Integrated Filters and Couplers for Next Generation Wireless Tranceivers

Olukoya, O.

UNIVERSITY OF WESTMINSTER

INTEGRATED FILTERS AND COUPLERS FOR NEXT GENERATION WIRELESS TRANSCEIVERS

Oludotun S Olukoya

A thesis submitted in partial fulfilment of the requirements of the University of Westminster for the degree of Doctor of Philosophy

January 2019

ABSTRACT

The main focus of this thesis is to investigate the critical nonlinear distortion issues affecting RF/Microwave components such as power amplifiers (PA) and develop new and improved solutions that will improve efficiency and linearity of next generation RF/Microwave mobile wireless communication systems. This research involves evaluating the nonlinear distortions in PA for different analog and digital signals which have been a major concern. The second harmonic injection technique is explored and used to effectively suppress nonlinear distortions. This method consists of simultaneously feeding back the second harmonics at the output of the power amplifier (PA) into the input of the PA. Simulated and measured results show improved linearity results. However, for increasing frequency bandwidth, the suppression abilities reduced which is a limitation for 4G LTE and 5G networks that require larger bandwidth (above 5 MHz). This thesis explores creative ways to deal with this major drawback. The injection technique was modified with the aid of a well-designed band-stop filter. The compact narrowband notch filter designed was able to suppress nonlinear distortions very effectively when used before the PA. The notch filter is also integrated in the injection technique for LTE carrier aggregation (CA) with multiple carriers and significant improvement in nonlinear distortion performance was observed. This thesis also considers maximizing efficiency alongside with improved linearity performance. To improve on the efficiency performance of the PA, the balanced PA configuration was investigated. However, another major challenge was that the couplers used in this configuration are very large in size at the desired operating frequency. In this thesis, this problem was solved by designing a compact branch line coupler. The novel coupler was simulated, fabricated and measured with performance comparable to its conventional equivalent and the coupler achieved substantial size reduction over others. The coupler is implemented in the balanced PA configuration giving improved input and output matching abilities. The proposed balanced PA is also implemented in 4G LTE and 5G wireless transmitters. This thesis provides simulation and measured results for all balanced PA cases with substantial efficiency and linearity improvements observed even for higher bandwidths (above 5 MHz). Additionally, the coupler is successfully integrated with rectifiers for improved energy harvesting performance and gave improved RF-dc conversion efficiency.

Table of Contents

Chapter 5: Compact Microstrip Coupler Design and its Next Generation Wireless Transceiver Applications

Chapter 6: Conclusions

List of Figures and Tables

Chapter 1

Chapter 2

Chapter 3

Chapter 4

Chapter 5

Chapter 2

Chapter 3

Chapter 4

Chapter 5

Acknowledgements

I would like to express my deepest appreciation to my director of studies, Dr. Djuradj Budimir, for offering the research opportunity at the University of Westminster and guiding me through my doctoral programme. Without your guidance, this thesis would not have been possible. I would also like to thank my second supervisor Dr. Andrzej Tarczynski for his advice on the PhD journey.

Special thanks to all my friends that have encouraged me and provided me with unconditional support.

Finally, I would like to dedicate this work to my family, my lovely wife and my son for their patience and continuous support. I would not have achieved this great milestone without you.

Author’s Declaration

I declare that all the material contained in this thesis is my own work.

List of Acronyms

1G	First Generation
2G	Second Generation
PA	Power Amplifier
GaN	Gallium Nitride
ADS	Agilent Design Software
3G	Third Generation
4G	Fourth Generation
LTE	Long Term Evolution
CA	Carrier aggregation
FBMC	Filter-Bank Multi-Carrier
UFMC	Universal Filtered Multi-Carrier
OFDM	Orthogonal Frequency Division Multiplexing
OFDMA	Orthogonal Frequency Division Multiple Access
CP-OFDM	Cyclic Prefix Orthogonal Frequency Division Multiplexing
ICT	Information and Communications Technology
IoT	Internet of Things
AI	Artificial Intelligence
VR	Virtual Reality
IF	Intermediate Frequency
RF	Radio Frequency
DPD	Digital Predistortion
MIMO	Multiple Input Multiple Output
OPBO	Output Power Back-Off
PhD	Doctor of Philosophy
MIC	Microwave Integrated Circuit
M2M	Machine-to-machine
PSTN	Public Switched Telephone Networks
MBPS	Megabits per second
MHz	Mega Hertz
RNC	Radio Network Controller

UMTS	Universal Mobile Telecommunication System
FDD	Frequency -Division Duplexing
TDD	Time-Division Duplexing
SNR	Signal-to-Noise Ratio
RN	Relay Node
SC	Single Carrier
ISI	Inter-Symbol Interference
QOS	Quality of Service
WLAN	Wireless Personal Area Network
WPAN	Wireless Personal Area Network
DLOS	Direct Line of Sight
ISI	Inter-Symbol Interference
SC-FDMA	Single Carrier – Frequency Division Multiple Access
BS	Base Station
HDSL	Asymmetric Digital Subscriber Lines
PAPR	Peak-to-Average-Power Ratio
CDMA	Code Division Multiple Access
MM-WAVE	Millimetre Wave
OOB	Out-of-Band
PAE	Power Aided Efficiency
GaAS	Gallium Arsenide
MIC	Microwave Integrated Circuit
HMIC	Hybrid Microwave Integrated Circuit
MMIC	Monolithic Microwave Integrated Circuit
DARPA	Defence Advanced Research Projects Association
DMS	Defected Microstrip Structure
BSF	Band-Stop Filters
ADS	Agilent Advanced Design System
PBG	Photonic Band Gap
DGS	Detected Ground Structure
EBG	Electronic Band Gap Structure
CAD	Computer Aided Design

EER	Envelope Elimination and Restoration
LINC	Linear Amplification with Nonlinear Component
DPD	Digital Pre-Distortion
PA	Power Amplifier
AM	Amplitude Modulation
PH	Phase Modulation
CA	Carrier Aggregation
ADS	Advanced System Design
BPF	Bandpass Filter
IM3	Third-Order Intermodulation Product
P_1DB	1-dB Compression Point
IM2	Second-Order Intermodulation
DUT	Device under Test.
LCP	Liquid Crystal Polymer.
BLC	Branch Line Coupler.
CRLH	Composite Left/right Hand

Chapter 1 Introduction

The way people communicate has been revolutionized by mobile communication systems. Communications evolved from being just stationary to being mobile and then wireless. The discovery of electromagnetism by Danish scientist Hans Christian Orsted and Andre-Marie Ampere early in the 1820's opened the door for the advent of mobile communications. He discovered that an electric current in a wire from a battery caused a compass needle to deflect. This finding led to the use of telegraph networks. The telegraph networks brought mobile communications to life and shortly afterwards, transatlantic cables were laid which made communications easier and faster in different locations. However, communications went into another gear when James Clerk Maxwell's postulated on wireless propagation which was also confirmed by Heinrich Hertz discovering radio waves some few years later when he found out that electric energy can be transmitted using electromagnetic waves.

These led to a radio-telegraph experiment by Marconi which led to the first complete wireless system in 1897. Marconi's idea became the backbone of other future mobile wireless systems. However, a breakthrough in the wireless journey was when Claude Shannon analysed the ability to send wireless information through a designated communications channel. This was due to the growing need for reliable and secure communications. Shannon was able to demonstrate that no matter how static and noisy a communication channel could be, perfect and reliable transmission was achievable. Therefore, different medium where no longer needed and his work transformed the mobile technology from analogue into the digital world. Mobile wireless communications have come a long way over the years and has become an ever-present part of modern day life, from global cellular telephone systems to local and even personal area networks. It has gone through the first, second and third industrial revolutions and it is still evolving as one of the fastest growing sectors today. Mobile wireless communications have been integrated into almost all industrial sectors like telecommunications, transportation, medical, energy, media and defence.

Mobile wireless technological discoveries have grown from the first to third industrial revolutions from the telephones to internet and ICT (information and communications technology). The internet has been the driving force for further developments of mobile wireless technology. Since the third revolution driven by internet and ICT, there has been great progress and a global expansion of mobile wireless methods of communications. Smart devices such as mobile phones, tablets, laptops have become an integral part of everyday life and led to more technological breakthroughs in the wireless industry. The new drive for data-hungry applications and high business needs all over the world has led to the fourth revolution of technology.

The fourth industrial revolution builds on the digital revolution (third revolution) which will present novel and advanced ways by which technology becomes embedded within societies and the human body. The fifth generation of mobile networks (5G) will be a major drive for all these fourth revolution technologies. The fourth revolution such as the advent of 5G has become massive for industries all over the world and would lead to emanating technological headways in technologies such as internet of things (IoT), artificial intelligence (AI), virtual reality (VR), and robotics.

1.1 Introduction

Mobile wireless communications have evolved over the years from analogue to the digital wireless systems of today over different generations. The first generation of mobile telecommunications also known as 1G introduced in the 1980's supplied voice services by using analog radio transmission techniques. The major drawbacks for 1G systems were unsecure communications, limited channel capacity, the large size of 1G mobile phones and it allowed calls in 1 country which did not fully support roaming. The second generation 2G networks were digital and improved on 1G's capacity and coverage [1.1]. 2G was able to digitally encrypt phone conversations, achieve better spectrum efficiency and introduce data services such as MMS (multimedia messages) [1.1]. However, 2G was only able to produce narrowband internet and could not meet data requirements as its speeds were low making it difficult to handle data like videos. Third generation (3G) mobile networks allowed mobile users to be able to download data and use internet on mobile phones which 2G could not reliably offer. It was able to provide high speed data connection with respect to previous generations [1.2]. 3G was well accepted for data and was instrumental during the fourth technological industrial revolution.

The increase in subscriptions and growing smart tablets, phones and laptops meant that 3G was not enough as mobile end users want to access multimedia data anytime anywhere with reliability and security. 4G improved on 3G's access methodology, transmission technology, data transfer rate and security. The emergence of new technologies, need for faster speeds and reliable connection for the growing millions of subscribers led to 4G (fourth generation mobile networks). The introduction of 4G LTE was driven by the industry's quest for a more efficient technology that could help achieve faster mobile broadband services, simplify network architecture, enhance coverage and subsidise reduce costs. 4G was developed to meet such high data speeds requirements and was predicted to achieve 1 Gbps in stationary cases and 100 Mbps for mobile cases. The upcoming 5G networks come with great prospects to achieve the data rates required with low latency by improving on the drawbacks of 4G LTE and LTE-Advanced.

However, for all these technologies from 2G to 4G, it was discovered that the predicted downlink and uplink speeds in theory were very less when compared to what was achieved in real life scenarios. Mobile users started becoming more aware of the fact that the speeds promised were never attained. For example, the maximum theoretical data transfer rate for 3G is about 2 Mbps. In Practice, the speeds achieved were mostly in the range from 0.5 to 1 Mbps even at locations not too far from the cell site. Same with 4G networks as it struggled to achieve even 50 Mbps. To be able to achieve such high data rates for 4G between 50 Mbps to 1 Gbps, it was observed that higher bandwidth and higher spectrum efficiency is required [1.3]. However, to get large bandwidths in a highly congested frequency band has limited the prospects of achieving the rates required. Also, the operational difficulties of combining different channels have been more pronounced than predicted. Due to this, 5G aims to use new frequency bands above and below 6 GHz where it could have the bandwidths required to achieve the necessary data rates and reduce interference. Higher bandwidths will affect the spectral efficiency/linearity and gain of the system. Therefore, techniques for achieving better

efficiency and improved linearity results for 4G LTE must continue to be improved for the 5G communications infrastructure. The linearity improvement is measured based on achieving significant reduction in nonlinear distortions (10 dB or more) with respect to the amplified fundamental input signals.

These issues affecting the required data transfer rates for these technologies are more prevalent in the wireless transmitters where the power amplifier operates as shown in Figure 1-1. The PA is a major component in the wireless transmitter system as it amplifies the signal prior to the antenna and its operation plays a vital role in determining the reliability of the signal.

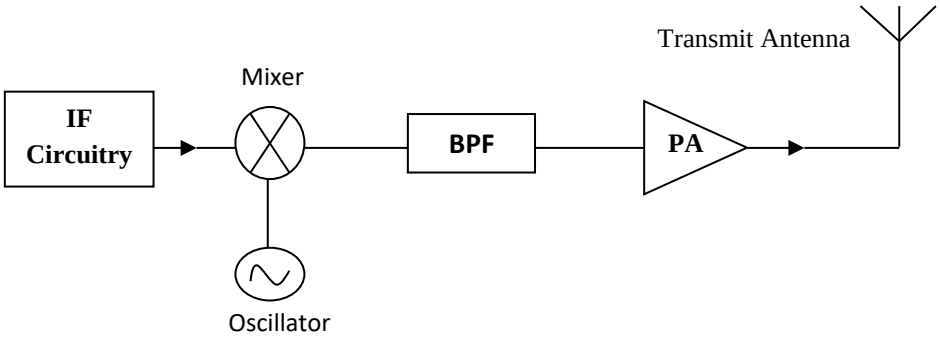

Figure 1-1: Wireless transmitter circuit.

To maximise efficiency, the power amplifier must operate very close to saturation because the highest transmit power possible impacts battery life positively and allows the system to operate more efficiently. However, at this stage, the power amplifier becomes nonlinear and its distortion adversely affects the performance of the overall system. As seen in Figure 1-2, the power amplifier (PA) increases linearly with input power until it gets to a point where the gain of the PA starts to reduce drastically with increasing power level until it becomes flat. This nonlinear behaviour is caused by the biasing of the active device in the PA and the power supply voltage.

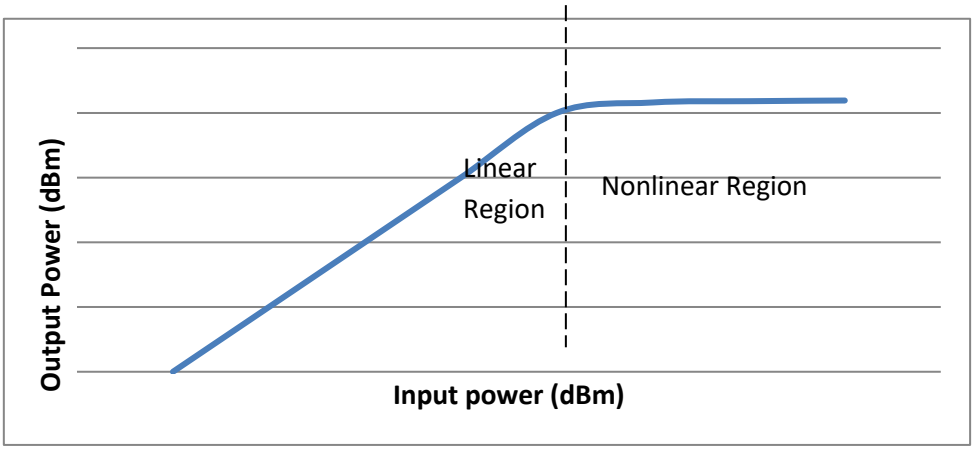

Figure 1-2: Linear and nonlinear region for PA.

These nonlinear distortions lead to low spectral efficiency which degrades performance and effectively shuts down the amplification process. Also, as frequency bandwidth increases, the higher order distortions become more pronounced [1.4]. These implies that techniques that helped improve linearity for 3G that utilized up to 5 MHz channel bandwidth may not be as effective when used for 4G LTE and LTE-Advanced that utilizes more bandwidth up to 20 MHz and 100 MHz respectively. Even more effective methods will be required for upcoming 5G networks that will use a minimum of 100 MHz channel bandwidth. Hence, it is best to find a way to maximise efficiency and linearity at saturation and effectively reject other forms of interference that could reduce system sensitivity.

The second harmonic injection linearization technique has achieved some good success in improving linearity and data rate reliability for 2G and 3G systems. Other techniques such as feedback, feedforward and DPD (Digital Pre-distortion) have also improved linearity but for smaller frequency bandwidths mainly below 5 MHz. Hence, the injection technique will form the basis of this thesis but emerging techniques such as filtering and different PA configurations will be combined and enhanced for better compensation of nonlinear distortions and interference suppression for newer generation of mobile wireless communication systems such as 4G LTE, LTE-Advanced and 5G.

1.2 Overview of Past Research

These issues affecting the required data transfer rates for these technologies are more prevalent in the wireless transmitters where the power amplifier operates as shown in Figure 1-1. The PA is a major component in the wireless transmitter system as it amplifies the signal prior to the antenna and its operation plays a vital role in determining the reliability of the signal.

Over the years, different research work has been aimed at developing and improving the performance of the wireless transmitters due to the meteoric growth of the wireless communication industry. Due to this, the efficiency and linearity requirements for these systems have become more important and previous techniques must be improved upon. High power applications have become ubiquitous, it has even become more vital to implement linearity techniques that will help reduce the distortions that occur due to the PA's nonlinear properties at the transmitting end. These demands have led to advancements in methods that will improve the nonlinear distortion performance of the PA.

Methods proposed over the years include feedback, feedforward, DPD, injection and even filtering [1.5] – [1.9]. In the feedback and feedforward methods, the loop control technique is limited to a few-gigahertz and may not be suitable for modern day communication systems and could be very complex as well [1.10]. Similarly, even though DPD is one of the most useful methods to diminish the distortions caused by PA nonlinearity and memory effects, for higher bandwidths there is a bandwidth mismatch between the PA and the feedback signal. This mismatch occurs because as the input signal bandwidth increases, the DPD feedback channel bandwidth becomes far larger but its limited by its non-ideal electronic components which degrade the linearization capabilities [1.7]. The injection technique has been explored in different ways and has achieved good linear improvements for 3G wireless systems [1.8]. In theory, the injection technique should be effective for low and high bandwidth situations but

however in practice, it has been observed that there could be increased complexity and linear performance degradation for MIMO and carrier aggregation systems that involve two or more components. This is very important as these disadvantages could negatively impact new networks like 4G and 5G. Filters such as band-pass and band-stop filters can also be used before or after the PA to eliminate unwanted signals, but its limitation comes from intra-band signals that cannot be removed without affecting the main signal [1.9]. More recently, the development of more efficient spectrum modulation schemes such as OFDM, improves the distortion performance of the overall system. However, poor efficiency has been observed in power amplifiers operating with such signals when operated at the output power back-off (OPBO) level [1.10]. In such cases, power amplifier configurations such as Doherty and balanced PA could be used as the efficiency of the Doherty PA is high at that region [1.11] - [1.13] and balanced PA could be configured with the aid of couplers to improve efficiency by limiting load insensitivities at the OPBO region for such signals with high PAPR [1.14].

These findings predict that the above techniques will be vital in improving the linear performance of next generation networks such as 5G. However, for different scenarios, they would have to be modified, combined and improved upon to achieve the results that will meet the demands of the industry.

1.3 Aims and Objectives of the Research

The major goal of this research is to explore novel ways to improve the efficiency and linearity in a 4G/5G wireless transmitter while considering size, complexity and cost. It is aimed at improving the reliability of the system in terms of data rates and spectral efficiency. This thesis will look at the most effective ways to reduce nonlinear distortions and suppress interference for these next generation networks. Also, due to higher bandwidths and combination of bands in LTE-Advanced carrier aggregation, there are other side effects that could affect the performance of the transmitter system. This PhD project aims to advance the second harmonic injection technique, combine it with other linearization techniques where possible and the use of appropriate power amplifier configurations that would boost efficiency, linearity and improve the sensitivity of 4G/5G wireless transmitter systems.

The research objectives are undertaken as follows:

- To perform detailed survey of the art on all the generations of mobile wireless communication systems and their data rates.
- Conduct a detailed investigation about nonlinear distortions in nonlinear RF/Microwave devices and systems.
- An in-depth study of the microstrip (MIC) technology and all the tools needed for design and implementation of the proposed circuits.
- Investigation of behavioural models of power amplifiers (PA) using the second harmonic injection technique.
- Investigating and providing a comparative overview on linearization techniques to find the best possible options for different cases.

- More detailed literature research on next generation 4G and 5G wireless systems with possible drawbacks and advancements.
- Simulation and experimental evaluation of nonlinear distortions in power amplifiers with and without the second harmonic injection linearization method.
- Advancing the injection technique for next generation networks.
- Designing novel notch microstrip filters using new technologies for nonlinear distortion and interference suppression in a multi-standard wireless system.
- Design and fabrication of compact microstrip couplers for multi-standard wireless applications.
- To fabricate the novel microstrip branch line couplers suitable for integration in balanced power amplifier (PA) configurations.
- Investigation and deduction of best approach for maximum efficiency and linearity of the 4G wireless transmitter systems.
- Experimental verification of the proposed balanced PA approach on the efficiency and linearity of different PA's in a 4G LTE transceiver system.
- Experimental evaluation on the best 5G waveform candidate for its wireless transmitters.
- Experimental verification of the proposed balanced PA configuration using the best 5G waveform candidates.

1.4 Thesis Organisation

This section summarises how this thesis written over a 3-year period has been organised into six distinct chapters.

Chapter 2 presents the theoretical background relating to this thesis. It looks at the evolution of all 5 generations of mobile networks. The data rates achievable and the rationale behind moving from one technology to another and the benefits of one over the other. The background theory of the microstrip technology in terms of designs and its pros and cons. The chapter then concludes with a summary of the nonlinear distortion theory and considers when it occurs and its effect in any wireless transceiver system.

Chapter 3 introduces novel band-stop filter designs using new technologies that could be used for different applications in the wireless transceiver. The design is focused on achieving a considerable size reduction. The chapter investigates the detailed analysis of the microstrip band-stop filter. The conventional design techniques were initially used to design the filter structures. The theory of the defected microstrip structure is investigated and used in conjunction with the emerging inkjet-printing technology to design single and dual-band new DMS band-stop/notch filters. Miniaturisation is achieved, and the performance of the filter is investigated at its frequency of operation.

Chapter 4 explores different compensation techniques for evolving next generation networks. This chapter presents the second harmonic injection technique and evaluates its compensation abilities over improved bandwidth for evolving LTE signal bandwidth. The band-stop filter introduced in chapter 3 is also implemented here to improve the nonlinear distortions for higher bandwidths and for interference suppression in LTE-Advanced inter and intra-band CA transmitters. Finally, different new 5G waveforms were evaluated for improved nonlinear distortion performance and spectral efficiency at saturation for different real power amplifiers.

Chapter 5 presents a new compact branch-line coupler design. The coupler was designed, simulated and fabricated. The coupler achieved great performance results. The coupler was used in different applications such as with rectifiers for improved energy harvesting. Also, it was used to design a new balanced power amplifier (PA). The balanced PA design with the aid of the coupler was then evaluated for increased efficiency and improved linearity in 4G and 5G wireless transceiver systems.

Chapter 6 gives the thesis conclusions with a summary of results and findings. The contributions to knowledge are noted and future work suggestions are also highlighted.

1.5 References

[1.1] T. Mshvidobadze, "Evolution mobile wireless communication and LTE networks," 2012 6th International Conference on Application of Information and Communication Technologies (AICT), Tbilisi, 2012, pp. 1-7.

[1.2] M. El-Sayed and J. Jaffe, "A view of telecommunications network evolution," in IEEE Communications Magazine, vol. 40, no. 12, pp. 74-81, Dec 2002.

[1.3] S. Yamanouchi, K. Kunihiro, S. Hori, M. Ikekawa and N. Nishi, "RF and signal processing technologies for 4G mobile networks," 2013 International Symposium on VLSI Technology, Systems and Application (VLSI-TSA), Hsinchu, 2013, pp. 1-2.

[1.4] L. Moller et al., "Higher order PMD distortion mitigation based on optical narrow bandwidth signal filtering," in IEEE Photonics Technology Letters, vol. 14, no. 4, pp. 558-560, April 2002.

[1.5] M. Faulkner, D. Contos and M. Johansson, "Linearization of power amplifiers using RF feedback," in Electronics Letters, vol. 31, no. 23, pp. 2023-2024, 9 Nov 1995.

[1.6] K. Konstantinou, P. Gardner and D. K. Paul, "Optimisation method for feedforward linearization of power amplifiers," in Electronics Letters, vol. 29, no. 18, pp. 1633-1635, 2 Sept. 1993.

[1.7] Y. Liu, W. Pan, S. Shao and Y. Tang, "A General Digital Predistortion Architecture Using Constrained Feedback Bandwidth for Wideband Power Amplifiers," in IEEE Transactions on Microwave Theory and Techniques, vol. 63, no. 5, pp. 1544-1555, May 2015.

[1.8] C.S. Aitchison, M. Mbabele, M.R. Moazzam, D. Budimir, and F. Ali, “Improvement of Third-Order Intermodulation Product of RF and Microwave Amplifiers by Injection,” Microwave Theory and Techniques, IEEE Transactions on, vol.49, no.6, pp.425-434, Feb. 2001.

[1.9] H. Uchida, H. Kamino, K. Totani, N. Yoneda , M. Miyazaki, Y. Konishi, S. Makino, J. Hirokawa, M. Ando, "Dual-band-rejection filter for distortion reduction in RF transmitters," Microwave Theory and Techniques, IEEE Transactions on, vol.52, no.11, pp.2550-2556, Nov. 2004.

[1.10] V. Paidi et al., “High linearity and high efficiency of class-B power amplifiers in GaN HEMT technology,” IEEE Trans. Microw. Theory Technol., vol. 51, no. 2, pp. 643–652, Feb. 2003.

[1.11] F. H. Raab, “Efficiency of Doherty RF power-amplifier systems,” IEEE Trans. Broadcast., vol. BC-3, no. 3, pp. 77–83, Sep. 1987.

[1.12] B. Kim, J. Kim, I. Kim, and J. Cha, “The Doherty power amplifier,” IEEE Microw. Mag., vol. 7, no. 5, pp. 42–50, Oct. 2006.

[1.13] D. Y.-T. Wu and S. Boumaiza, “A modified Doherty configuration for broadband amplification using symmetrical devices,” IEEE Trans. Microw. Theory Techniques, vol. 60, no. 10, pp. 3201–3213, Oct. 2012.

[1.14] H. Jeon, Y. Yoon, H. Kim, Y. Huang, and C. Lee, "Highly efficient balanced CMOS linear power amplifier with load immunity," IET Electronics Letters, vol. 47, no. 19, p. 1095, 2011.

Chapter 2 Theoretical Background

This chapter gives an overview and summary of the background theory behind this thesis. It covers various topics that will give clearer understanding of the work. To compensate for nonlinear distortions and suppress interference in advanced mobile networks such as 4G LTE, LTE-Advanced and the upcoming 5G networks, the history and evolution of mobile cellular networks needs to be effectively understood. The evolution of the generation of mobile networks from the first to fifth generation and the rationale behind the advancement to the next generation will be looked at. Evolution of analogue to digital and the data rates problem in theory have all led to the networks we have today. This day mobile wireless communications infrastructure is becoming more complex in designs as the new networks aim to support higher throughputs and reliability. The wireless transmitter is at the fore front of ensuring that these demands are met which has put strict requirements on its output power, efficiency and linearity performance.

This Chapter will also look at the theoretical background and literature review directly related to this thesis. The next generation networks will be looked at in more detail, the characteristics of the wireless transmitter and we also examine the microstrip technology which formed the basis of some novel structures that were built in this work.

2.1 Next Generation Mobile Wireless Communication Networks

Next generation mobile wireless communication networks encompass a series of architectural changes in the telecommunication core and access networks to improve performance and based on strategic requirements and targets such as increase in speed, overall efficiency, range and operating life time. Such next generation communication networks include 4G LTE, 5G, machine-to-machine (M2M) communications and IoT (Internet of Things).

Some of these are influenced not only by scientific factors but also physical and economic factors. Like in the 4G case, it shares some bandwidths with 2G and 3G networks which made it a bit difficult to have a large range of bandwidth which had to lead to the advent of LTE-Advanced carrier aggregation. The upcoming 5G systems have decided to use a new sets of frequency bands that is not congested so that it could be able to use more bandwidth to achieve very high speed and performance reducing interference.

4G LTE, LTE-Advanced and 5G will be discussed in the next sub-chapters to provide more knowledge about their advantages over older generation of communication networks.

2.1.1 History of Cellular Networks

There is a long history for communication devices that have a wireless connection to the public switched telephone network (PSTN). Although commercial mobile telephone networks existed as far back as the 1940s, the advent of analog cellular networks is widely accepted as the first generation (1G) wireless networks. The second-generation networks came up in the 1990s. The standards developed for 2G were the GSM standard from Europe and the CDMA standard developed by the USA [2.1]. The second generation used digital transmission instead of analog and was a great success. It was the advent of digital cellular networks and there was a rapid

increase in the use of second-generation mobile phone. The ability to view media on mobile phones also became popular with 2G.

The quest for more data due to the wide use of internet and higher data rates (speeds) led to the third generation (3G) technology as 2G data rates were not enough. 2G uses circuit switching while 3G utilizes packet switching for its transmission of data but still used circuit witching for voice. During the evolution between 2G and 3G systems such as GPRS and EDGE also referred to as 2.5G and 2.75G [2.1].

The specifications required aimed to produce up to 2 Mbps in stationary conditions and 384 Kbps in a moving vehicle with 5 MHz bandwidth. However, in practice, these expected rates were not attained [2.2].

The quest for higher data rates due to more demand has led to further upgrades on pre-existing technologies. Peak data rates EDGE/E-EDGE, W-CDMA, HSPA and HSPA+ were up to 1 Mbps, 2 Mbps, 10 Mbps and 28 Mbps downlink for these technologies. Further demand for higher speeds and data and higher bandwidth applications led to the industry moving towards the 4th Generation (4G) cellular networks such as LTE. 4G technologies would not employ circuit switching at all making it an all packet-based network [2.3]. LTE Release 8 gave further key data rates evolution with next generation networks such as LTE and Mobile Wi-Max offering downlink data rates up to 100 Mbps [2.4]. 4G LTE was very successful but the availability of bands was a real limitation as the bands were not readily available. Carrier aggregation was a good solution to that whereby different bands were combined but in practice it can become incredibly complex and tricky to know the right bands to combine. The issues with 4G LTE and LTE-Advanced are more with the reliability of the signal in mobile situations as it was not able to achieve the low latency expected. This has led to the advent of next generation 5G wireless communications. 5G will drive the fourth industrial revolution for smart devices, internet of things, artificial intelligence and virtual reality. It will use a new set of bands below and mainly above 6 GHz where it would readily have enough bandwidth to achieve the high throughputs expected with low latency. The next sub-chapters will focus mainly on the fourth generation LTE and fifth generation (5G) wireless networks. Their data rates, modulation schemes, signals and rationale will be closely looked at as they form the basis of this thesis.

2.1.2 LTE (Long Term Evolution)

Long Term Evolution (LTE) is a mobile network technology that was developed to succeed and update the generation of UMTS (Universal Mobile Telecommunications System) 3G technology which was based upon HSUPA, HSPA, HSDPA and WCDMA providing major data rate improvement for both downlink and uplink. The GSM and UMTS standards also generally referred to as 2G and 3G standards respectively have evolved towards LTE. LTE has been marketed as a 4G standard, but strict technical requirements placed by the ITU (International Telecommunication Union) shows that it does not meet all the requirements which are met by LTE-A. The International Telecommunication Union (ITU-R) and the 3GPP (3^{rd} generation Partnership Project) standard bodies have laid the foundations for its LTE successor counterparts such as the International Mobile Telecommunications –Advanced

(IMT-Advanced Standard) and LTE-A. The LTE standard aims to significantly increase capacity and data rates.

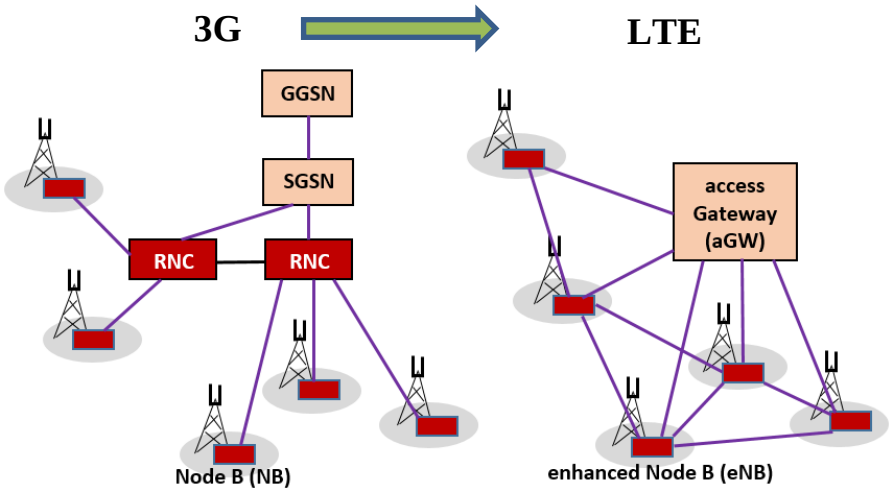

Figure 2-1: Evolution of 3G network architecture towards LTE.

LTE wireless communication standard was developed as part of release 8 of 3GPP and was updated in subsequent releases with major additions seen in release 9. LTE improved on the 5 MHz maximum bandwidth employed by 3G networks to flexible scalable frequency bands from 1.4 MHZ up to 20 MHz thereby increasing network capacity and coverage since increasing channel bandwidth could increase capacity and number of users.

Another vital feature of LTE is the use of scalable bandwidths for the channels. LTE uses bandwidths different from GSM and UMTS supporting scalable bandwidths from 1.4 MHz to 20 MHz. With these channel bandwidths and the MIMO technology, LTE could theoretically come up with peak data rates of 300 Mbps downlink and 75 Mbps uplink.

To reduce network complexity, LTE has removed the RNC (Radio Network Controller) from the network architecture of UMTS which helps to reduce size and complexity [2.5] as seen in Figure 2-1. This RNC elimination also gives room for better software-based advancements for the technology whilst reducing deployment and operation costs.

UMTS had been deployed successfully all over the world, hence, it was imperative that any new standard to be developed needed to be backward compatible. LTE also tries to simplify the network architecture whilst it achieves higher data rates as well. LTE aimed to achieve better speeds but to also reduce latency for packets that are transmitted. The upgrading process from UMTS towards LTE was done in a very simple way that could support interoperability.

For better wide channel bandwidth efficiency, LTE adopts the use of the OFDM (Orthogonal Frequency-Division Multiple Access) technology. This technology allows the use of FDD (Frequency-Division Duplexing) and TDD (Time-Division Duplexing). Unlike its 2G and 3G predecessors, LTE uses a different bandwidth allocation and would need a different spectrum of operation. For countries these days with insufficient spectrum, TDD is best suitable as it could decrease spectrum usage by 50 percent as it uses the same spectrum for downlink and uplink transmission in a time-duplexed mode [2.6].

Table 2-1: LTE operating frequency bands.

E-UTRA Band	Uplink band (MHz)	Downlink band (MHz)	Duplex-mode
1	1920 – 1980	2110 – 2170	FDD
2	1850 – 1910	1930 – 1990	FDD
3	1710 – 1785	1805 – 1880	FDD
4	1710 – 1755	2110 – 2155	FDD
5	824 – 849	869 – 894	FDD
7	2500 – 2570	2620 – 2690	FDD
8	880 – 915	925 – 960	FDD
9	1749.9– 1784.9	1844.9– 1879.9	FDD
10	1710 – 1770	2110 – 2170	FDD
11	1427.9– 1452.9	1475.9– 1500.9	FDD
12	698 – 716	728 – 746	FDD
13	777 – 787	746 – 756	FDD
14	788 – 798	758 – 768	FDD
17	704 – 716	734 – 746	FDD
33	1900 – 1920	1900 – 1920	TDD
34	2010 – 2025	2010 – 2025	TDD
35	1850 – 1910	1850 – 1910	TDD
36	1930 – 1990	1930 – 1990	TDD
37	1910 – 1930	1910 – 1930	TDD
38	2570 – 2620	2570 – 2620	TDD
39	1880 – 1920	1880 – 1920	TDD
40	2300 – 2400	2300 – 2400	TDD

LTE's frequency bands are summarized in the Table 2-1 below. Some bands have been skipped in the table. Band 6 which is commonly known as Japan's UMTS 800 is no longer used and

formerly reserved E-UTRA bands 15 and 16 (Center frequency f = 2600 MHz) have also become obsolete. Then other bands also used the FDD mode until band 33 (1900 - 1920 MHz) which uses a TDD duplex mode.

2.1.3 LTE - Advanced

As LTE could not meet many requirements for 4G communication systems, a new standard called LTE-Advanced was developed for cellular systems. Unlike LTE, LTE-Advanced meets the standardization body's 4G requirements. The formal evolution of LTE towards LTE-Advanced began with 3GPP release 10. LTE bodies such as IMT-Advanced and LTE-Advanced were aiming at downlink data rate of up to 1 Gbps for low mobility and 100 Mbps for high mobility applications [2.7]. This could help meet public demands such as downloads and the use of internet in fast moving trains.

When comparing this speed to the third generation (3G) requirement, that is a massive increase in data rates. LTE-Advanced aims to achieve higher data rates but not at the expense of spectral efficiency. Table 2-2 gives a better breakdown on how the data rate has evolved since UMTS as it continued to develop towards the fourth-generation networks and the state of art. Table 2-2 also shows how the standardization body's releases have evolved from release 4 till release 10. Even though there are plans for more releases as the advent of 5G gets closer and closer, LTE-Advanced has the prospect to meet the high demand in the mobile industry.

Table 2-2 Evolution from 3G to LTE-Advanced.

	UMTS (WCDMA)	**HSPA**	**HSPA+**	**LTE**	**LTE-Advanced**
Peak downlink speed (Bps)	384k	14M	28M	100M	1G
Peak uplink speed (Bps)	128k	5.7M	11M	50M	500M
Access Scheme	CDMA	CDMA	CDMA	OFDM/SC-OFDM	OFDMA/SC-FDMA
Year of Official Release	2003/2004	2005/2006; 2007/2008	2008/2009	2009/2010	2011
3GPP releases	Release 4	Release 5 /6	Release 7	Release 8	Release 10

LTE-Advanced requirements also included the fact that it should be compatible with other previous existing radio and mobile networks; it should be flexible and adaptable to support a wide range of services and applications in a cost-effective way. LTE-Advanced should also improve and achieve higher quality of service and should be very user friendly. LTE and LTE-Advanced have similar mobility capabilities but however, LTE-Advanced supports a throughput and spectral efficiency almost three times more than LTE. New bands have also been introduced with LTE-Advanced to add to the already existing bands listed in Table 1-1. The six additional bands are 450-470 MHz, 698-862 MHz, 790 - 862 MHz, 2.3 - 2.4 GHz, 3.4 - 4.2 GHz and 4.4 - 4.99 GHz bands.

A major significant improvement in LTE-Advanced when compared to LTE is the fact that theoretically, it could provide data rates up to 3Gbps as compared to 300 Mbps offered by LTE [2.8]. This significant increase and improvement is due to key technologies exploited by LTE-Advanced such as using more sophisticated MIMO technology techniques and wider channel bandwidths. For example, LTE-Advanced exploits downlink features using up to 8x8 MIMO and aggregation of up to five carriers to remarkably increase data rates and hence, end user throughput [2.8].

LTE-Advanced has also exploited beam-forming mechanism to improve practical performance when compared to LTE. For example, LTE-Advanced can beam-steer downlink sub-carriers to a end-user's handset. By doing this, the receiver of the handset will pick up a higher power of its own allocated resource block during transmission and a relatively lower power of the resource blocks that have been assigned to other end users. This beam-steering ability of LTE helps to improve strength of received signal by the handset and can also improve throughput for situations whereby the signal-to-noise ratio (SNR) is relatively low [2.9].

LTE-Advanced has some new functionalities that are specific to its standard which include carrier aggregation, enhanced multiple antenna transmission and support for relay nodes (RN). Carrier aggregation would be examined in more detail and experimentally in chapter 4 but for now, a general overview of LTE-Advanced carrier aggregation is described.

2.1.3.1 Carrier Aggregation (CA)

LTE-Advanced was introduced due to the quest for higher data rates. A well-known theoretical way to increase capacity is to increase the bandwidth according to Shannon's hypothesis. By increasing bandwidth, capacity is increased, and higher data rates could be achieved. LTE exploits this key basic idea to achieve very high-end user data transmission speeds. The technique to be used by LTE-Advanced is called carrier aggregation. This technique has to do with a flexible selection of multiple frequency bands to increase bandwidth. LTE carriers described in release 8 and 9 are also used to ensure backward compatibility and so the aggregation is down with these LTE carriers. According to release 8 and 9, the carriers can have a bandwidth of 1.4 MHz, 3 MHz, 5 MHz, 10 MHz, 15 MHz or 20 MHz. Each individual aggregated carrier in LTE-Advanced is called a component carrier (CC) and the limit placed on CC's to be aggregated is five (5). Therefore, the maximum bandwidth attainable in this case is 100 MHz as the highest bandwidth for any CC is 20 MHz [2.10].

CA can be used for both frequency division duplex and time division duplex modes. CA also supports aggregation of both downlink (DL) and uplink (UL) carrier components but only supports the case where the number of downlink component carriers cannot be less than the number of uplink carriers even though it is possible for them to be the same in some cases. This is further clarified in release 10 and release 11. For release 10, there are two downlink CC's but only one uplink component carrier implying that there is no CA foe the uplink case. Release 11 gives to downlink CC's and could support one or two CC's in the uplink. In this case, CA could be used for both uplink and downlink unlike the other example in release 10 above where CA was only used in the downlink scenario.

Now that the carriers to be aggregated have been established, there are different ways to arrange the carriers. The simplest way is to arrange the CC in a contiguous way within the same LTE operating frequency band known as intra-band contiguous CA. The drawback with this is due to the different frequency allocation scenarios in different countries; it may not be feasible to always get the contiguous case and so there has to another arrangement for cases where the other bands could be used. This is the non-contiguous case. The non-contiguous allocation is split into two scenarios. It could be intra-band in the case whereby the CC's are in the same LTE frequency band but are spaced by a frequency gap. It could also be the inter-band case in which the CC's belong to different operating LTE frequency bands [2.11].

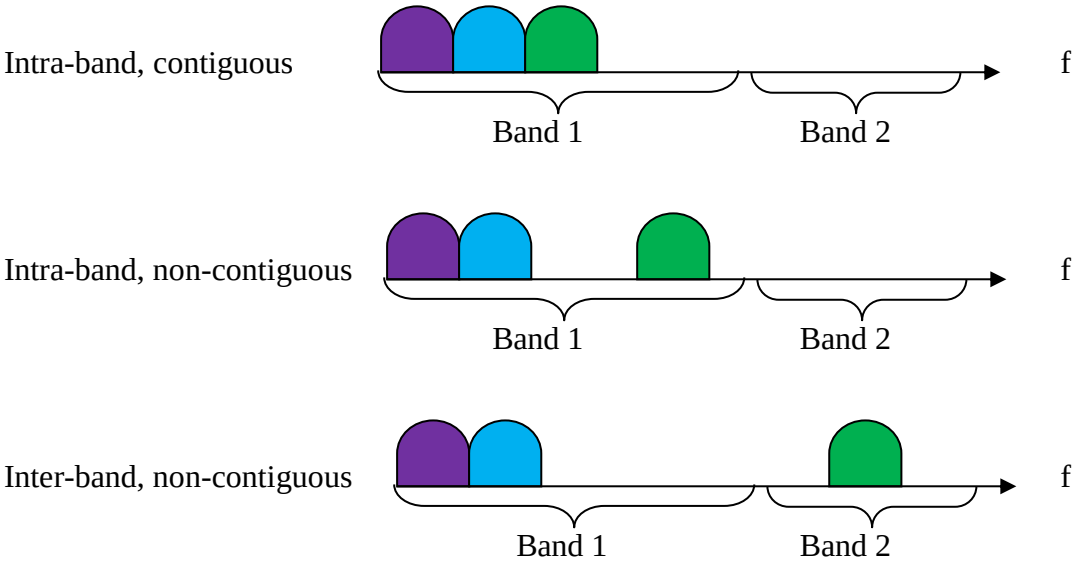

Figure 2-2: Intra- and Inter-Band carrier aggregation.

Figure 2-2 exposes the fact that it is easier to combine the frequency bands when they are in the same band and are contiguous carriers, but the frequency spectrum allocation does not permit that in all cases as some frequency bands or allocations within a band could be in use. For hardware purposes, the end user equipment (receiver) should support CA. Each component carrier (CC) is handled by a serving cell (transmitter). The main RRC (radio resource control) connection and all signal information messages with the end user is handled by the primary serving cell. The secondary component carriers are handled by the secondary serving cells and can be added and removed depending on the number of CCs required. The serving cell then scales the data link according to the capabilities of the end user device. For the intra-band non-contiguous case, the component carriers operate within the same LTE operating frequency band but are not next to each other and do not directly overlap as shown in Figure 2-2. The inter-band non-contiguous arrangement is one that would be very prominent for future LTE-Advanced applications but will require better adaptability techniques. The serving cells may be different, and the coverage could also be different based on the frequency of the CCs. In CA, there is always a primary serving cell and other cells are referred to as secondary serving cells [2.12].

Carrier aggregation for LTE-Advanced could also be used with MIMO (Multiple Input Multiple Output) techniques to increase total bit rate and end user speeds [2.13]. This is what

is referred to as enhanced multiple antenna transmission. LTE-Advanced aims to be able to support 8x8 MIMO downlink antenna configuration and 4x4 uplink to achieve higher peak rates when compared to LTE's ability whilst still maintaining good and acceptable spectral efficiency [2.14]. Also, the ability of LTE-Advanced architecture to support relay nodes which involves the mixing of small and large serving cells would help in efficient heterogeneous network planning for advanced mobile and wireless communication systems.

2.1.4 OFDM

The demand for higher data rates in the last few years for fixed and mobile communication networks has been on the rise. This led to more research interest for efficient modulation techniques such as OFDM.

OFDM is a multi-carrier modulation technique that involves the transmitting of information using numerous parallel narrow-band subcarriers rather than opting for a wide-band single carrier (SC). For modulation techniques that employ single carriers, when the information is transported over a multipath channel, it is possible that the symbol duration could be lesser than the delay spread of the channel which leads to what is called ISI (Inter-Symbol Interference) at the receiving end. Therefore, an equalizer is always required by the SC system to demodulate the transmitted signal correctly. The equalizer operates as a filter to reduce ISI. OFDM overcomes has that ability to operate even in such fading channels with a lot of multipath without the ISI problem with SC [2.15].

Parallel subcarriers are used in OFDM because in traditional series technique, the symbols are transmitted consecutively with all the bandwidth being fully occupied by the frequency spectrum of each symbol. For high data rate cases, several adjacent symbols may be completely distorted over frequency selective fading. In the parallel case, the subcarriers do not occupy the full channel bandwidth but instead the bandwidth is divided into several narrow sub-bands. This could help to eliminate the frequency selective fading problem as the frequency response over all the single separate sub-bands in the whole channel bandwidth is relatively flat.

2.1.4.1 Overview of OFDM

Trying to extend the available services on wired telecommunication networks to mobile networks and its end users has been very prominent on the agenda of mobile providers. Wired networks have high QOS (quality of service) and can achieve very higher end data rates than the mobile wireless and telecommunications users.

OFDM is also used in many other wireless communication systems such as wireless local area network (WLAN), wireless personal area network (WPAN) and Wi-Max among others.

The QOS for mobile wireless communication systems is affected by multipath reception. At the receiver there is a direct line of sight (DLOS) radio wave reaching the mobile radio channel. There are also many radio waves (reflected) reaching the receiving ends but at various times. Hills, tall trees, sky scrapers, mountains cause such reflections and when the signal passes through them, they are delayed.

Inter-symbol interference (ISI) occurs when such delayed signals interfere with the LOS wave and this interference leads to network performance degradation. To deliver high speeds for mobile communication systems, high-bit-rate transmission. If the digital data to be transmitted is sent at a data rate in the order of several Mbps (megabits per second), the delay time for the radio signals could be greater than a symbol time.

By using equalizers and other adaptive equalization methods, the receiver can demodulate the transmitted data correctly but there are a lot of stumbling blocks and limitations that have been observed when using equalizers at such high data rates in a couple of practical applications with the aim of low cost and compactness [2.16].

To avoid the use of equalizers which could not be totally relied upon, the OFDM transmission scheme has been developed and it uses the parallel sub-carrier transmission mode to subdue the multipath fading effect.

Figure 2-3 shows how the OFDM concept helps to achieve spectrum efficiency. The Figure shows about half of the spectrum being saved by OFDM rather than the conventional classical methods that consume a lot of bandwidth.

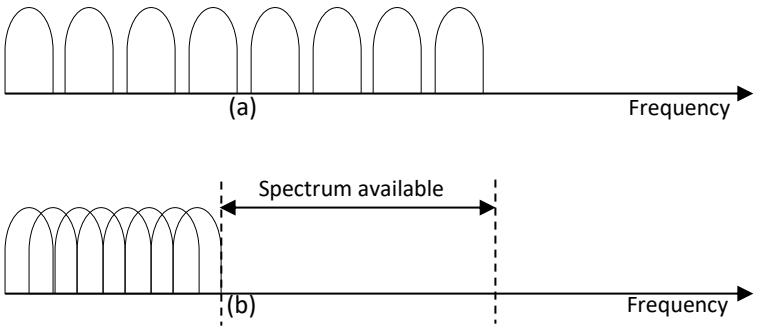

Figure 2-3: OFDM signal concept: (a) classical multicarrier method, and (b) orthogonal multicarrier modulation technique.

OFDM will be very important for advanced mobile communication systems that require a lot of bandwidth and spectral efficiency as the quest for higher data has led to more bandwidth consumption. This explains why 4G LTE signals are produced using OFDM.

2.1.4.2 OFDM Modulation

OFDM is a multi-carrier modulation or multiplexing technique that helps improve the toughness against frequency selective fading by transmitting a single data stream over a couple of lesser rate subcarriers. OFDM uses the parallel-data transmission scheme. In a conventional single-carrier system, the whole wireless link could break down by a specific interference or a fade on the link but in the multi-carrier network, for such fade or interference, the percentage of subcarriers to be affected will be on a small-scale. The small number of affected subcarriers can then be corrected using error correction coding techniques.

During implementation, the multiple access scheme supported for OFDM includes SC-FDMA (Single Carrier - Frequency Division Multiple Access) for uplink (End user to BS (base

station)) and OFDMA (Orthogonal Frequency Division Multiple Access). OFDM also supports all nodulation types such as QPSK, 16 QAM and 64 QAM.

When the parallel-data-transmission system was first developed, the whole frequency band is subdivided into several non-overlapping frequency sub-channels with each individual sub-channel being modulated with a separate symbol and then all the numerous channels are then combined. By doing this, inter-channel interference (ICI) could be gotten rid of as spectral overlap of channels are avoided but spectral efficiency is low and there are several wasted bandwidths.

A concept was developed in the 1960's to maximize the spectrum and cope with such inefficiencies. The idea was to use parallel data transmission and frequency division multiplexing (FDM) with overlapping sub-channels. Each sub-channel is being spaced in frequency by the same signalling rate that the channels are being transmitted with. By doing this, there would be no more need for high data rate equalisers. This concept as shown helps to increase robustness against multipath fading and impulsive noise and most importantly, as shown in the Figure 2-3, the spectrum bandwidth is utilised more effectively. Figure 2-3 shows how more bandwidth allocation could be created using the overlapping multicarrier technique. However, this could lead to cross talk between subcarriers and by achieving allowing distinct modulated carriers to be orthogonal to each other, cross talk could be used.

Therefore, specific mathematical expressions between the frequencies of the carriers are needed. In the traditional FDM system configuration, the carriers are well spaced with guard bands in the frequency domain which wastes bandwidth. In this OFDM technique, it is very much feasible to arrange the subcarriers in the signal such that the sidebands of separate carriers overlap and can be received without adjacent interference of carriers. To be able to achieve such minimum inter-channel interference (ICI), the carriers should be mathematically orthogonal to each other. The data is demodulated at the receiver whereby each carrier is then translated down and the signal that emanates is integrated over a symbol period (say T) retrieving the data.

At the receiver, if the other carriers all use frequencies that have a whole number of cycles in the symbol period, then the integration over the symbol period (T) will give a zero contribution from all other carriers. This implies that if the carriers are spaced (1/T) apart, the carriers are therefore linearly independent which implies that they are orthogonal [2.16].

OFDM has been used in different military high-frequency systems in the past. ANDEFT [2.17], KATHRYN [2.18] and KINEPLEX [2.19] are some examples. OFDM was also investigated for high-density recordings and high-speed modems and various developments have been made such as speed modems for telephone networks. In the last two decades, the use of OFDM has also been exploited for wideband communications over mobile radio channels such as high bit-rate digital subscriber lines (HDSL), asymmetric digital subscriber lines (ADSL) which were able to achieve up to 6 Mbps and the very high-speed digital subscriber lines (VDSL) which mostly uses fibre optic cable and could achieve very high data rates up to about 100 Mbps [2.16].

The OFDM transmission scheme has a lot of vital merits which will play a key role for next generation wireless communications. OFDM is a more efficient way to deal with multipath as the complexity of practical implementation is significantly lower than the use of an equalizer in a single carrier system. With OFDM, it is also possible to enhance capacity in slow-time varying channels, by modifying the data rate per subcarrier due to the SNR (Signal-to-noise ratio) of the subcarrier in question. OFDM offers great resistance and it's very tough against narrow-band interference as those kinds of interference can only have effects on a tiny percentage of the subcarriers. OFDM could also permit single-frequency networks and this is popular for broadcasting applications. OFDM also has its own drawbacks when compared to single carrier modulation as it is very sensitive to frequency offset and phase noise and it has a large PAPR (peak-to-average-power ratio) which has been known to reduce power efficiency of the RF (radio frequency) power amplifier.

OFDM and other such kind of multicarrier modulation methods will give the necessary way out from the problems associated with wireless communications and serve as the basis of next and future generation mobile wireless communications. Multicarrier modulation techniques such as orthogonal frequency division multiplex (OFDM) would help resist the frequency-selective fading problem that occurs in mobile wireless systems. For advanced mobile communication infrastructure that would be looking to achieve high-speed data transmission, the resistance against such frequency-selective fading is appealing and fascinating. Going further to combine OFDM with code division multiple access (CDMA) could also boost the robustness against such fading problem and attain higher scalability for high-speed data transmission. OFDM has really developed through research and it's well known to be an effective scheme for fourth generation (4G) and fifth generation (5G) signals.

The nonlinearities in LTE and LTE-Advanced wireless transmitters have also been on the rise due to the higher bandwidth specifications required. Other contributions to nonlinear distortions in such systems are the different carrier frequencies, the flexible channel bandwidths and carrier aggregation. Therefore, there should be plans in place for better linearity standards that would help improve the performance of such mobile networks. These nonlinearities should be suppressed and reduced to the barest minimum. This thesis would consider a host of ways and techniques to help these advanced mobile communication systems achieve a highly efficient and linear output whilst maintaining high data rates and throughput.

2.2 Fifth Generation Networks (5G)

The new network standard 5G will replace 4G in due course with potentially massive increased data speeds and incredibly low latency. It is not expected to be fully launched until 2020 and it's still at the stage of early testing. The requirement for the new standard is for it to be backward compatible with current wireless technologies like GSM, Wi-Fi, and LTE among others, combine them and use new radio access technologies as well. 5G is predicted to increase the data rates beyond 1 Gbps and offer higher broadband density to the end users. It is estimated that maximum data download and upload rate will be 20 Gbps and 10 Gbps respectively. However, the IMT 2020 requirements for 5G to achieve 20 Gbps peak downlink data rate and latency of 1 ms comes with major engineering challenges for the design of 5G mobile wireless

systems [2.20]. Demand for high data rates due to the growing popularity of hand-held smart devices mean that 5G must deliver faster speeds with low latency. The advent of IoT means that there is going to be a massive connection of devices to the network at the same time and reliability is important. 5G aims to achieve high mobile data rates (20 Gbps), low latency and increased battery life [2.21]. To be able to attain those high speeds, 5G will use less congested band as it requires very high bandwidth. This was one of the major issues with 4G's LTE. The millimetre wave (mm-wave) bands have emerged as the promising 5G candidates with Europe looking to use the 3.5 GHz band (3400 -3800 MHz) below 6 GHz and the 26 GHz (24.25 – 27.5 GHz) above 6 GHz. The mid-range bands such as the 3.5 GHz band for Europe with large bandwidths will be used to provide the necessary data rates and capacity to not only support a high number of connected devices but ensure that the devices can all be simultaneously connected at the same time. As for the spectrum above 24 GHz such as the 26 GHz band for, it ensures that very large bandwidths could be used to support ultra-high data rates and capacity and to support stationary and mobile services that require very low latency. Other lower frequency bands of interest such as 700 MHz and 1.5 GHz will still be used to enable coverage to wider areas. This is to ensure that 5G does not lack in one area over another. For instance, the RF/microwave bands provide great coverage capabilities, but bandwidth is scarce and limited due to band congestion, whereas the mm-wave bands have spectrum availability in abundance which could lead to increased data rates and low latency but possess coverage issues due to high electromagnetic attenuation [2.22]. This combination of low, mid and high frequency bands is proposed to take advantage of the major drawbacks of the previous generation and make 5G the network that will fulfil almost all demands and drive the fourth industrial and technological revolution.

The potential advantages of 5G cellular systems are numerous but one very vital to this research work is the fact that the signal waveform will improve on the spectral efficiency of LTE's OFDM signal. This will enable the wireless transmitters such as base stations operate better at the saturation level of the power amplifiers, thereby improving the overall efficiency and linearity of the system. 5G will have to use new, flexible waveforms that will be able to meet these new demands and overcome the draw backs of the 4G LTE signal. There are many contenders under consideration now which are unique for different scenarios. It has been suggested that 5G could even allow the use of different waveforms for different applications and systems [2.23]. Any alternative waveform candidate should achieve better spectral efficiency for various input power levels and increasing bandwidth. The modulation format and multiple access technique for 5G are not yet known, with many contenders under consideration, each proving advantages in certain scenarios and lacking in others.

Currently, there are several multicarrier waveform candidates that are being considered for 5G to address these limitations. The two leading candidates at the moment are Filter-bank multicarrier (FBMC) and Universal filtered multicarrier (UFMC). They also have the prospects of being used alternatively in different systems due to their similar charcteristics and performance for different use cases. Both signals will be compared with the current LTE OFDM signal for 4G systems. FBMC uses subcarrier filtering to attain better spectral efficiency whilst Universal Filter MultiCarrier (UFMC) is achieved by performing filtering operation per sub-band instead of per subcarrier and uses smaller filter length [2.24] –[2.25].

2.2.1 5G Waveform Candidates

In this section, the two leading 5G waveform candidates FBMC and UFMC explained above are further described in relation to LTE's CP-OFDM.

2.2.1.1 Cyclic Prefix OFDM (CP-OFDM)

The basic principle of CP-OFDM system is to use narrow, mutually orthogonal subcarriers. Cyclic prefix simply refers to prefixing of the OFDM symbol such that there is a repetition of that symbol at the end. The CP acts as a guard interval to protect the OFDM signals from inter-symbol interference from the previous symbol. CP-OFDM is the most prominent waveform, widely used in LTE. The signal design consists of many closely spaced sub-carriers and cyclic prefix length to carry data and control information. To design the signal, the end of the CP-OFDM symbol is and placed at the beginning of the symbol, for every symbol. In the cellular wireless transmitter system, CP-OFDM exhibits robustness against multi-path propagation but has drawbacks in its implementation. In the multi-path channel systems, the orthogonality between signal subcarriers cannot be easily accomplished. CP-OFDM signals use CP longer than time spread introduced by the channel, which leads to decrease of spectral efficiency. Due to its rectangular pulse, CP-OFDM has high OOB (out-of-band) emissions [2.26]. This results in larger side lobe levels with the elimination of sharp transition edges. There is spectral leakage at the end of each CP-OFDM symbol due to waveform discontinuity and this could limit its applications for 5G networks. Therefore, new multicarrier modulation scheme is proposed to overcome above drawbacks.

2.2.1.2 Filter Bank Multi-carrier (FBMC)

Filter bank Multi Carrier (FBMC) based systems can achieve better spectral efficiency and resilience to imperfect synchronization when compared to Orthogonal Frequency Division Multiplexing (OFDM) [2.27]. Filter Bank Multi-carrier (FBMC) transmits data by filtering each sub-carrier individually rather than the whole sub-band. The frequency and time domain are controlled by using prototype filters, which results in low side lobe levels in contrast to CP-OFDM. FBMC signal can achieve better spectral efficiency as it does not use cyclic prefix and respects Nyquist rate. In contrast to CP-OFDM, the low side-lobes, steep slope at the edges of the signal band and the use of larger number of subcarriers during transmission make FBMC more spectrally efficient at the output of the wireless transmitter [2.24]. One major advantage of FBMC over other waveform candidates (such as CP-OFDM, GFDM and UFMC) is that it enables fundamental spectral efficiency at low signal processing complexity. Better performance can be achieved comparable to CP-OFDM with the help of multiple prototype filters between spectrum confinement and orthogonality among adjacent sub-carriers. This waveform provides better performance in frequency selective channel with long delay spread as the delay spread (multipath difference) is known to have a significant impact on inter-symbol interference. FBMC possesses lower out-of-band emissions over CP-OFDM [2.27] and it has the capability to maintain system performance over a wide bandwidth which makes it a vital candidate for the 5G wireless transmitters.

2.2.1.3 Universal Filtered Multi-carrier (UFMC)

Universal Filtered Multi-Carrier (UFMC) is a waveform enhancement of CP-OFDM used in 4G LTE wireless transmitters. It works on the drawbacks of CP-OFDM whilst retaining some of CP-OFDM's unique properties such as high PAPR, flexibility and MIMO capability. UFMC filters a group of consecutive sub-carriers to reduce the out-of-band emissions and ICI between the adjacent users during asynchronous transmission [2.28]. This in turn provides the shorter impulse response in time domain. UFMC is spectrally more efficient compared to CP-OFDM because of the reduced guard bands in adjacent channels. Here the symbols are padded with zeros to perform the 2N-point FFT. This makes UFMC a better candidate for the 5G wireless transmitters. In UFMC systems, however, the resource block filtering is a major burden on the system complexity because it determines the number of discrete Fourier transform operation [2.29]. This is highly related to energy efficiency and system complexity at the user side which are important system performance metrics in a practical system.

The 5G FBMC and UFMC signals will be explored in this thesis below and above 20 MHz which is the maximum LTE frequency bandwidth in terms of their spectral efficiencies in a wireless transmitter system. UFMC and FBMC signals will be vital for 5G wireless communication system and different waveforms may be used for different applications and systems.

2.3 Wireless Transmitter System Parameters

This section briefly explains the main transmitter system parameters for this thesis. The major characteristics of the power amplifier will be examined and how it relates to intermodulation distortions of different orders.

2.3.1 Power Amplifier Characteristic Properties

Power amplifiers (PA) could be categorized in terms of output power, bandwidth, gain, input and output voltage standing wave ratio (VSWR), power aided efficiency (PAE) inter-modulation distortion and ACPR [2.30]. These characteristics are highlighted below.

2.3.2 Output Power

Output power (P_{out}) is defined as the power delivered to the load and it depends on the input power. The 1dB compression point also must be considered when designing power amplifiers. Equation (2.1) gives the relationship between the output power and input power.

2.3.3 Power Gain

Power gain (G) is defined as the ratio of power delivered to the load (P_{out}) to the power supplied from the source or at the input (P_{in}) of the amplifier. Equation 2.1 gives the relation between P_{in} and P_{out}. The power gain determines what the amplifier will deliver at its output once a signal is incident at its input port.

$$G = P_{out}/P_{in} \tag{2.1}$$

2.3.4 Bandwidth

Bandwidth is simply described as the range of frequencies for which the power amplifier performs as expected to meet certain specifications. It is the range of frequencies at which the PA could operate properly. It is mostly symmetrical from its center frequency point (f_0). Figure 2-4 gives the bandwidth as the (f_2-f_1) MHz.

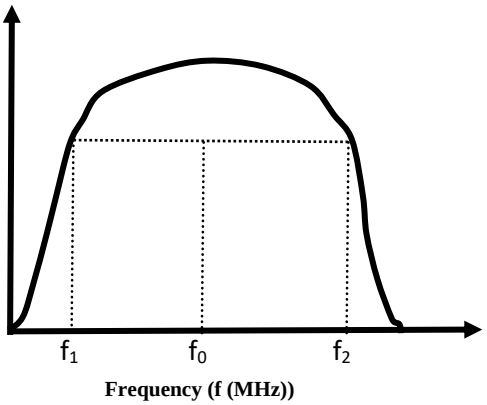

Figure 2-4: PA bandwidth.

2.3.5 VSWR (Voltage Standing Wave Ratio)

VSWR is a measure of the impedance matching of loads to the characteristic impedance of the transmission line. It is used to characterize amplifier's circuit match to source and load impedances respectively that is usually 50 Ω. It could be measured for both small and large-signal conditions. Power amplifier circuits are designed to deliver maximum power performance at the output and achieving good VSWR is not a necessity though this could also be achieved by using a balanced configuration or other good matching combining techniques [2.31].

2.3.6 Power Aided Efficiency (PAE)

PAs consume most of the direct current power in many handheld wireless devices and this makes the power efficiency of the amplifier very important in any design. A measure of the amplifier's efficiency is the ratio of RF output power to DC input power.

$$\eta = P_{out}/P_{DC} \tag{2.2}$$

Where η is the efficiency.

However, this definition does not account for the RF power delivered at the amplifier's input. This is because most power amplifiers have relatively low gains and hence, the efficiency defined in equation (2.2) tends to over-rate the actual efficiency. The power aided efficiency is a better measure for measuring efficiency. PAE includes the effect of input power and is defined as:

$$\eta_{PAE} = PAE = (P_{out} - P_{in})/P_{DC} = (1-1/G) \tag{2.3}$$

Where G is the amplifier's power gain.

Silicon transistor amplifiers in the 800-900 MHz band have been found to have power aided efficiencies on the order of about 80%, but that efficiency drops rapidly with increasing frequency. Hence, the use of GaAS (Gallium Arsenide) transistors which produce better efficiency at higher RF and microwave frequencies [2.31]. Power amplifiers prioritize efficiency over the gain and therefore designed to provide the best efficiency. High efficiency amplifier applications require single stage gain to be above 10 dB [2.30].

2.3.7 Intermodulation Distortion

Power amplifiers are generally utilised in the final stages of the wireless transmitters to increase the radiated power level prior to the antennas. The power amplifier should be able to deliver a microwave signal with sufficient power to present an easily detectable output at the receiver's end [2.31]. To get the maximum power efficiency from an amplifier, it should be operated close to saturation, but at that point, the amplifier is in non-linear mode. Therefore, when different signals with different carrier frequencies are passed through the power amplifier, because of the nonlinear mode, these signals will interact with each other causing inter-modulation products [2.30].

Two very important parameters that characterize inter-modulation distortion are the 1 dB compression point and the third-order intercept point.

2.3.7.1 P_1 dB (1 dB Compression Point)

The 1dB compression point also must be considered when designing power amplifiers. 1dB compression point is the output power at which the gain of the system's specified fundamental frequency has been reduce by 1 dB with respect to its small signal value. It indicates the power level that causes the gain to drop by 1 dB from its small signal value. Figure 2-5 shows the 1 dB compression point and how it relates to further increases in input power at the output.

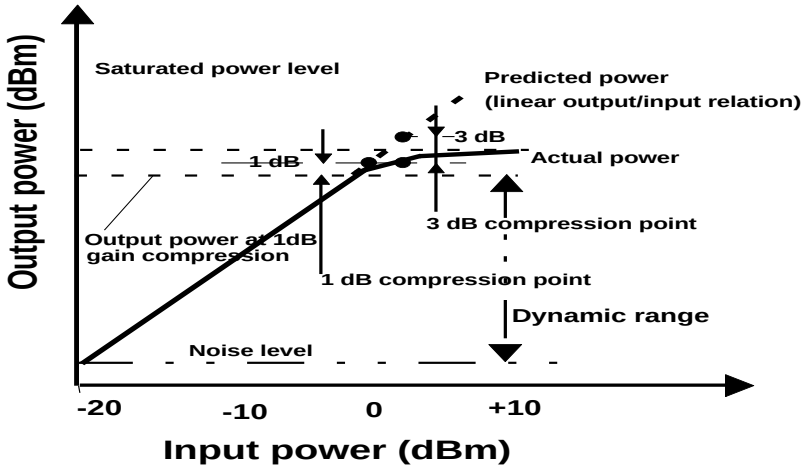

Figure 2-5: PA characteristics with 1 dB compression point.

2.3.7.2 Third-order Intercept Point

Third-Order Intercept Point (I) is the point at which the power in the third-order non-linear products and the linearly amplified signals meet. It corresponds to the input or output level at which the third order inter-modulation products exhibit the same output level as the fundamental tone when the amplifier is assumed to be linear [2.30]. Figure 2-6 shows the linear and non-linear range with the third-order intercept point.

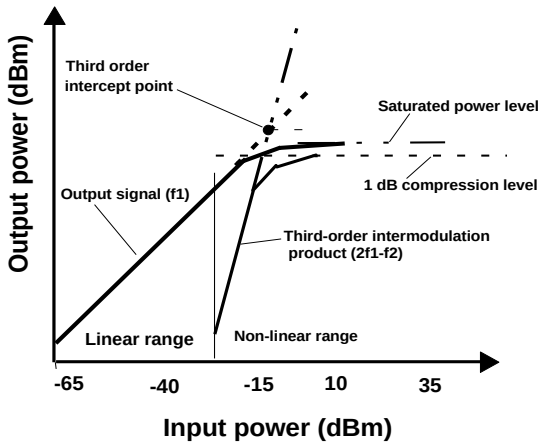

Figure 2-6: PA characteristics with third-order intercept point.

2.3.8 Adjacent Channel Power Ratio (ACPR)

The ACPR is the ratio of the total power of the adjacent channels due to intermodulation to the main or useful signal's power. It is used to evaluate the intermodulation distortion performance of power amplifiers for wireless communication systems. It is a measure of the spectral regrowth which appears in signal sidebands. It can be characterized with analog signals in terms of the 3rd and 5th order IM products for RF/microwave power amplifiers [2.31]. Figure 2-7 shows how ACPR between two signals could be compared for better linearity/spectral efficiency.

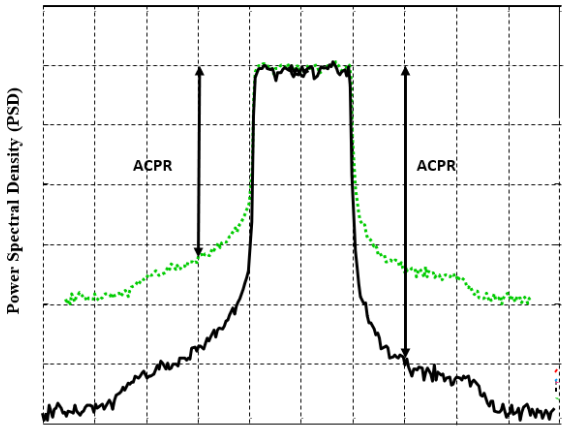

Figure 2-7: Improved adjacent channel power ratio.

2.4 Microstrip Technology

Size reduction and component miniaturizations of components have become vital when designing and developing low-cost passive and active circuits for modern day applications. Modern day technology prioritises compact techniques that will reduce the overall size of any circuit or integrated systems. Different methods such as the Lumped-element, high dielectric constant and monolithic integrated circuit-based technology have all been utilised over the years to achieve miniaturisation on a small scale. The microstrip technology is become ever significant in designing and fabricating devices to achieve a well reduced size, improve ease of fabrication and production and be cost effective [2.32]. In this section, the MIC technology is investigated and its transmission lines with focus on the microstrip lines are focused on for mobile wireless circuit designs. In this thesis, the microstrip technology would form the basis of RF circuits such as microstrip filters and couplers. The microstrip technology can be used with emerging printing technologies like 3D and inkjet printing to further meet modern day requirements for compactness and technological innovations.

2.4.1 MIC versus MMIC

The MIC (Microwave Integrated Circuit) technology is a common technology for circuit designs. It is divided into two main forms. The conventional MIC which is the HMIC (Hybrid Microwave Integrated Circuit) and MMIC (Monolithic Microwave Integrated Circuit). HMIC and MMIC are specified for high and low-power applications respectively. As far back as the 1980s, DARPA (Defence Advanced Research Projects Association) instigated the plan to develop solid-state microwave integrated circuits. These circuits were developed to replace tubes, cavities and discrete devices used in microwave radar and telecommunication systems. Initially this was only possible with HMIC but with advancement in semiconductor materials and related processes which aided the development and deployment of the MMIC technology which requires lower power than HMIC related applications. MIC also known as HMIC makes use of thick or thin films and substrate materials. An alumina substrate is mostly used as the substrate. This substrate is chosen to have low-loss in the microwave band, proper value of the dielectric constant, low in cost and an excellent resisting property against heat and chemicals [2.33].

MIC and MMIC at low frequencies uses components that have lumped inductors and capacitors in an order of magnitude that look smaller in size than the circuits using just distributed lines such as the coplanar waveguides or microstrip lines. At higher frequencies, such lumped elements have a lot of drawbacks that affect the efficiency of the circuit. At such RF and Microwave frequencies, lumped elements possess low Q and leads to higher loss and that makes the size advantage less pronounced as it is not just enough to produce a device with a smaller size but to also maintain good and acceptable efficiency for good performance.

MMIC components are very small, cost effective, offer less weight, and attractive for mass production which makes MMIC a very attractive technology fir the design of components and devices for future use. MMIC's normally use microstrip, inductors and MIM (metal-insulator-metal) capacitors for the matching networks at input and output. The distinctive feature of the MMIC technology is that all active, passive circuit devices and interconnections are deposited

together and patterned on the surface of the semi-insulating substrate. This is an integrated circuit whereby all active and passive elements are deposited on a single chip [2.34]. Main advantages of MMIC include reduced size, better cost, broadband performance, less weight and added simplification.

The fabrication process for HMIC technology, its fabrication method is achieved using 2 different ways. In the first process, the distributed circuit elements are fabricated on the substrate using a single-level metallization technique while other discrete circuit elements such as inductors, capacitors, resistors and distributed circuit elements get wire-bonded to the substrate. A printed circuit board is used for the single metallization process. The second process is called the miniature hybrid MIC. Components such as inductors, capacitors, resistors and distributed circuit elements are realized by depositing their metal patterns on the substrate. All devices are deposited apart from only solid-state devices such as chips which are directly linked to the substrate. The matching networks and passive circuits are realized by using printed metallization and discrete passive components. This helps achieve reduction in overall size and hence it is smaller than other traditional technologies [2.34].

2.4.2 MIC Transmission Lines

Lumped elements including capacitors and inductors could be used at low frequencies (Low RF and below) to design circuits and a wire could also be used to connect electronic components as well. However, at high frequencies (RF, Microwave and mm-wave), special transmission lines are used to connect the microwave circuit and its elements together as the wire is no longer sufficient. This is due to the observation that the wire/connector becomes very lossy and hampers performance and results [2.3**3**]. Such transmission lines include rectangular waveguide, strip line, coaxial line, coplanar waveguide (CPW) and microstrip line.

2.4.2.1 Microstrip Lines

Electromagnetic waves and other forms of power and energy can use transmission lines as the medium of propagation. Transmission lines are popular in many applications as they propagate electromagnetic waves with minimal interference and signal loss compared to other means of wave propagation. The microstrip line is the most commonly used transmission line for the microwave integrated circuit (MIC) technology due to its unique characteristics which will be summarized in this section. The microstrip line has been adopted for use for the design of the notch filter and other components as it is proven to achieve relatively compact size and is less costly. The microstrip line also integrates with active devices easily, compatible with monolithic circuits and aids mass reproduction. Other transmission lines such as strip line and fin line have been used as well but for designs such as filters for RF/Microwave applications. The microstrip line has been more prominent due to its attractive merits explained above.

Figure 2-8 shows the cross-section of the microstrip line. The microstrip structure is in such a way that the dielectric substrate is located between the metallic conductor and the ground plane as shown in Figure 2-8. The height and dielectric constant of the dielectric substrate is denoted by h and ε_r respectively.

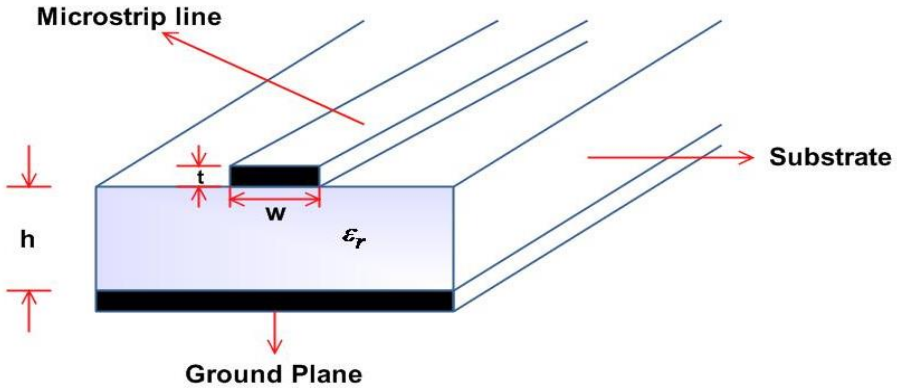

Figure 2-8: Cross section of microstrip transmission line.

The metallic conductor for the microstrip line is very thin with thickness (t) and width (W). The microstrip structure also puts into the consideration the amount of air located in the layer of the structure therefore the properties of air used are very important in any design. Because two dielectric mediums are present for the structure, the EM field is not homogeneous. The electric field (EF) remains concentrated within the substrates medium whilst the magnetic field (MF) extends into air's dielectric medium as well. This inhomogeneous characteristic of the electromagnetic filed in the microstrip line allows for the quasi-TEM (Transverse Electric and Magnetic) assumption for empirical solutions rather than a pure TEM [2.35]. Figure 2-9 gives a better view on how the dielectric mediums extend into each other which affects the overall electromagnetic property of the structure.

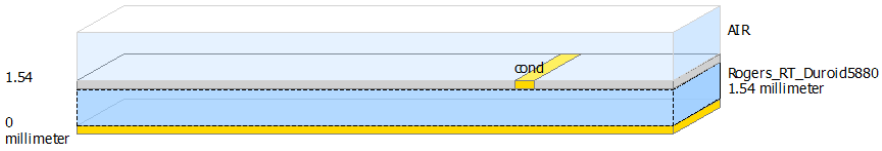

Figure 2-9: 3D Substrate view showing 2 dielectric mediums.

This open microstrip line structure also has its own drawbacks. It could be very lossy as well. The microstrip line could be affected by loss from different mediums such as the conductor loss, radiation loss, dielectric loss and surface wave propagation.

When designing components such as filters using microstrip technology, the discontinuities in the microstrip line is a vital property that is investigated to give the desired results. Discontinuities could be gaps, junctions, bends or sudden change in the regular pattern of the structure. An example is the discontinuity that formed the basis of the defected microstrip structure (DMS). When the discontinuity is produced on the transmission line, some properties of the line is altered, and this property has been used to offer compact size designs of microstrip filters [2.35].

This thesis would involve using the microstrip technology to design and fabricate novel structures like the band-stop filters and microstrip branch line couplers which will be used to improve the performance of the mobile wireless transmitters for next generation networks such as 4G and 5G. This thesis would consider a host of ways to use the unique properties of the

microstrip designs in these advanced mobile communication systems to achieve a highly efficient and linear output power spectra density whilst trying to produce higher data rates. For example, the filter proposed would be designed using microstrip technology with the aim to achieve the best possible size reduction, be environmental-friendly whilst suppressing interference and being integrated with different applications to improve linearity performance.

2.5 References

[2.1] T. Halonen, J. Romero and J. Melero, “GSM, GPRS and EDGE Performance”, *2nd Edition, John Wiley and Sons*, 2003.

[2.2] B. Gudmundson, “UMTS/IMT2000 Based on WideBand CDMA”, *Proc. Intl Conf. on Communication Tech. (Icct)*, 1998, Beijing, China, vol. 1, pp. 490-494, 22 Oct.1998.

[2.3] A. Rusan and R. Vasiu, “Assessment of packet latency on the 4G LTE S1-U interface: Impact on end-user throughput", *Proc. Intl. Conf. on Software, Telecommunications and Computer Networks*, pp. 305-309, 16-18 Sept. 2015.

[2.4] S.Z. Asif, “Next Generation Mobile Communications Ecosystem: Technology Management for Mobile”, *1st edition, John Wiley and Sons*, 2011, pp. 23.

[2.5] A.-C. Pang, Y.-B. Lin, H.-M. Tsai and P. Agrawal, “Serving Radio Network Controller Relocation for UMTS All-IP Network”, *IEEE Journal. Selected Areas in Comm.*, vol. 22, no. 4, pp. 617-629, May 2004.

[2.6] J. Brown and J. Khan, "Performance Comparison of LTE FDD and TDD Based Smart Grid Communications Networks for Uplink Biased Traffic", *IEEE 3rd International Conference on Smart Grid Communications*, Tainan, 2012, pp. 276-281, 5-8 Nov. 2012.

[2.7] M. Sawahashi, Y. Kishiyama, H. Taoka, M. Tanno, and T. Nakamura, “Broadband radio access: LTE and LTE-advanced,” *in Intelligent Signal Processing and Communication Systems, 2009. ISPACS 2009. International Symposium on*, pp. 224 –227, Jan. 2009.

[2.8] G. Carullo, M. Tambasco, M. Mauro and M. Longo, “A performance evaluation of WebRTC over LTE”, *IEEE 12th Annual Conf. on Wireless On-demand Network Systems and Services (WONS)*, 2016, pp. 1-6, 20-22 Jan. 2016.

[2.9] Y.-S. Cheng and C.-H. Chen, “A novel 3D beamforming scheme for LTE-Advanced system,” *in Proc. 16th Asia-Pacific Network Operations and Management Symp. (APNOMS)*, pp. 1–6, Sep. 2014.

[2.10] R. Ratasuk, D. Tolli, and A. Ghosh, “Carrier aggregation in lte-advanced,” *in 2010 IEEE 71st Vehicular Technology Conf. (VTC 2010- Spring)*, pp. 1 –5, May 2010.

[2.11] Z. Shen, A. Papasakellariou, J. Montojo, D. Gerstenberger, and F. Xu, “Overview of 3gpp lte-advanced carrier aggregation for 4g wireless communications,” *IEEE Commun. Mag.*, vol. 50, pp. 122 –130, February 2012.

[2.12] H. Wang, C. Rosa, and K. I. Pedersen, “Performance analysis of downlink inter-band carrier aggregation in lte-advanced,” *in VTC Fall*, pp. 1–5, IEEE, 2011.

[2.13] Y. Peng, W. Yang, Y. Zhu, and X. Chen, “Transmission scheme for 2D antenna array MIMO systems with limited feedback,” *Wireless Pers. Commun.*, vol. 75, no. 1, pp. 759–774, 2014.

[2.14] K. Werner, H. Asplund, B. Halvarsson, A. Kathrein, N. Jalden, and D. Figueiredo, “LTE-A field measurements: 8x8 MIMO and carrier aggregation,” *in Proc. IEEE Veh. Technol. Conf. (VTC Spring)*, pp. 1–5, 2013.

[2.15] E. Dahlman, S. Parkvall, J. Sköld, “4G LTE/LTE-Advanced for Mobile Broadband”, *Elsevier Ltd*., 2011.

[2.16] R. Prassad, “OFDM for Wireless Communication Systems”, *2nd Edition, Artech House Inc.*, Boston-London, 2004.

[2.17] G. C. Porter, “Error Distribution and Diversity Performance of a Frequency Differential PSK HF Modem”, *IEEE Trans. Communications*, Vol. COM-19, pp. 628-634, October 1971.

[2.18] M.S. Zimmerman, and A.L. Kirsch, “The AN/GSC-10 (KATHRYN) Variable Rate Data Modem for HF Radio”, *IEEE Trans. Communications*, Vol. COM-15, pp.567-575, April 1967.

[2.19] R.R. Mosier, and R. G. Clabaugh, “Kineplex, a Bandwidth Efficient Binary Transmission System,” *AIEE Trans.*, Vol. 76, pp. 723-728, January 1958.

[2.20] R. Ford, M. Zhang, M. Mezzavilla, S. Dutta, S. Rangan and M. Zorzi, "Achieving Ultra-Low Latency in 5G Millimeter Wave Cellular Networks," *in IEEE Communications Magazine*, vol. 55, no. 3, pp. 196-203, March 2017.

[2.21] P. Guan, D. Wu, T. Tian, J. Zhou, X. Zhang, L. Gu, A. Benjebbour, M. Iwabuchi, and Y. Kishiyama, “5G Field Trials - OFDM-based Waveforms and Mixed Numerologies,” *IEEE Journal on Selected Areas in Communications*, vol. PP, no. 99, pp. 1–4, 2017.

[2.22] C. T. Neil, M. Shafi, P. J. Smith, P. A. Dmochowski and J. Zhang, "An Evaluation of Channel Models, Frequency Bands and Antenna Topologies for 5G," 2017 *IEEE 85th Vehicular Technology Conference (VTC Spring)*, Sydney, NSW, 2017, pp. 1-7.

[2.23] C. Sexton, Q. Bodinier, A. Farhang, N. Marchetti, F. Bader and L. A. Da Silva, "Enabling Asynchronous Machine-Type D2D Communication Using Multiple Waveforms in 5G," *in IEEE Internet of Things Journal*, vol. PP, no. 99, pp. 1-1, 2018.

[2.24] F.-L. Luo and C. Zhang, “From OFDM to FBMC: Principles and Comparisons,” Signal Processing for 5G: Algorithms and Implementations, *Wiley-IEEE Press*, 2016.

[2.25] D. Na and K. Choi, "Low PAPR FBMC," *in IEEE Transactions on Wireless Communications*, vol. 17, no. 1, pp. 182-193, Jan. 2018.

[2.26] Ç. Göken and O. Dizdar, "Performance of edge windowing for OFDM under non-linear power amplifier effects," *MILCOM 2017 - 2017 IEEE Military Communications Conference (MILCOM)*, Baltimore, MD, 2017, pp. 219-224.

[2.27] A. Saljoghei, F. A. Gutiérrez, P. Perry, D. Venkitesh, R. D. Koipillai and L. P. Barry, "Experimental Comparison of FBMC and OFDM for Multiple Access Uplink PON," *in Journal of Lightwave Technology*, vol. 35, no. 9, pp. 1595-1604, May1, 1 2017.

[2.28] Hyunsoo Kim, Jonghyun Bang, Sooyong Choi and D. Hong, "Resource block management for uplink UFMC systems," 2016 *IEEE Wireless Communications and Networking Conference Workshops (WCNCW)*, Doha, 2016, pp. 477-480.

[2.29] Vakilian, V.; Wild, T.; Schaich, F.; ten Brink, S.; Frigon, J.-F., “Universal-filtered multi-carrier technique for wireless systems beyond LTE,” 2013 *IEEE Globecom Workshops (GC Wkshps)*, pp.223-228, 9-13 Dec. 2013.

[2.30] Chang, K and Bahl, I., "RF and Microwave Circuit and Component Design for Wireless Systems", *USA, John Wiley and Sons, Inc.*, pp. 406-425, 2002.

[2.31] Olukoya, O.S., Msc. final year project, "Design of Power Amplifiers for LTE-Advanced Applications", *Msc Mobile, Wireless and Broadband Communications, University of Westminster*, pp. 10-22, July 2013.

[2.32] K. Chang, and I. Bahl, "RF and Microwave Circuit and Component Design for Wireless Systems", *USA, John Wiley and Sons, Inc.*, pp. 42-43, 2002.

[2.33] Pozar, D.M., "Microwave and RF Design of Wireless Systems", *New York, John Wiley and Sons*, pp. 189-221, 1998.

[2.34] E. Niehenke, I. Bahl, N. Consulting and M. Baltimore, "Microwave and millimeter-wave integrated circuits", *IEEE Trans. Microwave Theory Tech.* 50(3), pp. 846-857, March 2002.

[2.35] J-S. Hong, "Microstrip Filters for RF/Microwave Applications", *NewYork, John Wiley and Sons, Inc.*, pp. 77 – 190, 2001.

Chapter 3 Compact Microstrip Band-stop Filter Design

The ever pressing need to suppress interference makes band-stop filters (BSF) very important in RF/Microwave systems. In applications such as the case whereby some certain frequency bands need to be suppressed, band-stop filters are essential. Wireless systems are always very susceptible to interference as a strong interfering signal could adversely affect the fundamental signal and cause serious perturbations on the spectrum of the signal. Band-stop filters have become a vital component of noise reduction devices that are embedded in mobile phones, satellite systems, local oscillators and other wireless communication system applications. Band-stop filters have been preferred to bandpass filters for cases whereby the interfering signals lie in the passband or even very close to the pass band. With the aid of a highly narrowband band-stop or notch filter, even interfering signals very close to the passband could be effectively suppressed.

Because of these unwanted signals, nonlinear distortions become more pronounced in the system. For unwanted signals very close to the main band, bandpass filters cannot suppress those signals effectively. However, band-stop filter can attenuate such signals, but narrowband band-stop filters or notch will be more effective in dealing with such nonlinear distortions due to those interfering signals. The increase in nonlinear distortions could degrade and adversely affect system performance and as such by using a band-stop filter to reject such interfering signal, nonlinear distortions could be suppressed thereby making the system more linear and more efficient. The advantage of using the band-stop filter is that it is simple and straight forward to use which is better than having to use algorithms and methods that are very complex and expensive.

There are some major things to consider when designing such filter. Apart from its simplicity and cost advantage, size is a critical factor. When designing such a filter, the size must not be too big so as not to complicate the system but help to reduce network complexity and achieve compactness. This is basically due to a known fact that in the world today, there is a massive public demand on size reduction for mobile and wireless devices such as mobile phones and tablet computers.

Also, due to the unwanted signals interfering very close to the main signal, the specification for the band-stop filters requires stringent requirements. The main use of a band-stop filter is to reject unwanted signal and the filter design would require the filter to show a relatively narrowband band-stop response with high attenuation capability to successfully reject the interfering signal.

This chapter presents a novel design of microstrip band-stop filters and embraces new technologies such as inkjet printing. In the next section, the history and evolution of microstrip band-stop filters that have been developed up until recent times is explained leading up to the rationale behind choosing this design.

3.1 Microstrip Band-stop Filter Design

The advent of Microstrip stems as far back as 1952 when strip-lines were first published by Grieg and Engelmann in the IRE proceedings. Microstrip was then designed as a new transmission technique to compete with the strip-lines for the kilomegacycle range. Microstrip lines were designed to compensate for disadvantages such as large size, bulkiness, difficulty and cost of manufacturing of waveguide and coaxial component structures [3.1].

Initial design of microstrip band-stop filters have included the use of different kind of stubs such as open circuit stubs [3.2] - [3.3].The Fold-line configuration was one of the first types of microstrip band-stop filters designed which was able to achieve a reduction in size by utilizing the substrate surface area more efficiently and also allowing for flexibility by using its hybrid geometry [3.4]. Another compact filter was designed to subdue the surface wave radiation problem in in open stubs [3.5]. This filter designed was also compact and radiates far less power than open stub filters. A related compact filter to [3.3] was later designed to further reduce radiation effects observed with conventional shunt stub and coupled-line filters [3.5] and has been used in other applications such as antenna designs that put stringent conditions on its radiation patterns [3.6]. In the early 1980's, a new approach was used to accurately predict and evaluate the parameters such as the external quality factor that characterise the coupling between a microstrip line and a dielectric resonator. These results aided in the design and fabrication of a band-stop filter based on microstrip technology and a dielectric resonator [3.7]. From then, the resonators became popular and were used in various configurations to achieve good band-stop response [3.8] - [3.9].

Direct coupled realisations for microwave band-stop filters came about in 2004 [3.10]. One of such filters uses a zig-zag resonator to reduce the effect of direct resonator to resonator coupling [3.11] and the use of a quarter-wavelength open stub resonator with strong direct coupling between the resonator and the microstrip line which further helps to reduce radiation loss [3.12]. Other microstrip filters designed over the past decade include [3.13] - [3.16].

In recent years, there have been a lot of developments and improvements in the theory of original and new microstrip BSF and this has been combined with the photonic band gap (PGB) theory to design a new phase of microstrip band-stop filters. There has been a shift from old technologies towards planar microstrip band-stop filters. A band-stop filter of such could comprise of ninety degrees (90^0) short circuited stub coupled through a capacitive gap and linked to the fundamental transmission line. In trying to retrieve the lumped element equivalent of the band-stop filter design, these stubs behave as inductors and the capacitance is calculated through the gap. The enthusiasm to realize a compact filter has been there for many years and a lot of microstrip BSF has been designed over the years with their respective advantages.

A design of one of such conventional microstrip band-stop filter using the Agilent Advanced Design System (ADS) is shown in the Figure below. As seen in Figure 3-1, the designs consist of open circuit stubs which are linked to the microstrip line.

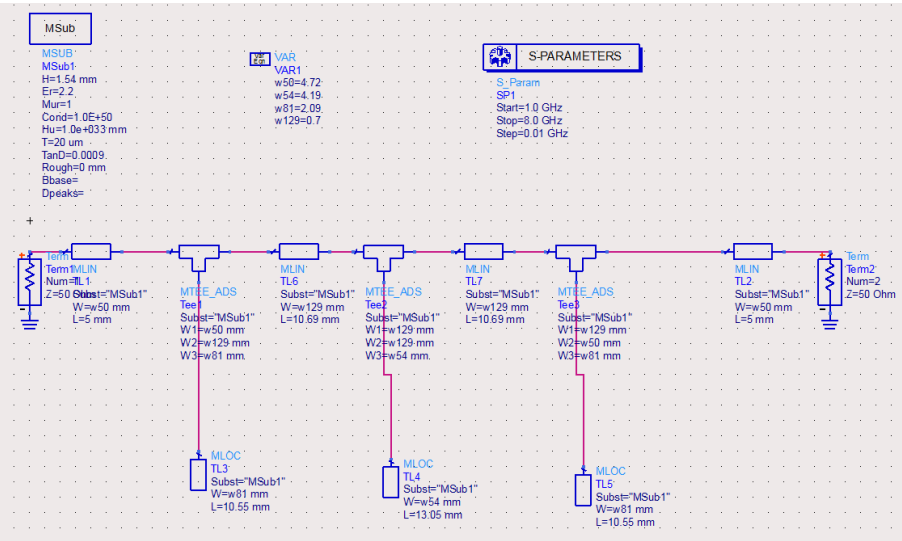

Figure 3-1: ADS stub filter design.

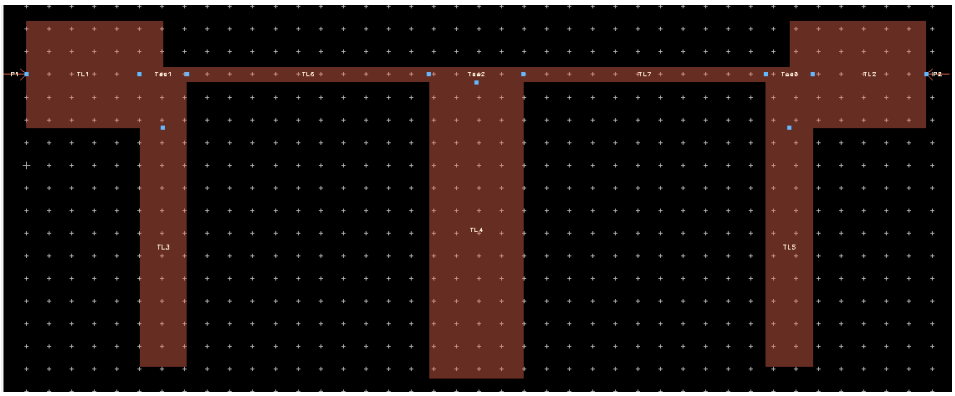

Figure 3-2: Stub filter layout.

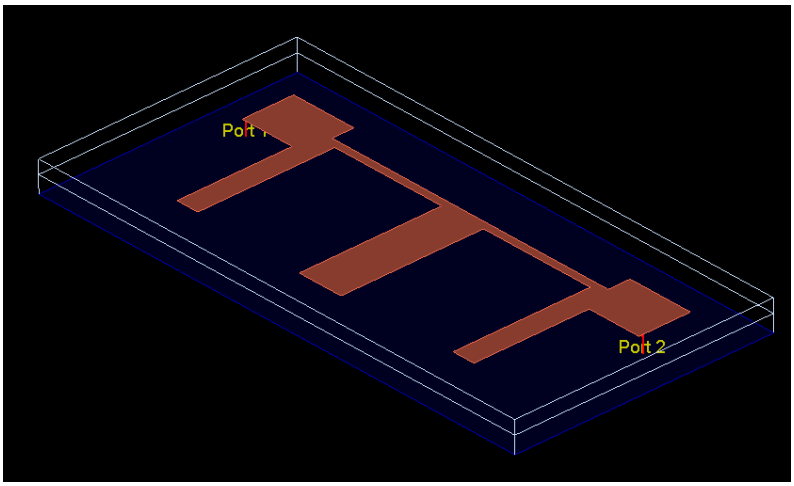

Figure 3-3: 3D view of designed filter.

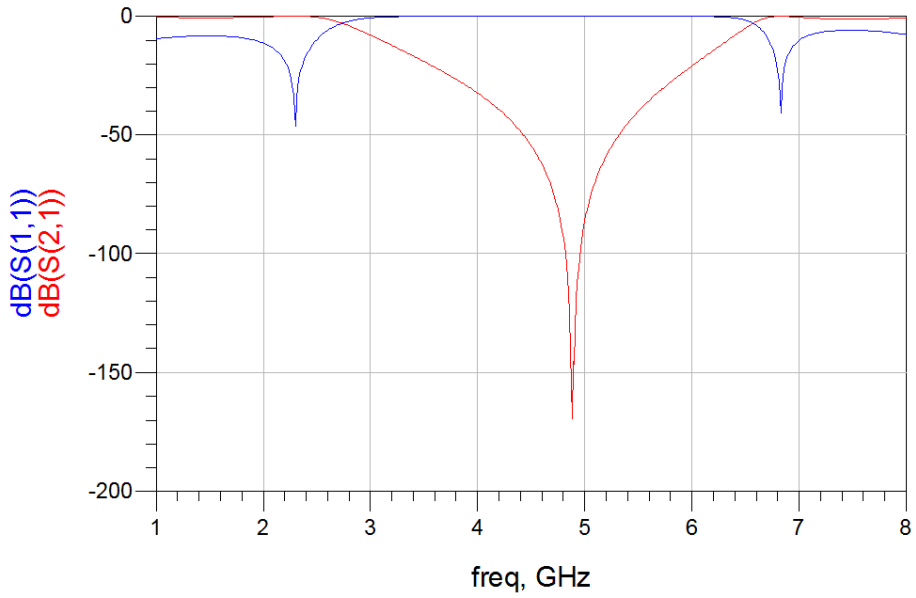

Figure 3-4: Simulated s-parameter response of stub filter.

Figure 3-1 shows the design of the filter using microstrip lines and technology. By using Quasi TEM assumptions, the parameters have been calculated and designed. The layout of the filter and its 3D equivalent are visible in Figure 3-2 and Figure 3-3. The simulated response of the band-stop filter designed in Figure 3-1 is seen in Figure 3-4. The filter does not give a narrowband but has good rejection over 160 dB at its center frequency of 4.9 GHz. Apart from its excellent stopband attenuation at its resonant frequency, it has many draw backs such as its return loss performance outside the stop band as shown in Figure 3-4 above. The designed filter is also very large in size which is also a very big disadvantage as compactness should be achieved in any design.

Another of such filter is a double bended stub filter as presented in Figure 3-5. This design helps to achieve a reduced size as compared to the above design by bending the stub. This design produces a dual band microstrip filter with narrower bandwidth and a compact size but lesser attenuation. The structure was developed and simulated using EM sonnet. The simulated response is shown in Figure 3-7. The fact that the design gives a dual band response shows that it could be used to reject interfering signals at some other frequencies as well and not only the stopband of the filter. Hence it is not limited to just one band.

The two distinct bands of the filter at different frequencies has its applications in systems that would need to deal with interference at either side of the main passband. A better and cost-effective way would be to design a tuneable filter that could be tuned to any kind of frequency needed. With defected microstrip structure design as well, any filter could be designed at any frequency by just modifying dimensions.

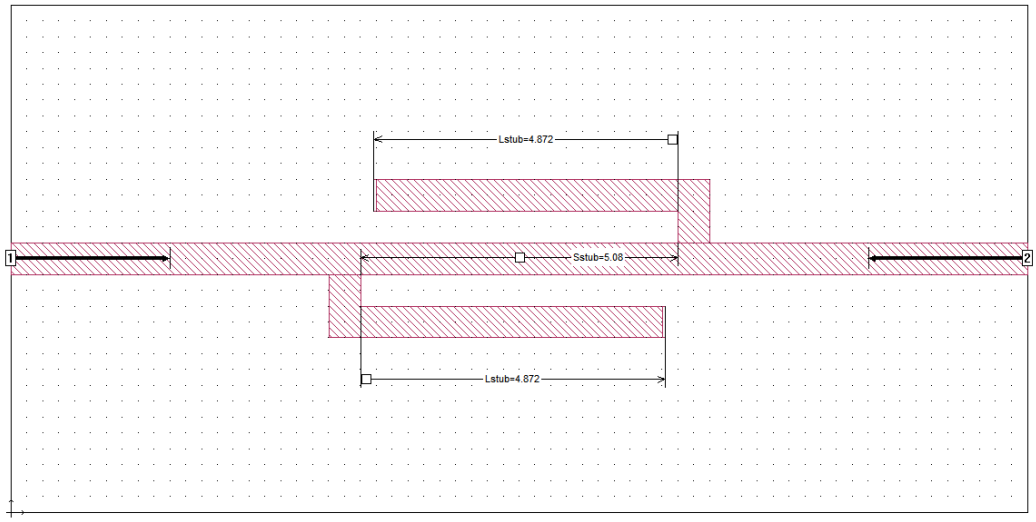

Figure 3-5: Compact double-bended stub filter.

The Figure above is a compact dual-band microstrip filter with the stubs being bent on either side of the main transmission line. The filter is designed and simulated using Keysight/Agilent ADS software on alumina substrate with dielectric constant of 9.8 and thickness (h) of 0.508 mm. It is a compact filter with its overall dimension size being 16.26 mm by 2.54 mm. Figure 3-6 is the 3D view of the filter design showing its substrate architecture with the alumina substrate below and air above.

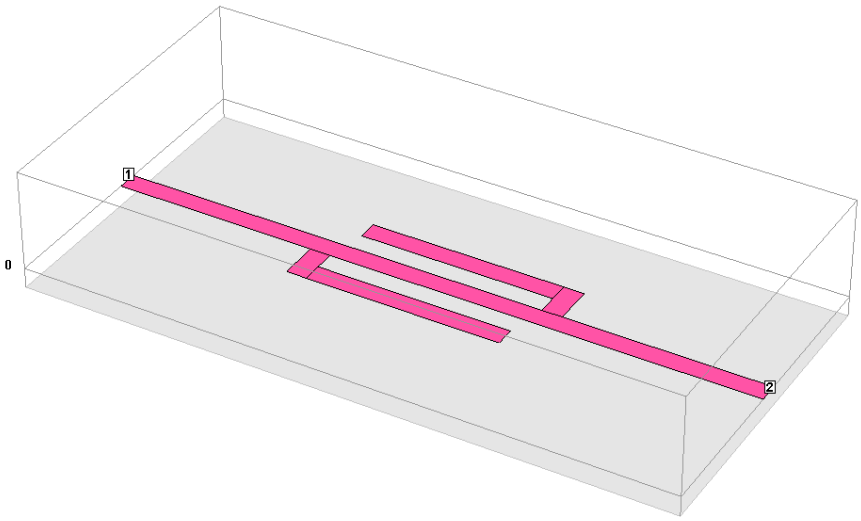

Figure 3-6: Double-bended stub filter layout

Figure 3-7 shows the simulated S-parameter response of the wideband band-stop filter. The filter response shows that it is dual-band with transmission zeroes at 5.2 dB and 5.9 dB with attenuation of about 70 dB and 57 dB respectively. This filer has a good potential to be used in rejecting two interfering signals effectively at 5.2 GHz and 5.9 GHz but the fact that the stopband range is very wide from about 3.5 GHz to 7 GHz means that it could not be effectively used when the unwanted signal is very close to the main band.

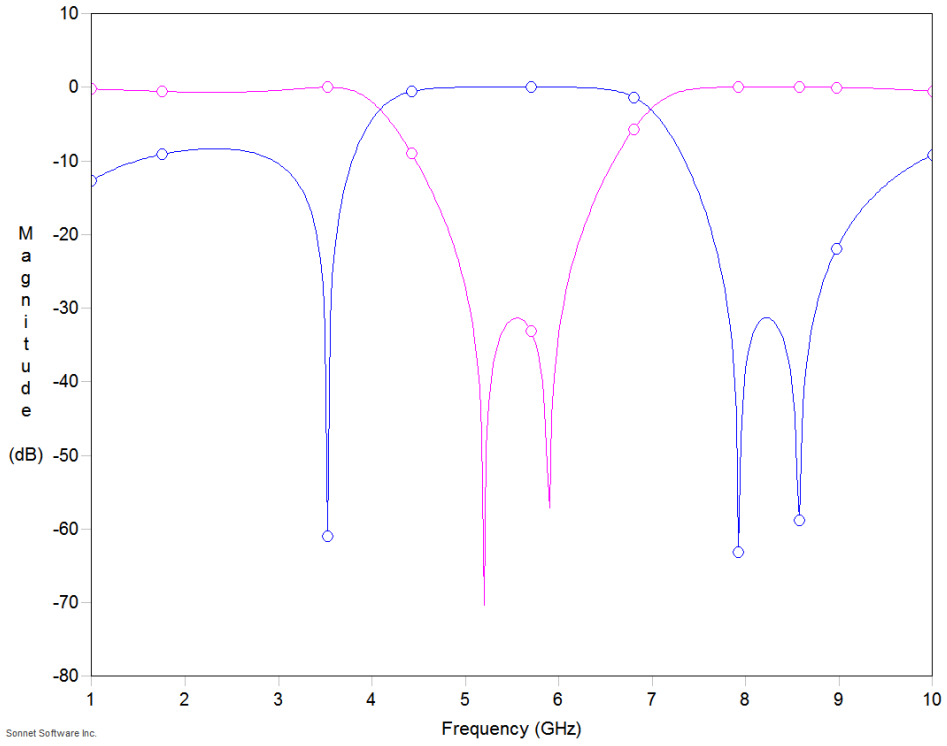

Figure 3-7: Simulated s-parameter results for double-bended stub filter

The filter design in Figure 3-5, has a lot of challenges with size when trying to design at frequencies below 4 GHz. The size keeps on increasing at such lower frequencies. Also, there is space for a lot of improvement for the return loss performance of the filter which is below 10 dB.

Majority of the conventional RLC (Resistor, inductor, capacitor) band-stop filters incorporates diverse kinds of open-circuit shunt stubs or even use open circuit stubs of a quarter wave length ($l = \lambda_g /4$). These filters have been relatively easy to design and implement. Even though such RLC filters have been used successfully in band-stop filter design, it is however affected by some technical constraints. Some of such limitations are based on its large size which is a main disadvantage, larger power consumption, its high susceptibility to parasitic effects which is very much pronounced in the gigahertz bands. A major disadvantage of these kinds of filters is that it is very difficult to integrate them with other planar structures and modern communication systems as such. Hence, the need to focus more on microwave planar structures for modern communication systems.

3.2 Defected Microstrip Structure

In recent years, Band-stop filters (BSF) have become very important components in RF, Microwave and mm-wave communication systems to reject spurious responses, discard higher harmonics and reduce nonlinear distortions. Various BSF have been designed but due to technical limitations such as large size, larger power consumption and its performance in the Gigahertz frequency range, there has been a shift from the conventional RLC band-stop filters to microstrip filter planar structures. Future and evolving wireless communication systems and applications have placed paramount importance on compact size and cost effectiveness. These

stringent requirements led researchers to explore techniques that could reduce the size of the BSF and perform better in higher frequency bands such as the Photonic Band Gap (PBG) structure and the Detected Ground Structure (DGS) [3.17].

Due to the size constraint problem with conventional band-stop filters, there has been a lot of research into the issue of size reduction in the realization of band-stop filters of different kinds and at different frequency bands (lower or higher). With the rapid evolvement of modern wireless communication systems, microstrip planar structures such as the electronic band gap structure (EBG), the defected ground structure (DGS) and the defected microstrip structure have all been explored and has continued to attract the attention of researchers and developers as they aim to achieve better and more compact size. These structures are based on several kinds of discontinuities that affect the microstrip lines.

The electronic band gap (EBG) structure uses the principle of forbidding the propagation of electromagnetic (EM) waves within a band (Band gap) whilst permitting the propagation in other bands known as the energy bands. These periodic structures then interact with EM waves to form stop bands. The periodic structure of the EBG enables it to produce band-stop characteristics based on the band gap effect. EBG has some concerns and draw backs. Size and compactness were a major challenge with EBG as it occupies a large overall size. Other limitations include wide bandwidth, low attenuation level and tunability.

On the other hand, the defected ground structure (DGS) initially proposed by park [3.20], emerged from the EBG principle. By creating a defect on the ground plane, the effective inductance and capacitance are altered and provides band rejection from the resonance character of the structure transmission. The DGS uses the slow-wave effect to achieve size reduction. The slow wave factor is the relationship between the wave number in free space and the propagation constant of the transmission line. The slow wave factor for the defected structure is increased as discontinuities are introduced in the electromagnetic wave path. As the slow wave factor is increased due to the discontinuities, the impedance of the line also increases. This is a very important phenomenon used for planar structures as it could be used to achieve an overall size reduction for planar circuits like coupling lines, microstrip antennas and microstrip line lengths. However, DGS has disadvantages such as back radiation and ground plane leakage or crosstalk.

In the past decade, DGS has attracted a lot of interests due to slow wave effects, size reduction and high selectivity with narrow stopband but draw backs such as ground plane leakage, back radiation which could considerably affect performance and measurements led to the exploration of the Defected Microstrip Structure (DMS) [3.18].

The Defected DMS on the other hand has similar characteristics with DGS without the draw backs earlier associated with DGS. The defected microstrip structure (DMS) was developed based on DGS but mainly to avoid the drawbacks that affected DGS. The structure configuration of DMS is very similar to DGS and they could be integrated together [3.19]. Both methods can produce a very narrowband stopband response. DMS is easy to design with a very simple configuration; it could achieve very good notch response with a very low loss [3.17]. The main difference between DGS and DMS is that DMS involves etching different patterns on the transmission line or signal plane itself rather than on the ground plane which was the

case for DGS which eliminates the ground plane leakage problem and also radiation through the slotted patterns. DMS advantages include high attenuation level, ability to achieve narrower bandwidth, compact size, simplicity in design and implementation and tunability.

In recent years, many of such defected microstrip structures (DMS) designed as band-stop filters [3.17] - [3.21] have had applications in various applications. Thus, this notch filter design mainly focuses on using DMS for simplicity, low loss and compactness.

3.3 Inkjet-printed Band-stop Filters

With the rapid emergence of printed electronics, Inkjet printing technology is becoming more prominent since it aids mass production and the technique used helps to reduce manufacturing costs, shorten fabrication time and boost production flexibility [3.22]. Inkjet printing makes use of nanoparticle inks rather than the conventional copper and it permits the use of flexible substrates. Rather than etching, inkjet printing utilizes low cost processes such as the additive measures. Inkjet printing is being utilized more often than conventional etching techniques owing to its direct-write method without masks which reduces material utilisation and waste produced from wet processes in different design patterns. The actual droplet is placed only where it is needed and that's why it can reduce waste which makes it energy conservative and environmentally friendly.

With the advancement of flexible electronics, and the push for low cost and efficiency, the flexible materials used for applications with ever keen interest such as wireless, cognitive radio and other high frequency applications are been critically investigated [3.23]. One of such materials is kapton polyimide. The flexible kapton polyimide substrate is durable and maintains its electrical and physical properties over a wide temperature range withstanding high temperature levels [3.24].

A lot of Microwave and mm-wave components and systems attributed to inkjet printing and different specific substrates have been published, for instance the design of RFID antenna on paper substrate. Paper is an acceptable substrate though due to its low cost, rapid and straight forward inject printing but it still has drawbacks in terms of its high frequency absorption abilities and a range of humidity issues such as moisture absorption. Due to this, other substrates have been used for inkjet printing such as Injected Printed Humidity Sensor on kapton Substrate [3.24], Hairpin Bandpass filter [3.25] and Flexible Microwave filter on Liquid Crystal Polymer (LCP) Substrate [3.23], Coplanar waveguide (CPW) bandpass filter on plastic substrate [3.26].

Recently, inkjet-printed filtenna using kapton substrate has been investigated [3.27], however to the extent of the author's knowledge on literature, no band-stop filter (BSF) using kapton substrate and its flexible polyimide film have been worked on or published. In this thesis, the design of inkjet-printed BSF based on using DMS technology on flexible kapton substrate is investigated.

The Defected Microstrip Structure (DMS) is structured to create band-stop response at arbitrary frequency. The principle behind the design of this DMS structure is to create a defect on the microstrip structure. This defect provided by the slot line modifies the current distribution flow

across the transmission line obtaining a stopband response. The aim of this study is to design a narrow band filter with compact size, good selectivity and band-stop response at cut-off frequency that could help reject unwanted signals and with improved return loss performance.

The configuration of the proposed microstrip BSF using DMS is shown in Figure 3-8. On the microstrip line, an inverted T-shaped DMS pattern is etched on the U-shaped slot thereby changing the current distribution and altering the effective capacitance and inductance. This defect leads to a reduction in the occupied circuit area and hence overall size of the filter. Modifying dimensions within the circuit area allows the structure to be designed at different frequencies. This structure in Figure 3-8 was chosen because the line labelled X and the T-shaped slots (with dimensions Y and Z) were observed to improve the stopband attenuation and return loss performance for almost half the circuit area of the conventional structure represented by Length(L) * Width (W).

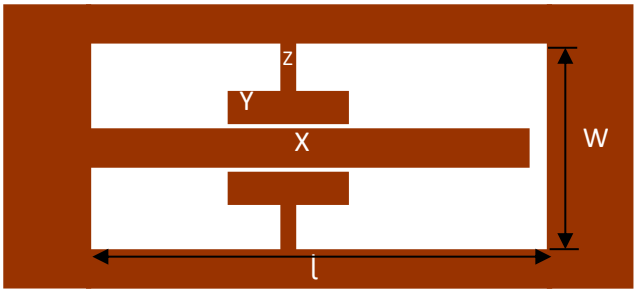

Figure 3-8: Structure of the proposed U-shaped notch filter.

Using Quasi-TEM approximation equations, the width (W) of the microstrip line, effective dielectric constant (ε_{eff}) and guided wavelength (λ_g) can be obtained using empirical expressions as shown in equations (3.1) – (3.3). To calculate the effective dielectric constant (εeff), still considering the quasi-tem approximation and a homogeneous dielectric material with an effective dielectric permittivity, the ε_{eff} is obtained using quasi-static analysis whereby the fundamental wave propagation mode is completely TEM for the microstrip. It is mainly obtained from equation (3.1).

$$\varepsilon_{eff} = C_d / C_a \tag{3.1}$$

Where C_d and C_a are the capacitance of the transmission line per unit length with dielectric substrate and air respectively. For this kind of filter design to achieve compactness, very thin conductors are used. For tiny conductor cases of thickness tending towards zero (such as t = 1 μm in this case), the expression for the effective dielectric constant is calculated in terms of the width W of the conducting strip of the microstrip line and the thickness (h) of the dielectric substrate. For such inkjet-printed DMS design that requires ultra-thin substrate thickness, the ratio of width to thickness is greater than one (1) and such the relative expression for ε_{eff} is given in equation (3.2) below:

$$\varepsilon_{eff} = \frac{\varepsilon_r + 1}{2} + \frac{\varepsilon_r - 1}{2}\left[1 + \frac{12h}{W}\right]^{-1/2} \tag{3.2}$$

Where h is the thickness of the substrate and ε_r is the dielectric constant.

When trying to design a filter using microstrip technology, you could know the height and dielectric constant of the substrate. To calculate the width of the microstrip line to be used in simulations, the next two equations in (3.3) and (3.4) could be used for W/h >2 [3.28].

$$\frac{W}{h} = \frac{2}{\pi}\left[A - 1 - \ln(2A - 1) + \frac{\varepsilon_r - 1}{2\varepsilon_r}\left\{\ln(A - 1) + 0.39 - \frac{0.61}{\varepsilon_r}\right\}\right] \quad (3.3)$$

$$A = \frac{377\pi}{2Z_O\sqrt{\varepsilon_r}} \quad (3.4)$$

Where Z_0 represents the characteristic impedance.

By obtaining the effective dielectric constant, other parameters such as the guided wavelength, propagation constant, phase velocity and electrical length among others, the filter could be designed. For the purpose of this filter design, the immediate calculations for this design would be the guided wavelength (λ_g) and the electrical length (l). These values would be used to determine the parameters during the filter software design.

$$\lambda_g = \lambda_0/(\varepsilon_r)^{1/2} \quad (3.5a)$$

$$\lambda_g = \frac{c}{f_O\sqrt{\varepsilon_{eff}}}\,m \quad (3.5b)$$

Where λ_0 is the wavelength of free space, c is the speed of light in free space and f_0 is the resonant frequency.

The electrical length used for the conventional microstrip filter design is the quarter wavelength microstrip line as shown in (3.6). This length reduces as the length (X) is increased from the input port towards the output port thereby reducing size.

$$l = \lambda_g/4 \quad (3.6)$$

Using equations (3.1) - (3.6), the initial dimensions for the filter design could be calculated. The thickness (h) of the kapton substrate to be used for inkjet printing is 50 µm, with dielectric constant (ε_r) of 3.4. A 50 ohms line is used (Zo = 50 Ω). At the required center frequency, using equations (3.1) - (3.6), all the required dimensions are determined. However, to obtain better band-stop response from the simulations, the circuit had to be optimised.

The dimensions of the inkjet-printed based DMS circuit area as shown in Figure 3-1 are as follows: l = 15mm, W = 0.11 mm, X = 14.98 mm by 0.01 mm, Y = 0.6 mm by 0.05 mm and Z = 0.005 mm by 0.39 mm. Silver with thickness of 1µm is used as the metallisation for the kapton polyimide substrate. This was adopted because of the ultra-thin silver nano-particles used in the inkjet printing technology.

Simulations are done using the em sonnet commercial software. The electromagnetic em sonnet software was used for this design as it allows the structures to be modified physically rather than using ADS whereby the lumped inductance and capacitance values are used to form the structure. In this case, it is easier to etch different defects on the transmission line using the em sonnet software. The filter is simulated using kapton polyimide with thickness of 50 µm, dielectric constant (ε_r) of 3.4 and loss tangent (tanδ) of 0.0021.

Figure 3-9 shows the simulated result of the filter. The narrow band BSF has fractional bandwidth of 14%, stopband rejection ($|S_{21}|$) of 39 dB at the resonant frequency of 3.25 GHz with its return less than -0.14 dB exhibiting a very low loss. The insertion loss performance ($|S_{11}| > 35$ dB) is better when compared with other published filters in Table 3-1.

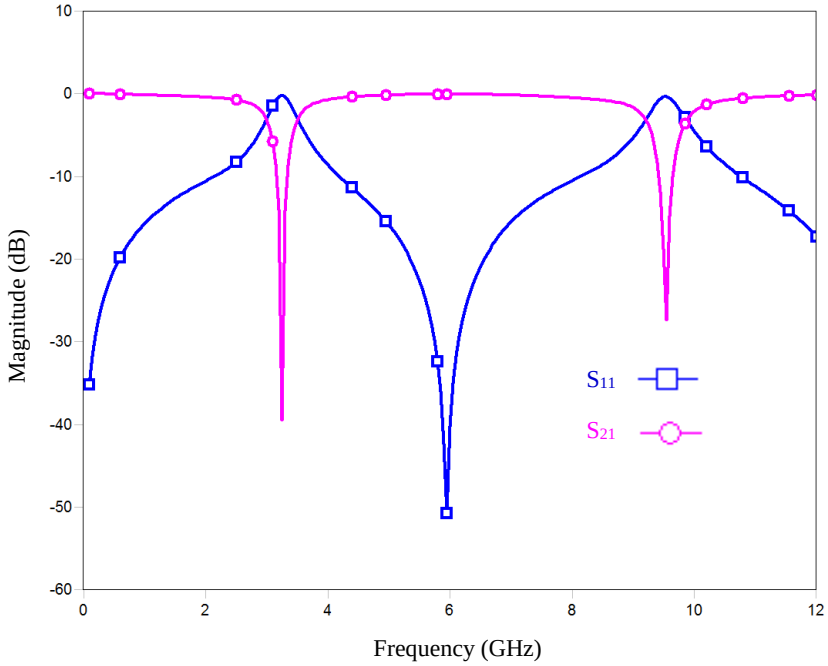

Figure 3-9: S-parameter simulation response of the proposed notch filter.

Figure 3-9 shows the simulated response of the filter design with two transmission zeros at 3.25 GHz and 9.55 GHz with stopband attenuation of about 40 dB and 30 dB respectively. This filter could be used to reject two bands of interfering signals at 3.25 GHz and 9.55 GHz and it maintains a very good return loss performance in the passband over the whole bandwidth. Between the two stopbands, a good return loss performance tending towards 50 dB is observed. Prior to the first transmission zero, and after the second transmission zero, the return loss also shows good performance tending towards about 40 dB. The two stopbands at 3.25 GHz and 9.55 GHz could also be used independently if required such as a case whereby an interfering signal at 9.55 GHz needs to be rejected as it may be affecting a signal at over 10 GHz.

The unloaded Q-factor Q_u is a dimensionless parameter that indicates energy losses. The higher the unloaded Q factor, the lower the loss. The 3 dB bandwidth of the filter is about 0.4 GHz and therefore a Q-factor around 16.3 could be achieved. The unloaded Q-factor, Q_u can be expressed in terms of resonant frequency (f_0) and 3 dB bandwidth Δf_{3dB}.

$$Q_u = 2\ f_0 / \Delta f_{3dB} \qquad (3.7)$$

$$Q_u = 2 \times 3.25 / 0.4$$

$$Q_u = 16.25.$$

Because of the good response with a narrow bandwidth and good selectivity, the notch design could be used to reject unwanted signals close to the router. This would be explored in the next chapter on how effective the filter could be in suppressing nonlinear distortions and to reject

interfering signals close to the main fundamental signal. Owing to the satisfactory stopband performance, it is very useful for modern communication technology such as the evolving WiMAX applications. The designed BSF could be used to suppress nonlinear distortions most especially for the 3.5 (3.3 – 3.7 GHz) GHz WiMAX licensed spectrum profile.

Table 3-1: Simulated band-stop response comparison for different reported DMS filters.

DMS (BSF)	**Resonant Frequency** (GHz)	**Bandwidth (GHz)**	**Insertion Loss, S_{11}** (dB)	**Rejection Level, S_{21}** (dB)
Ref. [3.18]	2.75	0.3	> -10	> -45
Ref. [3.19]	3.825	0.55	> -10	> -25
Ref. [3.20]	5.31	0.44	> -15	> -25
Ref. [3.21]	2.45	0.5	> -5	> -35
This work	3.25	0.4	> -35	> -35

Apart from the satisfactory band-stop performance, the presented filter also shows some good advantages over existing published filter designs. As shown in Table 3-1, it is obvious that the filter has shown a great deal of improvement in terms of the return loss performance over the whole bandwidth. This is a very critical response performance for practical realisation of the filter as this helps to reduce the loss observed in the filter when it is used for experimental verifications and in system components. The designed filter has better stopband attenuation when compared to band-stop filters designed in [3.19] – [3.21]. However, another band-stop filter designed in [3.18] had slightly better stopband attenuation above 45 dB at its resonant frequency of 2.75 GHz but at the expense of a good return loss performance as the input return loss (S_{11}) is just above 30 dB.

Table 3-2: Physical size for BSF with substrate properties.

DMS (BSF)	**Dielectric Constant, ε_r**	**Substrate thickness** (mm)	**Rectangular area** (mm^2)	**Normalised area** (λ_g x λ_g)
[3.17]	3.48	0.508	12.1*2.7	0.32*0.07
[3.18]	2.2	1.54	16.2*4.8	0.35*0.065
[3.19]	2.55	1.5	9.0*4.5	0.201*0.101
[3.20]	2.65	1.6	8.5*4.1	0.22*0.11
[3.21]	2.5	2.63	14.15*6.2	0.17*0.07
This work	3.4	0.05	15*0.11	0.27*0.002

The BSF is compact and its overall physical length and width is 15 mm x 0.11 mm. The normalised area of other similar band-stop filters is calculated using equations (3.1) - (3.6) and compared in Table 3-2.

For the filter designed in this chapter using Figure 3-8, The thickness of the Kapton substrate to be used for inkjet printing (h) is 50 um, with dielectric constant (ε_r) of 3.4. A 50 ohms line is used (Zo = 50 ohms). From the design above, we also know that W = 0.11 mm.

To calculate the effective dielectric constant (ε_{eff}), equation (3.2) is used.

$$\varepsilon_{eff} = \frac{\varepsilon_r + 1}{2} + \frac{\varepsilon_r - 1}{2}\left[1 + \frac{12h}{W}\right]^{-1/2}$$

$$\varepsilon_{eff} = \frac{4.4}{2} + \frac{2.4}{2}\left[1 + 5.45\right]^{-1/2} = 2.67$$

$$\varepsilon_{eff} = 2.67 \tag{3.8}$$

The guided wavelength can be calculated from (3.5b).

$$\lambda_g = \frac{c}{f_o\sqrt{\varepsilon_{eff}}}\ \text{m}$$

Where c is the speed of light (3 x 10^8 m/s) and f0 is the resonant frequency which is 3.25 GHz for this filter design.

$$\lambda_g = \frac{3\ \text{x}\ 10\text{^}8}{3.25\ x\ 10\text{^}9\sqrt{2.67}}\ \text{m}$$

$$\lambda_g = 56.49\ \text{mm}$$

Therefore, the overall dimension of the filter could be calculated in terms of the guided wavelength. The length and width of the designed structure is 15mm by 0.11 mm.

$$\text{l}\ (\lambda_g) = 15/56.49 = 0.27$$

$$\text{W}\ (\lambda_g) = 0.11/56.49 = 0.002$$

Therefore, the presented structure in Figure 3-8 occupies an overall area of 0.27 λ_g x 0.002 λ_g in terms of the guided wavelength. The dimensions of all the other published filters using the same DMS technology have been evaluated and compared in terms of the guided wavelength as shown in Table 3-2. The presented structure thereby occupies the smallest rectangular area and has the least normalised area (0.27 λ_g x 0.002 λ_g). The results in Table 3-2 and by evaluating equations (3.1) – (3.6), it could be observed that the flexible substrate properties necessary for inkjet printing have also played a vital role in the miniaturisation of the structure. The DMS of the band-stop filter designed to be suitable for inkjet printing has shown a miniaturized normalised area and overall size reduction.

With the DMS, by simply modifying the defects on the main transmission line, different stopband characteristics could be obtained which helps to reduce size which would have required larger dimensions for smaller frequencies. Figure 3-10 is a modification of Figure 3-8 to achieve a narrower stopband for a different center frequency of 2.4 GHz. It was also more compact as it would be slightly bigger to design at 2.4 GHz using Figure 3-8. The dimensions Y and Z are investigated carefully to achieve a narrower stopband while the T-shaped slots are to achieve the highest stopband attenuation possible. The filter aims to reject wireless (Wi-Fi) interference at 2.4 GHz. On the microstrip line, an inverted T-shaped DMS pattern is etched on the U-shaped slot along with the stepped impedance slots, thereby modifying the current distribution and changing the effective inductance and capacitance. This defect leads to a compact filter size and by simply modifying its dimensions within the circuit area, the structure could be designed at different frequencies.

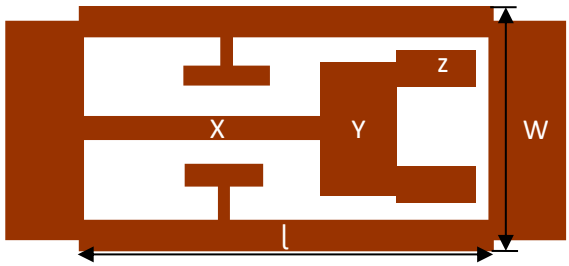

Figure 3-10: Structure of the modified U-shaped notch filter.

This filter is also designed to be suitable for inkjet printing. The properties for simulation were to be adaptable for the inkjet printer. The chosen metal for the inkjet-printed substrate is Silver. This is because kapton polyimide substrate makes use of silver nano-particles for inkjet printing. Silver with thickness of 1µm (0.001 mm) is used in simulations. It is also a single layer circuit and the T-shaped patches also manipulate the stopband attenuation, but the aim is to get good stopband attenuation and a good return loss performance.

By following similar design specifications as described above, using equations (1) – (6) and optimising by tuning, the dimensions are obtained. The dimensions of the structure in Figure 3-10 are as follows: l = 15mm, W = 0.12 mm, X = 11.03 mm by 0.01 mm, Y = 3 mm by 0.08 mm and Z = 1 mm by 0.02 mm. The Dimensions of the inverted T-shaped DMS patch could be varied for better Q-factor and stopband attenuation at cut-off frequency.

Simulations are done using the em sonnet commercial software. The filter is simulated using kapton polyimide with thickness of 50 µm, dielectric constant (ε_r) of 3.4 and loss tangent (tanδ) of 0.0021. The simulated result of designed filter is shown in Figure 3-11 with stopband rejection (S21) of -38.44 dB, fractional bandwidth of 16.84 % and Q-factor of 14.6 at the resonant frequency of 2.375 GHz with its passband less than -0.14 dB exhibiting a very low loss.

Figure 3-11 also presents the insertion loss performance (S_{11}>-30 dB) which is very useful in filter fabrication and when it is used for nonlinear distortion evaluation. At the center frequency of 2.375 GHz, a sharp narrowband notch response could be observed. This rejection could be used for interfering signals very close to the main band or even within the main signal as it also

exhibits good return loss which tends towards zero (0). The second transmission zero from the stopband response is at 9 GHz. It also has a narrowband response even though it is not as narrow as the first transmission zero at 2.375 GHz. Its stopband attenuation is also approaching -30 dB which also means it could be useful to reject unwanted signals. For this actual research, the frequencies being focused on is mainly the ones closer to the first transmission zero but the rejection properties at 9 GHz could still be very useful as it shows not only good rejection but low loss as well as the first stopband response at resonant frequency of 2.375 GHz.

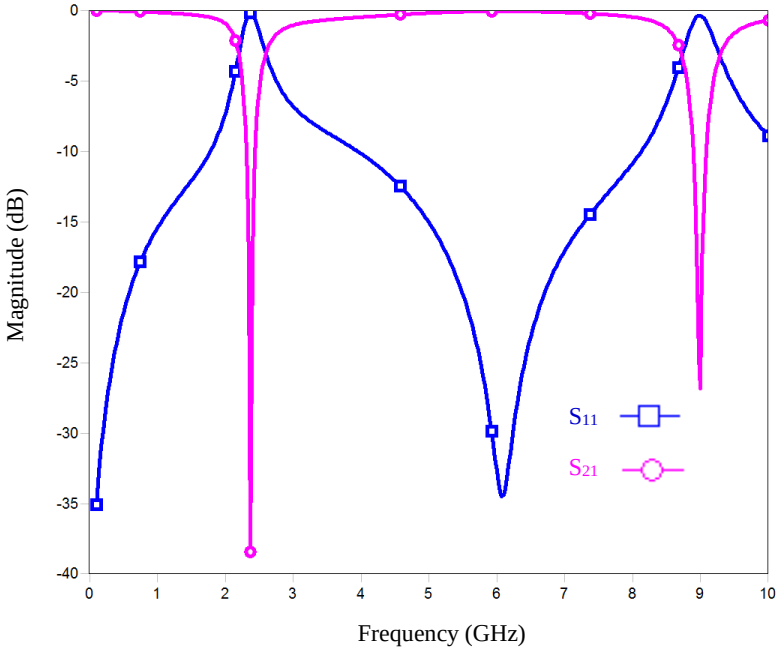

Figure 3-11: Band-stop response of designed notch filter at 2.375 GHz.

The designed filter shows a narrow band with compact size, good selectivity and band-stop response at the cut-off frequency of 2.375 GHz. The Q- factor is also calculated using equation (7).

$$Q_u = 2\ f_0 / \Delta f_{3dB} \qquad (3.7)$$

$$Q_u = 2 \times 2.375 / 0.325$$

$$Q_u = 14.6$$

This filter also has its applications in successfully rejecting unwanted signals and suppressing nonlinear distortions and it would be investigated in chapter 4. This also proves that with DMS, by simply modifying the dimensions of the defect placed on the microstrip line, filter could be designed at any arbitrary frequency. Both structures give good response, but Figure 3-10 is more complex to design than the DMS in Figure 3-8. This filter is also very useful for modern wireless communication technology such as the wireless transmitters at 2.4 GHz, the evolving WiMAX applications and other wireless systems. The designed notch filter could be used reject unwanted signals and to suppress nonlinear distortions at the output of PA for specified frequency bands close to its bands of operation.

To obtain an improved rejection level, a DMS spur-line configuration was explored and one of such structure was designed as shown in Figure 3-12. Two adjacent L-shaped defects have been

used to alter the effective capacitance and inductance of the microstrip line thereby increasing the slow wave factor and the impedance o the line. This has also slightly modified the dimensions of the filter as compared with Figure 3-8 and Figure 3-10. All these structures are designed with inkjet printing in mind and so the same specifications for the flexible kapton substrate have been used for all the configurations. Using CAD (Computer aided design) and mathematical expressions have enabled us to get the dimensions required for the microstrip design.

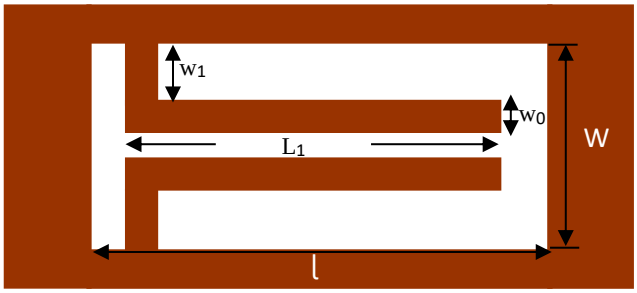

Figure 3-12: Double spur-line band-stop DMS configuration.

After generating length (l) and width (W) of the design, further optimisation techniques are required to be able to get the right band-stop response with the aim to achieve higher stopband attenuation whilst maintaining low loss, good return loss performance and compactness in size. Using the same silver metallisation and steps used in the initial design with U-Shaped slots, the spur-line structure is designed with these dimensions: l = 14.6 mm, w = 0.1 mm, L_1 = 14.58 mm, w_0 = 0.01 mm and w_1 = 0.034 mm.

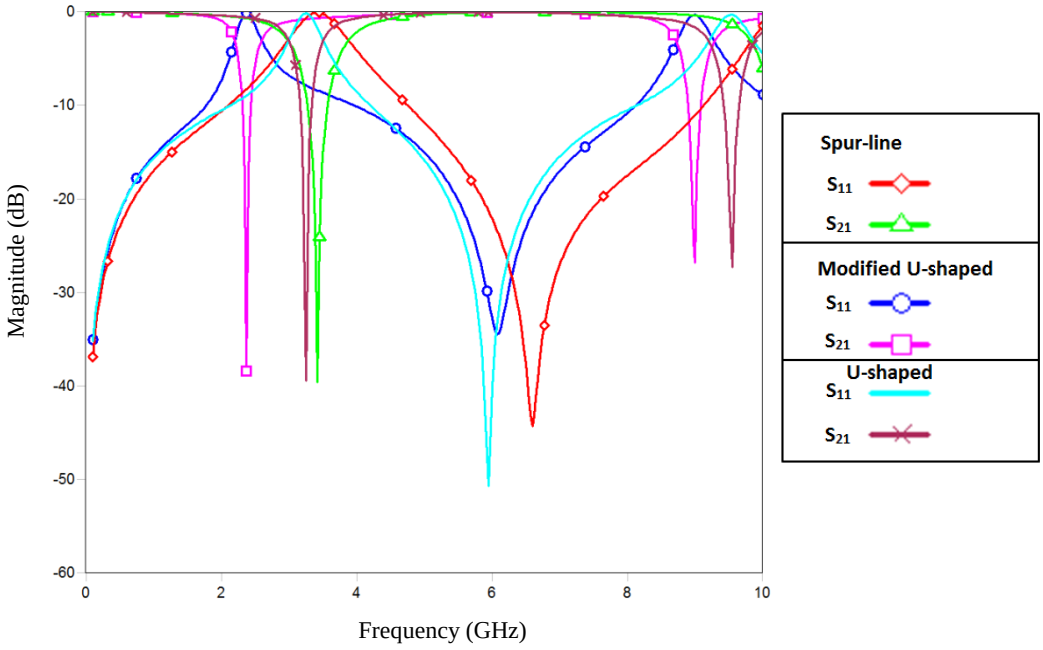

Figure 3-13: Comparison of Simulated s-parameters of spur-line and u-shaped DMS.

By varying the values of all the dimensions within the structure, we get a different response. Figure 3-13 compares the spur-line DMS results with both U-shaped band-stop filters designed

in Figure 3-8 and Figure 3-10. The spur-line structure has a slightly smaller area (14.6 mm by 0.1 mm) with a normalised size of 0.27 λ_g x 0.0019 λ_g showing an overall physical reduction. The simulated result in Figure 3-13 shows a higher stopband attenuation of about 44 dB and improved return loss performance with the passband return loss almost zero (-0.09 dB) at the resonant frequency of 3.425 GHz. The spur-line achieved attenuation better than the U-shaped DMS. From Figure 3-13, it can be observed that the modified U-shaped DMS has the narrowest band, followed by the initial U-shaped and then the Spur-line. Also, in terms of the out-of-band return loss (S11), the U-shaped achieved about 50 dB while the Spur-line achieved about 45 dB and the modified U-shaped achieved about 38 dB. The 3 designs have all unique qualities. The modified U-shaped is more compact than both and has the narrowest band while the initial U-shaped design is also narrow and possesses the best out-of-band return loss performance with better attenuation than the modified U-shape. The spur line has the highest attenuation and better out-of-band return loss compared to the modified U-shaped but its not as narrow as both U-shaped filter designs.

The filters have been specifically designed to reject interference for Wi-Fi, WiMAX and other wireless systems. The novel compact DMS filters in this section will be integrated into transceiver circuits of next generation wireless networks in the next chapter for different applications.

3.4 Conclusions

This chapter has presented novel ways of designing compact band-stop filters for RF/Microwave wireless communication systems. The conventional RLC bandstop filters have been limited by their large sizes in the Gigahertz frequency range. This thesis has achieved further miniaturisation by applying defects on microstrip filter planar structures. The aim is to achieve compactness, narrowband and maintain the excellent stopband performance properties of the conventional BSF. A U-shaped transmission line concept which could be designed at any desired center frequency was proposed in this thesis. The filter was designed to be suitable for inkjet printing due to its ultra-thin and flexible kapton substrate that also improves on compactness of the overall structure. The U-shaped slot was observed to achieve the same excellent stopband attenuation and return loss performance for almost half the size of the conventional structure. The proposed structure also achieved the smallest rectangular and normalised area over other published filters.

To achieve a narrower band, the U-shaped structure was further modified but with a slight trade-off on stopband attenuation. However, this design also reduces the size more as it will take a bigger area for a lower center frequency (from 3.5 GHz to 2.4GHz) using the same U-shaped design. To achieve a higher stopband attenuation whilst maintaining other stopband properties led to a similar design in a spur-line shape. The spur-line was able to improve stopband attenuation but at the expense of a wider band and return loss performance between bands. All 3 structures were narrowband (notch), similar in compactness and gave excellent properties which make them outstanding candidates for filtering modern day communication systems. These filters will be integrated in RF/Microwave transceiver systems for non-linear distortion and interference suppression.

3.5 References

[3.1] D. D. Grieg and H. F. Engelmann, “Microstrip—A new transmission technique for the kilomegacycle range,” *Proc. IRE*, vol. 40, pp. 1644–1650, Dec. 1952.

[3.2] G. L. Matthaei, L. Young and E. M. T. Jones, Microwave Filters, Impedance-Matching Networks and Coupling Structures, *McGraw-Hill, New York*, 1964.

[3.3] B. M Schiffman and G. L. Matthaei, “Exact Design of Band-stop Microwave Filters”, *IEEE Trans. Microwave Theory Tech.*, vol. 12, no. 1, pp. 6-15, Jan 1964.

[3.4] P. A. Dupuis, and E. G. Cristal, "Folded-Line and Hybrid Folded-Line Band-stop Filters," *Microwave Symposium Digest, 1974 S-MTT International*, vol.74, no.1, pp.162, 164, 12-14 June 1974.

[3.5] R. N. Bates, “Design of microstrip spur-line band-stop filters,” *Microwaves, Optics and Acoustics, IEEE Journal on*, vol.1, no.6, pp.209, 214, November 1977.

[3.6] D. Sanchez-Hernandez, and I.D. Robertson, “Dualband Microstrip Rectangular Patch Antenna Using a Spur-line Filter Technique,” *23rd European Microwave Conf: Proceedings*, pp. 357-360, Madrid 1993

[3.7] P. Guillan, S. Mekerta, and Y. Garault, “Microstrip band-stop filter using a dielectric resonator,” *Microw. Opt. Antennas IEEE Proc. H*, vol. 128, no. 3, pp. 151-154, June 1981.

[3.8] A. Abramowicz, "MIC Realization of Dielectric Resonator Elliptic Filters," *Proc. 19th European Microwave Conf.*, London 1989.

[3.9] A. Brucher, Ph. Meunier, C. Cenac, B. Jarry, R. Guillon, "Broadband and tunable negative monolithic circuits for microwave active filters compensation," *IEEE MUT-S Symp. Dig.*, Vol. 2, pp. 745-748, 1995.

[3.10] R. J. Cameron, Ying Wang and Ming Yu, "Direct-coupled realizations for microwave band-stop filters," Microwave Symposium Digest, 2005 *IEEE MTT-S International*, vol., no.4, pp. 12-17, June 2005.

[3.11] G. Zhang, M. J. Lancaster, F. Huang, and N. Roddis, “A superconducting microstrip band-stop filter for an L-band radio telescope receiver,” *in 35th Eur. Microw. Conf.*, pp. 1–4, Oct. 4-6, 2005.

[3.12] Won-Gyu Lim, Wan-Kyu Kim, Dong-Hoon Shin, Jong-Won Yu, “A Novel Band-stop Filter Design Using Parallel Coupled Line Resonators,” *IEEE European Microwave Conference*, pp. 878- 881, Oct. 2007.

[3.13] D. R. Jachowski, “Compact Frequency-Agile, Absorptive Band-stop Filters”, *IEEE MTT-S, Digest*, pp. 1-4, 2005.

[3.14] L. Cheng-Jung, K. M K H Leong, and T. Itoh, "Metamaterial Transmission Line Based Band-stop and Bandpass Filter Designs Using Broadband Phase Cancellation", *Microwave Symposium Digest, 2006. IEEE MTT-S International*, vol., no., pp.935, 938, 11-16 June 2006.

[3.15] D. R. Jachowski, "Cascadable lossy passive biquad band-stop filter", *IEEE Microwave Symposium Digest, 2006. IEEE MTT-S International*, pp. 1213-1216, 2006.

[3.16] J. Dong, L. Liu, D. Gao, Y. Yu, A. Zheng, T. Yang, and X. Zhang, "Compact notch microwave photonic filters using on-chip integrated microring resonators," *IEEE Photon. J. 5*, 5500307 (2013).

[3.17] W. Y. Sam, Z. Zakaria, M. A. Mutalib, M. F. M. Fadhli, A.R. Othman, and A.A.M. Isa, "A Compact DMS Triple-Band Band-stop Filter with U-slots for Communication Systems", *Proc. Int. Conf. on Electronic Design*, Penang, Malaysia, pp. 383-386, 2014.

[3.18] K. Chakrabarty, and D. Budimir, "Compact tunable bandstp filters using Defected Microstrip Structure for multi-standard wireless systems", *Proc. 43rd Eur. Microw. Conf.*, Nuremberg, Germany, pp. 1031-1034, 2013.

[3.19] J. Wang, H. Ning, L. Mao, and M. Li, "Miniaturized Dual-Band Band-stop Filter Using defected Microstrip Structure and Defected Ground Structure", *IEEE-MTT-S Int. Microw. Symp. Dig.*, Montreal, Canada, pp. 1-3, 2012.

[3.20] D. La, Y. Lu, and S. Sun, "Novel Band-stop Filter Using Dual-U Shape Defected Microstrip Structure", *Proc. Int. Symp. Signals, Systems and Electronics*, Nanjing, China, pp. 400-402, 2010.

[3.21] S .R. Choudhury, T. Mondal, S. K. Parui, and S. Das, "Compact Stopband Filter Based on Double Tuned rectangular Split Ring Defected Microstrip Structure for ISM Band Applications", *Int. Conf. on Computers and Devices for Communication*, Kolkatta, India, pp. 1-4, 2012.

[3.22] H. Saghlatoon, L. Sydänheimo, L., Ukkonen, and M. Tentzeris, "Optimization of Inkjet Printing of Patch Antennas on Low-Cost Fibrous Substrates", *IEEE Antennas Wireless Propag. Letters*, vol. 13, no. 1, pp. 915-918, 2014.

[3.23] Y. Lan, Yuehang Xu, C. Wang, Z. Wen, Y. Qiu, T. Mei, Y. Wu, and R. Xu, "Flexible Microwave filters on Ultra-Thin Liquid Crystal Polymer substrate", *IEEE MTT-S Int. Microw. Symposium*, Phoenix, Arisona, pp. 1-3, 2015.

[3.24] J. Virtane, L. Ukkone, T. Bjorninen, A. Elsherbeni, and L. Sydandnheimo, "Inkjet-printed humidity sensor for passive UHF RFID systems", *IEEE Trans. on Instrum. Meas.*, vol. 60, no. 8, pp. 2768-2777, 2011.

[3.25] H. L. Kao, C. L. Cho, X. Dai, C. S.Yeh, X. Y. Zhang, L. C. Chang, and H. C. Chiu, "Hairpin Bandpass Filter on Liquid Crystal Polymer Substrate using Inkjet Printing Technology", *IEEE MTT -S Int. Microwave Symposium*, Seattle, W A, pp. l- 4,June.2013.

[3.26] K. Hettak, T. Ross, R. James and A. Momciu, " Low-Cost mm-Wave Coplanar Waveguide Bandpass Filter using Inkjet Printing of Silver Nano-Particles on Flexible Plastic Substrate", *IEEE MTT-S Intl. Microwave Symposium,* Phoenix, AZ, pp. 1-3, 17-22 May 2015.

[3.27] W. Ahmad, and D. Budimir, "Inkjet-printed bandpass filters and filtennas using silver nanoparticle ink on flexible substrate", *IEEE Intl. Symposium on Antennas and Propagation*, pp. 145-146, 19-24 July 2015.

[3.28] Pozar, D. (2011), "Microwave engineering", *3rd Ed. New York: John Wiley & Sons*, pp.143-147.

Chapter 4 Nonlinear Distortion Evaluation and Suppression for Evolving Next Generation Networks

The comprehension of the different kinds of distortions in wireless systems is a necessity as that helps when planning the necessary techniques to adapt to various kinds of distortions. The methods to improve linearity and efficiency of the system whilst effectively suppressing nonlinear distortions and intermodulation products will depend mainly on the kind of distortion that is produced, and which makes it very essential to evaluate the behaviour of the system and its distortion properties. The distortion produced by the amplifier itself, would be different to the case whereby there is one interfering signal or even more interfering signals and therefore, the way to suppress each case would differ.

Different types of linearization techniques have been used over the years with the primary aim of producing highly efficient and linear systems. The main categories of these techniques include feedback, feed forward, digital pre-distortion, EER (Envelope elimination and restoration), LINC (Linear amplification with nonlinear components), filtering and injection [4.1] - [4.4].

In the feedback linearization technique, a portion of the amplifier's inverted waveform output is sampled and summed up with the input which then aids in the partial cancellation of the distortion products. This technique mainly feedbacks the distorted output signal thereby forming an error signal when compared to the input. The main limitations of this technique occur from the fact that overall system gain is reduced; it is not very much stable, and the time delay introduced by the feedback signal path limits the upper frequency range as well. To try to overcome some of these limitations, came about the feedforward equivalent [4.1].

The feedforward technique is like the feedback technique, but splits into two loops from the input and does the signal and error correction towards the output as shown in Figure 4-1. One of the signals which is observed to be highly linear and carries a sample of the undistorted input signal is compared with a sample of the main signal output and these results in an error signal of distortion products. Delays are then introduced to match the main signal and the error channels.

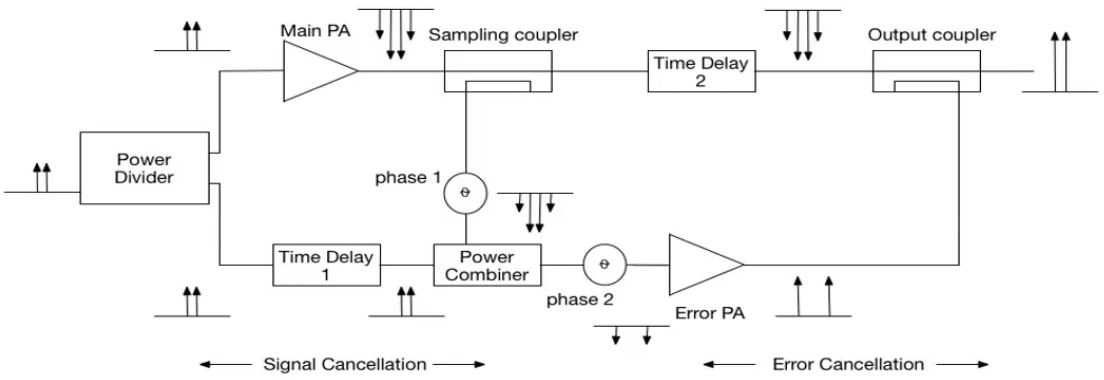

Figure 4-1: The feedforward linearization block diagram.

In summary, this technique utilizes the concept of having a signal cancellation and error cancellation loop. So, the fundamental signal at the input is sent through the PA operating in its nonlinear region and intermodulation products are obtained when the resulting signal is subtracted from a delay also placed on the main input signal. Then by amplifying the intermodulation products to a certain level, it very much possible to get a distortion free signal at the output [4.2]. One major drawback of this technique is the fact that another class A linear amplifier is required which leads to system complexity and could be expensive.

Digital pre-distortion (DPD) is another linearization technique that has been used in literature. The pre-distortion technique could be analog or digital [4.3]. They are alike but just the fact that analog could be used in the RF domain and digital is used in the digital domain. DPD works with the concept of creating an inverse transfer function of the power amplifier (PA) and adding to the transfer function of the PA thereby giving a linear output. The problem with DPD techniques is its complexity. It is very complex mainly due to the memory effect problem along with an increase in overall size and cost as well. Its analog equivalent also has power loss constraints due to the use of more RF components. To overcome these problems, adaptive DPD techniques with better memory effects must be implemented [4.4].

In the case of the EER (Envelope elimination and restoration) technique, the input signal is split into two producing amplitude modulation (AM) and phase modulation (PM). The first part is sent via an envelope detector for the amplitude modulation and the second part through a limiter to give the phase modulation (PM) part. The AM and PM equivalents are then amplified by a baseband and RF amplifier simultaneously. To restore the envelope, the AM signal is used to modulate the RF signal. By doing this in conjunction with the limiter to eliminate AM/PM distortions, linearity at the output is achieved [4.5]. Its limitations include the nonlinearity observed in components such as the baseband amplifier and the envelope detector. In this technique, delays in the path and less efficiency also contribute to doubts about the effectiveness of the technique.

The next technique which is like EER is the linear amplification using nonlinear components (LiNC). As the name states, this method uses nonlinear components to achieve linearity. By using an AM-PM modulator, the signal is divided into two parts/components. Individual parts are then amplified by PA with very high efficiency and then finally added at the output. Distortions are eliminated as there is a linear relationship between the signal and the input signal [4.6]. The realization of the right AM-PM modulator, complexity and the phase and gain imbalances that occur in the two parts using the highly efficient power amplifiers are some of the disadvantages that has been widely attributed to this technique [4.7] - [4.8].

Filtering has become very much popular among researchers due to new technologies of its design that could achieve simplicity and compact size. It eliminates the need to have to use complex algorithms for linearization or reducing of nonlinear distortions. A filter can be used either before the PA or after the PA to reject unwanted signal [4.9] - [4.10]. The filtering technique could be used by a bandpass filter or band-stop filter. The bandpass filter is limited in the case of operating close to saturation whereby the third order inter-modulation products have become more pronounced and is so close to the main signal and cannot be effectively

suppressed by the bandpass filter. For this case, a narrowband band-stop filter (notch) is required with a very high Q and low loss.

Band-stop filters are mostly used after the PA to reject unwanted signals. However, in this thesis, the notch would be used before the PA to effectively suppress such inter-modulation distortion products that affect the linearity of the output signal. The band-stop filter could still play important roles when used after the PA for cases whereby both sides of the main signal has interfering signals that have accumulated distortions into the PA's operating band. However, in this case, a dual-band narrow band band-stop filter is required to reject both sides of such distortion. But these filters will have to be designed with stringent requirements for power and with enough attenuation to fully suppress such nonlinear distortions. When interfering signals that could contribute to nonlinearity are present, inter-stage band-stop filters could be used effectively because by attenuating those interfering signals, the nonlinear distortions due to the interference also reduces.

For the injection technique which will form the basis of this research, it involves injecting specific frequency components into the fundamental signal circuit to mainly cancel out the third-order intermodulation products (IM3) and suppress other nonlinear distortions. This could be implemented by the frequency difference between spectral components (such as cos $(w_2 - w_1)$ t) of the input signal and adding them alongside with the input signal that is to be amplified [4.11]. This technique has seen to help reduce third-order intermodulation products (IM3). Another way of using the injection technique is by using the second harmonics of the signal. This is referred to as second harmonic injection. The second harmonics along with its intermodulation products are fed back into the input of the amplifier to cancel out the third-order intermodulation products with the aim to suppress nonlinear distortions. The second harmonic injection technique will be fully explained in section 4.2 as it forms the basis of the technique to be used in this thesis.

In this chapter, the filtering and second harmonic injection techniques are going to be considered and investigated with next generation systems such as 4G and 5G in mind.

Section 4.1 goes further to evaluate distortions and investigate the second harmonic injection technique and with novel ideas to effectively suppressing nonlinear distortions for advanced mobile wireless communications such as LTE, LTE-Advanced and 5G communication systems.

Section 4.2 explores new ways in which a well-designed narrowband band-stop (notch) filter can be used effectively in rejecting interfering signals and effectively suppress nonlinear distortions that occur in wireless transmitters due to the nonlinear characteristics of the power amplifier at the saturation point. A narrower filter is better as it tries to ensure that the stopband does not extend into the passband of the main signal. However, the filter design must still meet specifications such as compact size, low loss, and good inter-stage and integrating properties with other technologies and techniques.

Section 4.3 combines the techniques and used in carrier aggregated systems for LTE-Advanced systems. Carrier aggregation (CA) wireless transmitter signals are used to evaluate nonlinear distortions in the power amplifier under test. The injection technique has never been utilised

for carrier aggregation and has been modified in this chapter to accommodate for nonlinearities in two and three intra-band components aggregated carriers. The injection technique is then further modified with the aid of the band-stop filter designed in chapter three for inter and intra-band CA. Both intra-band and inter-band contiguous and non-contiguous CA cases are considered.

In Section 4.4, the band-stop filter is tested in an LTE transmitter system for interference suppression. The use of the designed band-stop filters before and after the PA in the wireless transmitter architecture is investigated and results are also presented for carrier aggregation.

4.1 Compensation based on Second Harmonic Injection

Due to the nonlinear characteristics of the power amplifier (PA), it imposes spectral and power constraints whilst designing any transmitters for mobile wireless communication systems. Any signal passing through the PA is highly susceptible to nonlinearity and the easiest way would have been to operate the PA in its linear region to avoid nonlinear distortion. But to maximize efficiency, the PA should be able to operate close to saturation. Hence, techniques required for linearization and efficiency are required and should be simple, cost effective and aim to achieve a reduced size.

This work features advances in different proposed techniques and novel ideas on how to effectively suppress such nonlinear distortions.

4.1.1 Theoretical Analysis

The injection technique is analysed theoretically assuming a nonlinear power amplifier (PA). The linearity of the PA is then expressed function of the drain current (i_d) to the gate voltage (v_{in}) using power series as shown in equation (1) and equation (2).

$$i_d = g_{m1} v_{in} + g_{m2} v^2_{in} + g_{m3} v^3_{in} \quad (1)$$

$$v_{in} = A_1 \cos w_1 t + A_2 \cos w_2 t \quad (2)$$

Where A_1 and A_2 are the amplitudes and w1 and w2 denote the angular frequency. By putting equation (2) into equation (1) and solving for the drain current in the power series, the current term for the third-order intermodulation product ($2w_2 - w_1$) is derived in equation (3).

$$0.75 A_1 A_2^2 g_{m3} \cos (2w_2 - w_1) t \quad (3)$$

The second harmonic injection technique requires the second harmonics to be fed back into the amplifier. Therefore, from equation (2), if the second harmonic of the two input frequencies is added to the amplifier input voltage components, then input voltage changes and results in equation (4)

$$v_{in} = A_1 \cos w_1 t + A_2 \cos w_2 t + A_{11} \cos (2w_1 t + \varphi_1) + A_{22} \cos (2w_2 t + \varphi_2) \quad (4)$$

Where A_{11}, A_{22} are the amplitude of the second harmonics in addition to the initial amplitudes in equation (1) and φ_1, φ_2 represents the phase of the harmonics. By putting equation (4) into equation (1), the resulting expression for the drain current at the frequency of the third order intermodulation products becomes:

$$0.75A_1A_2^2g_{m3}\cos(2w_2 - w_1)\,t + A_1A_{22}\,g_{m2}\cos(2w_2t - w_1t + \varphi_2) \quad (5)$$

The term g_{m1} does not have any third order intermodulation products and so is not present in equation (5). By analysing equation (5), it could be deduced that by manipulating A_{22} and φ_2, it is very much possible to obtain equal amplitude and opposite phase relationship between the two terms. This would then give a net zero drain current component at $(2w_2 - w_1)$. Hence, by systematically feeding back the amplitude and phase of the second harmonics into the input of the PA, the IM3 components in the drain currents could be eliminated or sufficiently suppressed and aids in reducing nonlinear distortion [4.1]. This is the theoretical background of how this technique operates. This technique would now be considered in simulations and tests to prove on how it could be effective for advanced mobile wireless communication systems.

4.1.2 Second Harmonic Injection Technique

The injection of the second harmonics could be done at the input alone. It could also be explored at the output and both input and output. For simulation purposes, the above possibilities (input and output) were explored. Figure 4-2 presents the schematic block of the proposed injection technique to be used in this research. The circuit diagram in Figure 4-2 is designed in Keysight/Agilent ADS (Advanced System Design). The feedback loop consists of ideal components in ADS library such as the power splitter, bandpass filter (BPF), phase shifter, variable attenuator, and the gain amplifier which were used to alter the second harmonic signal to the right requirements to be added back into the PA's input. The amplifier including all additional components (Signal Modulator, power splitter, phase shifters, variable attenuators, bandpass filters and gain amplifiers) were designed using Keysight/Agilent ADS software. The components used apart from the amplifier are ideal elements from the ADS library.

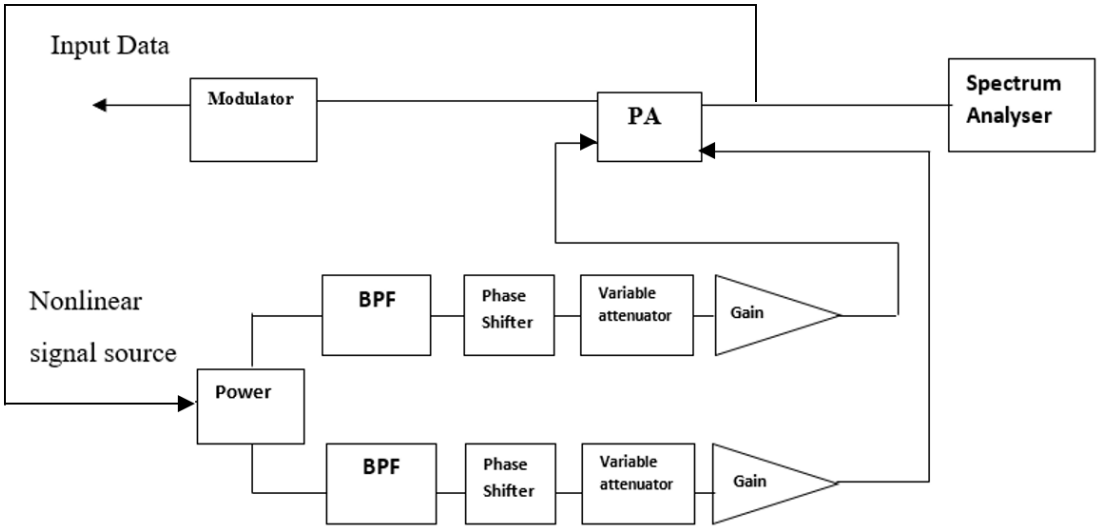

Figure 4-2: Second harmonic injection circuit diagram.

Initially, a gallium nitride (GaN) power amplifier was designed using ADS and was used as the amplifier under test for simulations. This amplifier would be evaluated using the injection circuit shown in Figure 4-2. Simulated results are shown below. The amplifier behaviour is

shown in Figure 4-3 and it could be seen that the 1-dB compression point is at about 20 dBm. The GaN amplifier is designed at 3.3 GHz center frequency and is characterized by 17 dB gain and 20 dBm P_1dB as shown in Figure 4-3.

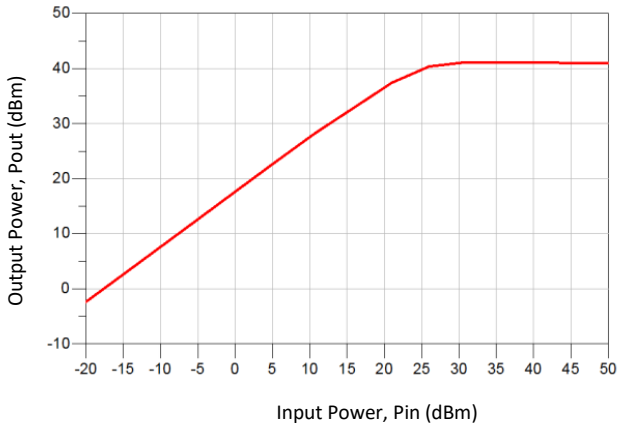

Figure 4-3: GaN transistor PA behavioural modelling.

4.1.2.1 Compensation of Nonlinear Distortion with Analog Signals on GaN Amplifier

Two-tone analog signals are fed into the input (gate) of the amplifier and tested with the linearization circuit in Figure 4-2 above. In this case, the technique uses the gate of the GaN transistor amplifier rather than the input as the GaN PA used for simulations was designed at transistor level. Different frequency spacing can be used. LTE frequency bandwidths range from 1.4 MHz to 20 MHz and LTE-Advanced through carrier aggregation could go up to 100 MHz by aggregating up to a maximum of 5 carriers.

Two tone fundamental signals spaced 5 MHz apart at frequencies 3.3 GHz and 3.305 GHz are tested at different power levels of 5 dBm, 10 dBm and 18 dBm (which happens to be 2 dB below the 1-dB compression point). The spectra after and before applying this injection technique for input level of 5 dBm is shown below in Figure 4-4.

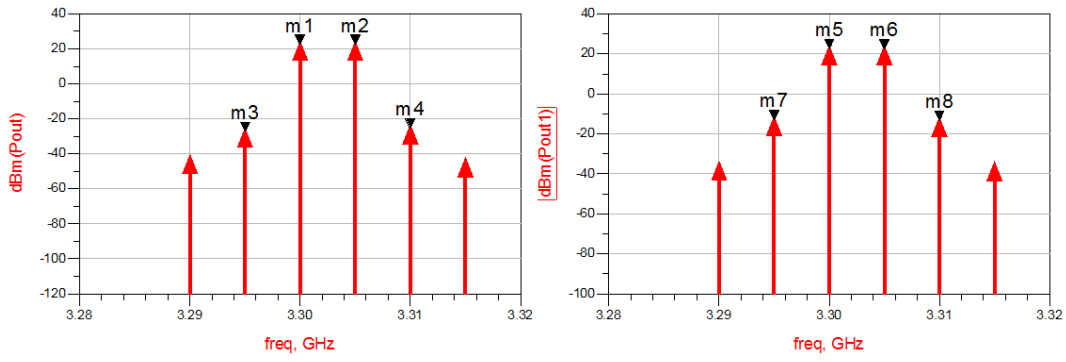

(a) (b)

Figure 4-4: Simulated PA output spectra for 5 dBm input: (a) With injection, and (b) Without injection.

Analysing markers (m7-m3; m8-m4), 15 dB IM3 reduction is observed in this case. Figure 4-5 also shows output spectra with reduction for input power levels of 10 dBm with similar IM3 reduction.

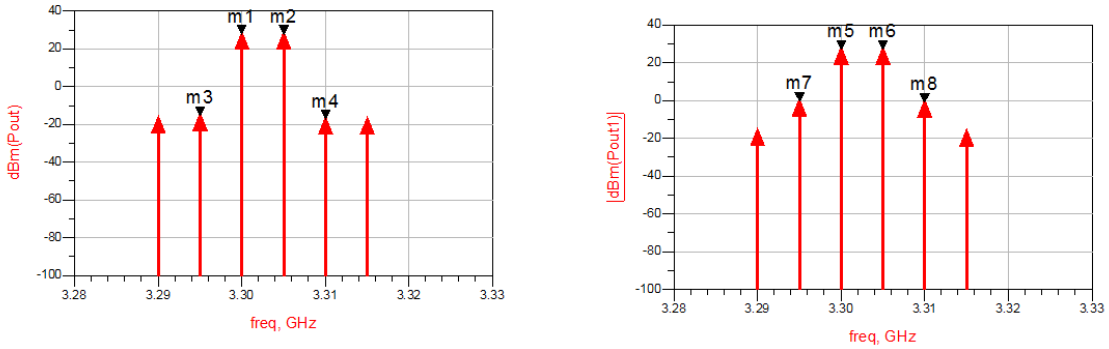

(a) (b)

Figure 4-5 Simulated PA output spectra for 10 dBm input: (a) With injection, and (b) Without injection.

By going pretty much closer to saturation at the input power level of 18 dBm at the gate of the GaN transistor and with the same 5MHz frequency spacing, further reduction could be observed in Figure 4-6. This time we have a reduction of about 20 dB which is about 5 dB more than the other spectrum at input gate levels of 5 dBm and 10 dBm which gave a reduction of about 15 dB.

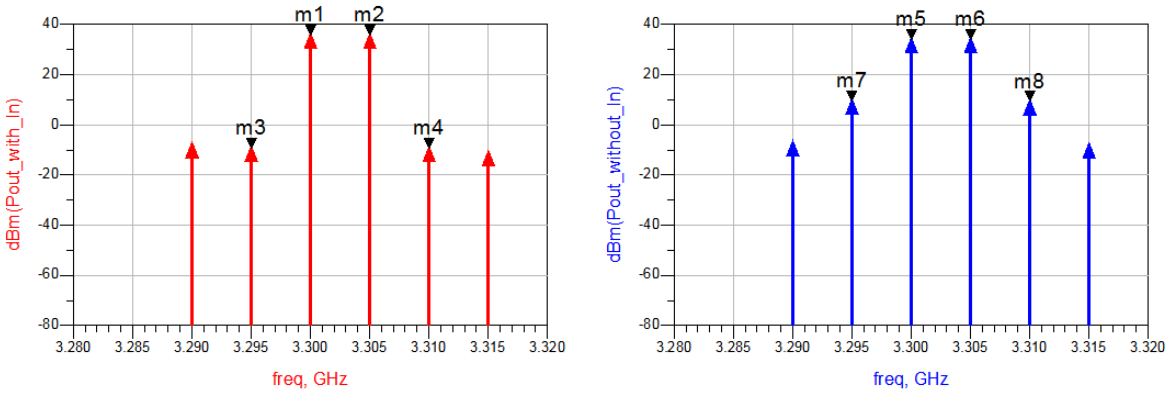

(a) (b)

Figure 4-6: Simulated PA output spectra for 18 dBm input: (a) With injection, and (b) Without injection.

From the results presented in Figure 4-4, 4-5 and 4-6, intermodulation distortions have been observed at the output spectrum when input signals go through the amplifier's input (gate of the Transistor). By applying the injection technique proposed at the gate and drain of the GaN amplifier under test, a reduction in nonlinear distortions has resulted due to the simultaneous injection of the second harmonics at the amplifier's input (gate) and output (drain).

Digital signals would be used in the next section to investigate the implementation of the technique for mobile communications technology such as 3G, 4G and 5G communications systems.

4.1.2.2 Compensation of Nonlinear Distortion with Digital Signals on GaN Amplifier

As observed from the earlier analysis of the analog signals, the technique works better when it operates close to the 1 dB compression point. Digital signals such as QPSK and QAM would be sent through the GaN transistor amplifier at input power level of 18 dBm using different range of LTE specified frequency bands. The IM3 for the digital signals were taken at the same frequencies (marked m3 and m4) for the analog cases described in Figure 4-4, 4-5 and 4-6 described above. LTE requires band of 1.4 MHz, 3 MHz and 5 MHz up to 20 MHz. Tests with 1.4 MHz, 3 MHz and 5 MHz have been presented in this report as it is very much possible to do experimental verifications in the Laboratory.

These simulations were done using the block diagram in Figure 4-2. The digitally modulated (64-QAM) signals were used transmitting 6 bits per symbol. The second harmonics were taken from the output and fed back through a bandpass filter. The gain amplifier and phase shifters are used to carefully adjust the amplitude and phase by using tuning optimisation techniques. The Keysight/ADS optimisation parameter was used to achieve the optimum value for amplitude and phase for each symbol. The injection is done by feeding back second harmonics back into the gate and the drain of the GaN transistor amplifier and the simulated results are shown in Figure 4-7, 4-8 and 4-9 for different LTE frequency levels at 1.4 MHz, 3 MHz and 5 MHz respectively.

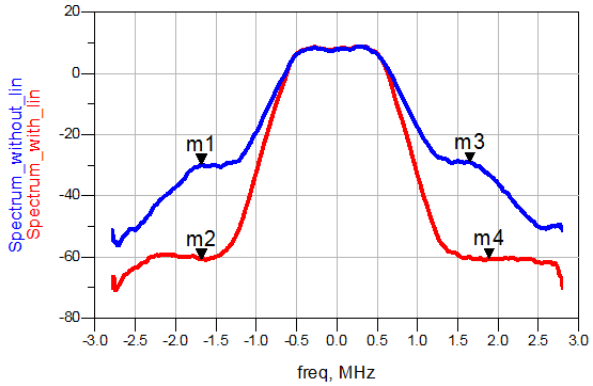

Figure 4-7 Simulated PA output spectra for 1.4 MHz digital modulated signal with and without injection

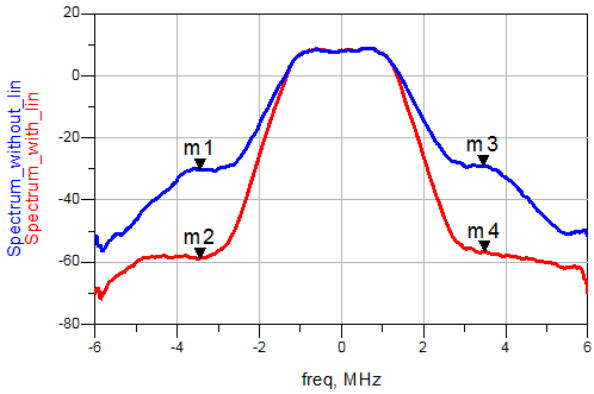

Figure 4-8 Simulated PA output spectra for 3 MHz digital modulated signal with and without injection.

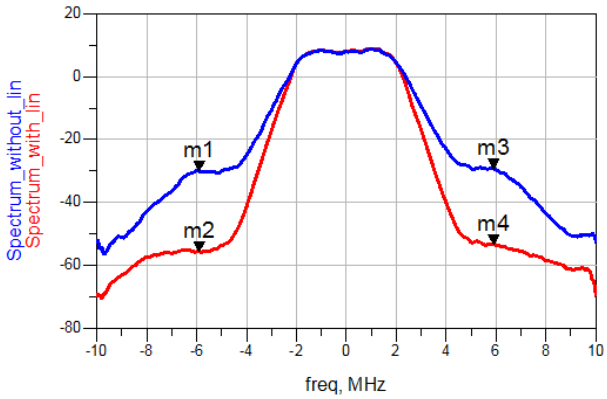

Figure 4-9 Simulated PA output spectra for 5 MHz digital modulated signal with and without injection.

By analysing tuning and optimizing the amplitude and phase of the second harmonics and feeding it back into the gate and drain of the amplifier, the nonlinear distortions have been effectively reduced by 31 dB in Figure 4-7, 28 dB in Figure 4-8 and 25 dB in Figure 4-9. It could be observed that as the bandwidth increases, there is a slight reduction in improvement based on the technique. This technique has been very effective in reducing nonlinear distortions that occur at the output of the designed GaN transistor PA.

Furthermore, a real power amplifier (PA) is used to compare simulations with measurements. A fabricated PA is needed for experimental verification. Figure 4-10 shows the picture of the real mini-circuits ZFL-500 PA available in the laboratory. The technique is going to be slightly modified as we cannot directly utilize the gate and drain of the PA as in the case of the designed GaN transistor amplifier. The measured results of this PA are then used in Keysight/Agilent ADS instead of the GaN. The ZFL-500 amplifier is designed to operate mainly at 500 MHz center frequency and is characterized by 20 dB gain and 4.5 dBm input power 1-dB compression point (P_1dB) as shown in Figure 4-10.

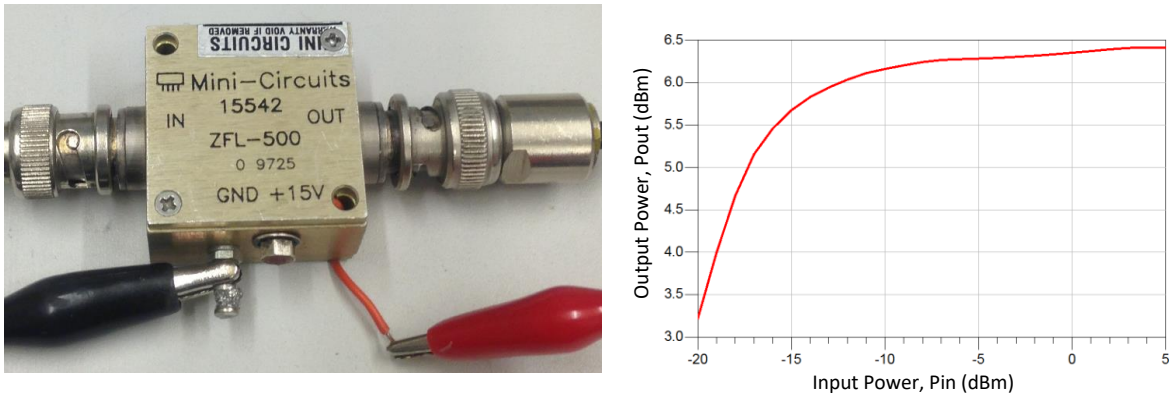

Figure 4-10: ZFL-500 PA under test with its input/output relationship.

The second harmonic injection circuit in Figure 4-2 is slightly modified as the Device under test (DUT) this time is the real power amplifier ZFL-500 mini-circuit and it's no longer at transistor level. Only the feedback that requires the second harmonic to the input is maintained whilst the output feedback loop is neglected. This time, the second harmonics is injected into the input of the PA rather than the gate and drain for the GaN transistor amplifier at center frequency of 500 MHz.

Digitally modulated QAM signals are used to test the real amplifier to see how it responds to the injection technique. The harmonic injection technique is implemented on the ZFL-500 PA at LTE frequencies of 1.4 MHz, 3 MHz and 5 MHz. The input power level used for this test is 3 dBm which is about 2 dB less than the 1 dB compression point. Two tone fundamental signals at frequencies 500 MHz and 501.4 MHz were initially used with power levels 3dBm at the amplifier input which is 2dB below 1-dB compression point shown in Figure 4-10. The spectra after and before applying this injection technique are shown in Figure 4-11 and Figure 4-12 below. A reduction of about 10 dB is still being observed in this case but with great potential for further improvement. This same technique will be used further for increasing bandwidths such as 3 MHz and 5MHz analog and digital signals.

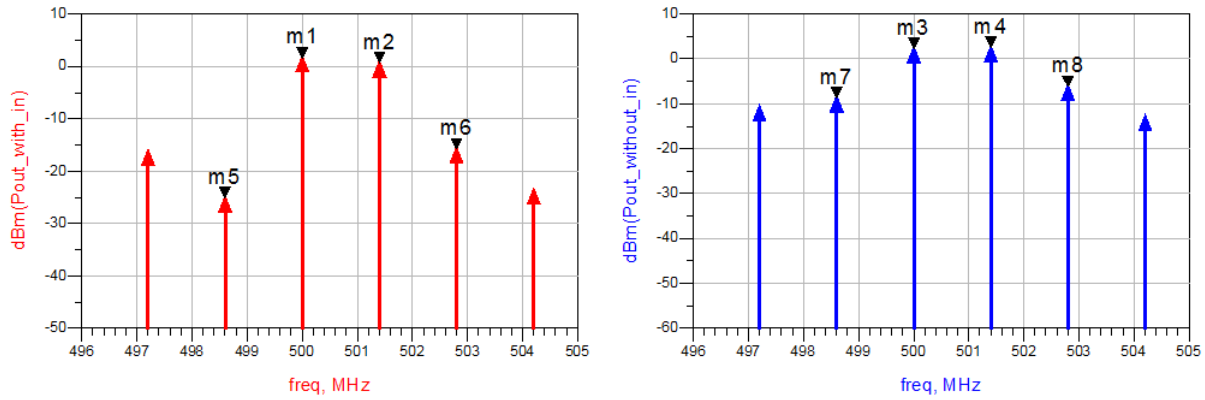

Figure 4-11: Measured PA output spectra for two analog signals spaced 1.4 MHz after and before injection.

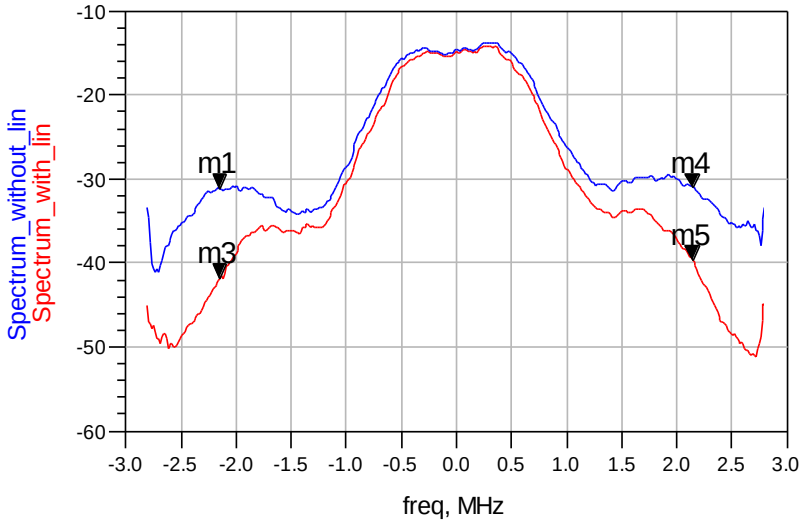

Figure 4-12: Measured PA output spectra for 1.4 MHz digital modulated signal with and without injection.

Figures 4-12 to 4-15 also give output spectrum with nonlinear distortion reduction for 3MHz and 5 MHz bandwidth respectively.

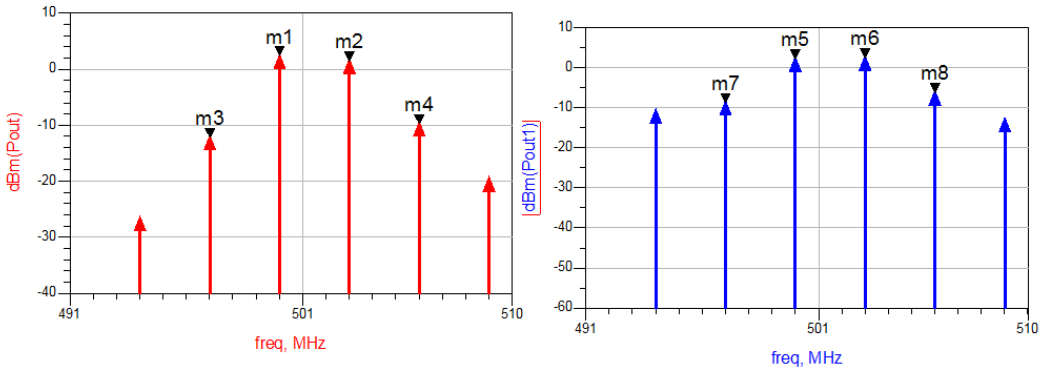

Figure 4-13: Measured PA output spectra for two analog signals spaced 3 MHz after and before injection.

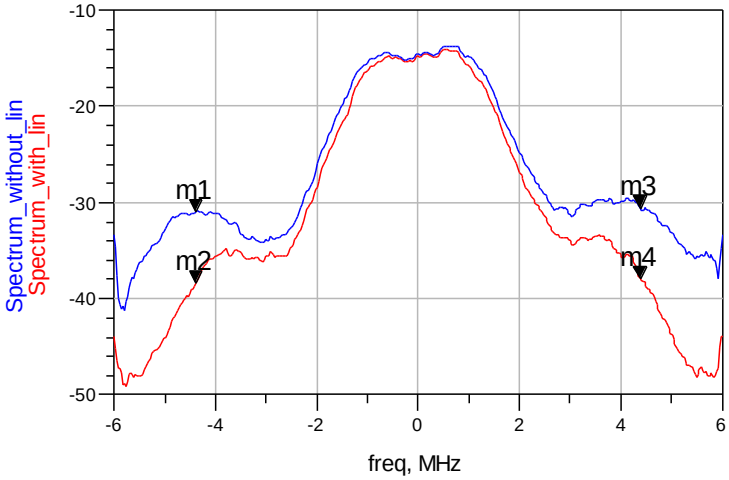

Figure 4-14: Measured PA output spectra for 3 MHz digital modulated signal with and without injection.

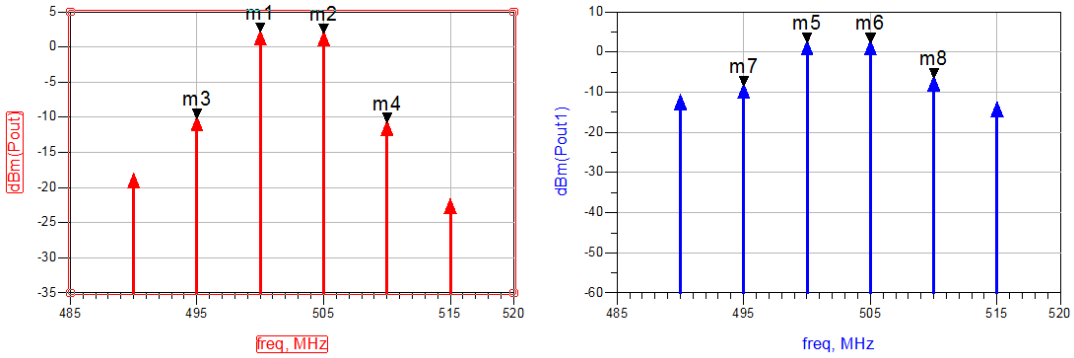

Figure 4-15: Measured PA output spectra for two analog signals spaced 5 MHz after and before injection.

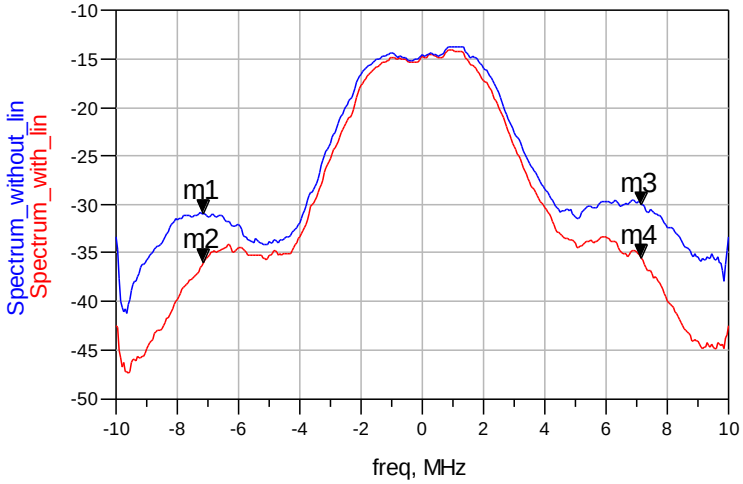

Figure 4-16: Measured PA output spectra for 5 MHz digital modulated signal with and without injection.

The output response is different when using a real PA compared to the designed GaN transistor amplifier. The analog tests show that the real amplifier behaviour can be influenced by different distortions and behave differently. From the two-tone test results in Figure 4-11, 4-13 and 4-15 it could be observed that the technique could be flexible to achieve more reduction on either side of the fundamental signals. Hence, it is very possible to achieve more reduction at one side than the other and it could also lead to a slight trade-off of the gain. However, with digital signals the nonlinear reductions behave more symmetrical in nature.

Figure 4-12 gave a reduction of about 10 dB, Figure 4-14 recorded a 7 dB reduction and Figure 4-16 shows an improvement of about 4 dB. From these results, it was observed that there was a steady decrease in performance using the technique for higher bandwidths. This led to further scrutiny as even though the technique has been successful in suppressing nonlinear distortion, it is important that it could be effective for higher bandwidth cases as those will be needed for advanced wireless systems that require high data transmission. Hence, for higher bandwidth cases, the technique must be modified to adapt to increasing bandwidth applications. Based on this, the next sections will look to modify the second harmonic injection technique with the aid

of the inkjet-printed band-stop filters designed in Chapter 3. This modified technique would also be utilised for LTE's advanced carrier aggregation networks that require band combinations. Any successful modifications will be vital in suppressing distortions for advanced mobile communication systems such as 4G's LTE and LTE-Advanced.

4.2 Compensation Using Band-stop Filters

Figure 4-17 gives the proposed concept of using a band-stop/notch filter to effectively suppress and curtail nonlinear distortions in the power amplifiers of wireless transmitters. Previously, band-stop filters are mainly used at the output to reject unwanted signals. In this case, the nonlinear distortions are so close to the signal that it will be very difficult to reject unwanted signals without altering the signal itself.

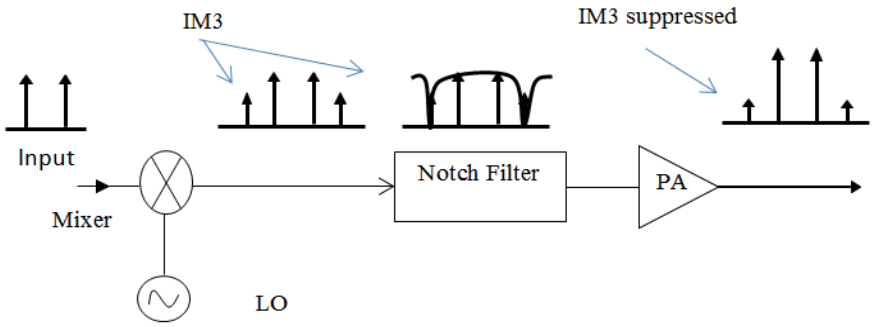

Figure 4-17: Suppression of IM3 with the aid of a narrow-band band-stop filter.

In this proposed concept as shown in Figure 4-17, the fundamental tones f_1 and f_2 are fed into the input and intermodulation products are produced due to the mixers nonlinearity as well. The third-order intermodulation products (IM3) $2f_1$-f_2 and $2f_2$-f_1 are mostly evident as they are very close to the main signal, have the highest power level and cannot be easily removed by the mere use of a bandpass filter. These IM3 products acts as additional interfering signals to the main signal and they should be suppressed to have a more efficient and linear output. By using a narrowband band-stop (notch) filter in front of the power amplifier, interfering signals and intermodulation products (IM3) are minimised before amplification by the PA. This allows for a more linear output as the fundamental tones are amplified more thereby suppressing the nonlinear distortions at the output of the PA.

The filter designed in chapter 3 would be used for this process of reducing nonlinear distortions by filtering. Initially, the filter designed as shown in Figure 3-8 will be used at the output of the PA to show its rejection capabilities. The power amplifier (PA) in question is the ZFL-500 PA. The rejection using this notch is used after the PA as the power level of the PA is low and for the notch to attenuate sufficiently, its output needs to be amplified. Figure 4-18 shows the rejection powers of the designed notch filter at its center frequency of 3.25 GHz when the filter is used after the PA at the output of the power amplifier.

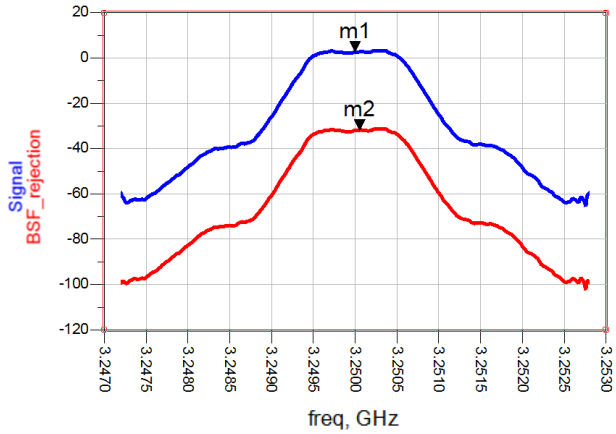

Figure 4-18: Band-stop filter rejection at 3.25 GHz.

The signal sent into the PA at the center frequency of the designed filter at 3.25 GHz. The notch filter is used after the PA. The signal at the output with and without the notch filter is seen in Figure 4-18 with about 34 dB of rejection observed. The notch filter can also be used to reject nonlinear distortions by following the process shown in Figure 4-17.

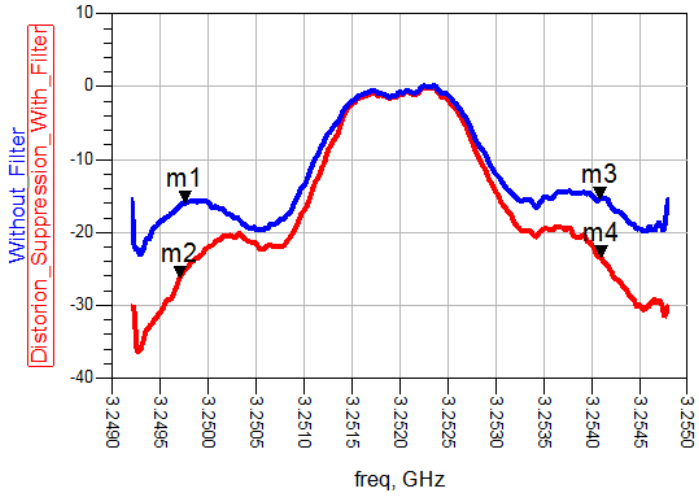

Figure 4-19: Suppression of nonlinear distortion by notch filter.

By using the resonant properties of the notch filter before the PA at frequencies where the third-order intermodulation products operate, nonlinear distortions could be reduced. Figure 4-19 shows the reduction of about how the notch filter designed in this paper with resonant frequency was able to suppress nonlinear distortions at the carrier frequency of 3.252 GHz giving a reduction of about 10 dB. However, the signal at the output of the ZFL-500 had to be amplified further as the output signal was at -16. A gain amplifier was used to achieve an output above 0 dB so that the rejection of the notch filter could be fully observed. Due to this another amplifier ZHL 4240W would be used for further tests to eliminate further amplification at the output of the amplifier.

Another filter designed in Figure 3-10 to reject Wi-Fi signals is studied extensively and investigated to compensate for nonlinear distortions. The power amplifier used this time is the ZHL 4240W as it can operate at higher powers than the ZFL-500 PA. For the notch filter to reject unwanted signals properly for simulations, the actual signal should be above 0 dB. The ability of the designed filter to attenuate signals at its center frequency prior to the PA is examined. Figure 4-20 shows the rejection powers of the designed notch filter at its center frequency of 2.375 GHz.

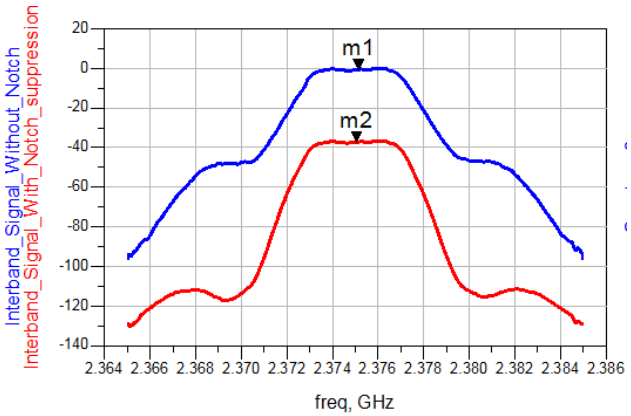

Figure 4-20: Band-stop filter rejection at 2.375 GHz.

64 QAM digitally modulated signal is sent into the PA (ZHL 4240W) at the center frequency of the designed filter at 2.375 GHz. This is to be able to observe how effective the notch filter could be when rejecting interfering signals at that frequency. By choosing different input power levels, different rejection values could be observed when the notch is used to reject the signal before the PA. At input power level of -23 dBm, the highest rejection powers of the notch are noticed to be about 37 dB as shown in Figure 4-20.

The notch filter will also be implemented using the proposed filter concept described in Figure 4-17. The filter is used prior to the ZHL 4240W PA. By using the resonant properties of the notch filter before the PA at frequencies where the third-order intermodulation products operate, nonlinear distortions could be reduced. In this case, with the PA operating at a frequency of 2.39 GHz, by careful observation of the IM3 products, the notch filter designed at resonant frequency of 2.375 GHz could reject such interference without affecting the fundamental signal too much due to the low loss and high Q characteristics of the notch filter.

Figure 4-21 shows the reduction of about how the notch filter designed in this paper with resonant frequency was able to suppress nonlinear distortions at the carrier frequency of 2.39 GHz giving a reduction of about 12 dB.

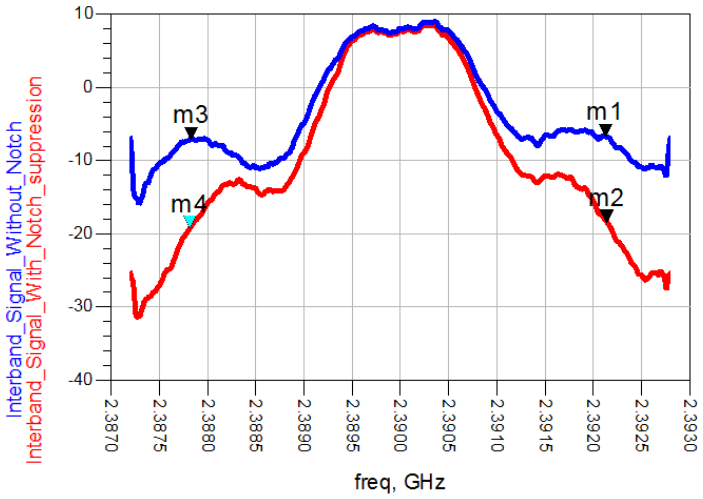

Figure 4-21: Suppression of nonlinear distortion by notch filter for 1.4 MHz bandwidth.

Furthermore, it could be observed that unlike the injection case above whereby the suppression abilities were reducing for increase in bandwidth, it is not the case with the notch filter suppression technique. With good adaptation, the suppression at 3MHz and 5 MHz are at about 12 dB as well as shown in Figure 4-22 and Figure 4-23.

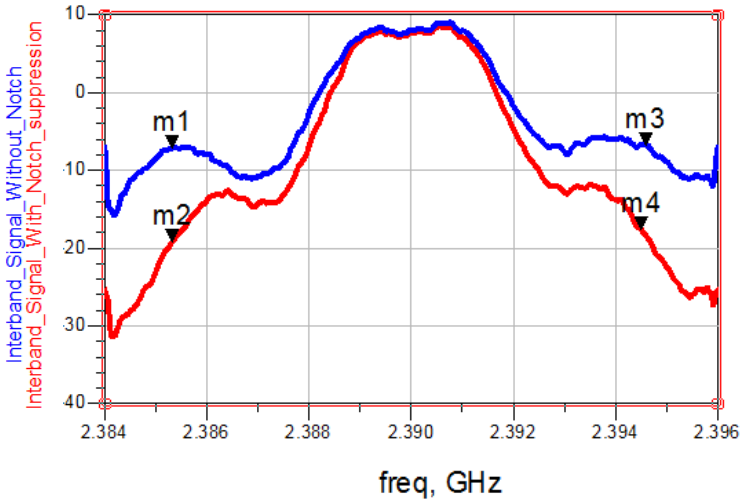

Figure 4-22: Suppression of nonlinear distortion by notch filter for 3 MHz bandwidth.

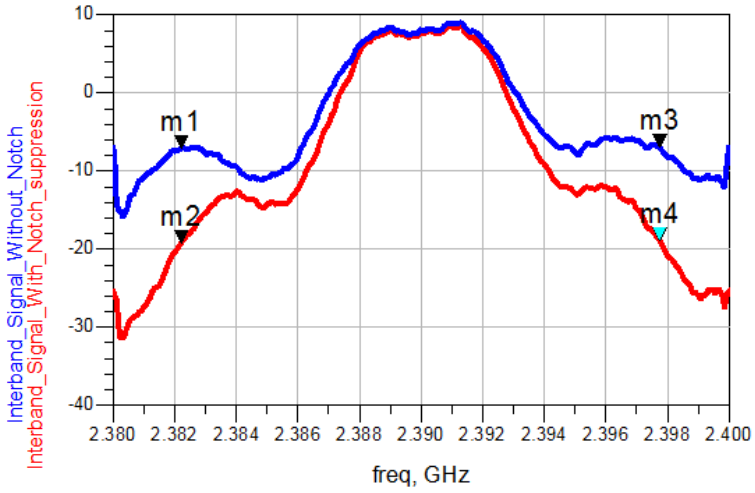

Figure 4-23: Suppression of nonlinear distortion by notch filter for 5 MHz bandwidth.

It was further noticed that the properties of the band-stop filter used has maintained reduction performance for even higher bandwidths. This technique also compensates for higher band width cases because the band-stop filter can reject such 3rd order intermodulation products without necessarily affecting the main signal and it would be easier to design a dual-band notch filter to reject such distortions. Such kind of compact filters can also be incorporated into the second harmonic linearization technique. To reduce size, the linearization architecture in chapter 4.1 can still be modified by replacing the bandpass filter with the miniaturised notch filter. However, that implies that would mean that the second harmonics may have to be fed back in by passing through the band-stop filter. By removing the BPF, the circuit component size is reduced as the designed narrow band notch filter is very small in size and RF bandpass filters are generally large at such frequencies. The two techniques are to be combined in the next section for next generation networks such as 4G LTE and LTE-Advanced carrier aggregation. These networks utilize multiple carriers with higher bandwidths which would be a limitation for either of the techniques to handle on its own.

4.3 LTE-Advanced Carrier Aggregation

The enormous rise in the use of smart phones and tablet computers have led to demands for higher data rates and the need for more bandwidth-intensive applications. Currently, about 2.6 billion smart phone subscribers and users exist all over the world. It is not just smart phones that have risen tremendously; in general, mobile subscriptions that include tablets, mobile broadband, PCs have all recorded huge increases in subscriptions. The total number of mobile subscriptions globally is still expected to rise further due to the recent increase in popularity of Internet of Things (IoT) devices [4.12]. It is also predicted that by the end of this decade, mobile subscribers would be close to 9 billion.

Such global desire for higher data and faster mobile data services means that mobile network providers must persistently seek efficient and economical solutions that will help to satisfy the needs of their customers. Challenges such as limited spectrum allocations and non-contiguous spectrum blocks also emphasize the need for mobile network operators to find reasonable solutions even as the end-user crave for video applications and other social media apps become

more popular each day. Operators require more capacity and would like to provide higher end user data rates but are also limited by segmented spectrum in multiple bands and regions. These challenges and subscriber demands have driven network operators into deploying carrier aggregation (CA) which happens to be one of the ways to address such issues. CA is a vital trademark of LTE-Advanced applications that permits the combination of two or more resource blocks into a broader channel. This technique has helped operators to improve capacity and network performance, increase capacity and utilize signals with larger bandwidths among others [4.12].

One of the biggest challenges facing operators now is the adequate provision of spectrum. Carrier aggregation is used to solve this spectrum problem which has been adopted for LTE-Advanced Applications. Swisscom became the latest operator to announce the end of its 2G network to free up resources for LTE and 5G. LTE-Advanced is the technology that has been chosen to be the priority of mobile operators in the coming year according to Mobile Europe's annual survey with a high percentage of 42.86%.

4.3.1 Carrier Aggregation with ZFL-500 Mini-Circuits Amplifier

The simultaneous Injection technique has been proven to be successful in reducing nonlinear distortions significantly but as could be seen with the test on the ZFL-500 Mini circuit amplifier, as bandwidth increased from 1.4 MHz to 5MHz, there was a consequent decrease in its suppression abilities.

Next generation networks such as LTE-Advanced require high bandwidths up to 100 MHz for 4G communication systems. For 5G communication systems that will also operate at higher frequency bands with more bandwidth capabilities, the injection technique would need to be investigated and modified to suit such high bandwidth requirements. Therefore, it is very important to modify the technique for carrier aggregation as LTE-Advanced supports the aggregation of 5 carriers up to 100 MHz bandwidth [4.13].

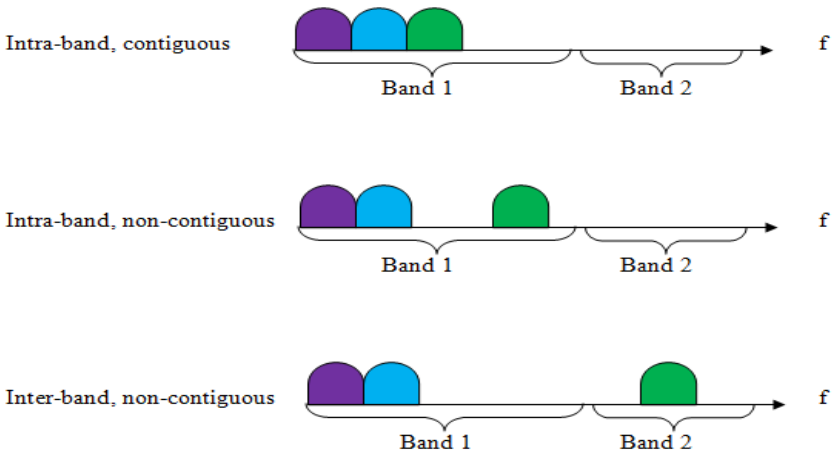

Figure 4-24: Inter and intra-band carrier aggregation with 3 carriers.

In this thesis, this notch filter will be used in rejecting unwanted signals as well as limiting nonlinear distortions for non-contiguous inter-band wireless transmitters for LTE applications. Other techniques have not considered the impact of nearby interference which could affect the

way the third order IM products will occur at the output which limits the impact of the injection technique. It is observed that the novel notch filter in chapter 3 could also play a vital role in the linearization circuit of the proposed technique. Therefore, the circuit in Figure 4-2 is modified as shown in Figure 4-25, with the adaptation of an inter-stage notch filter.

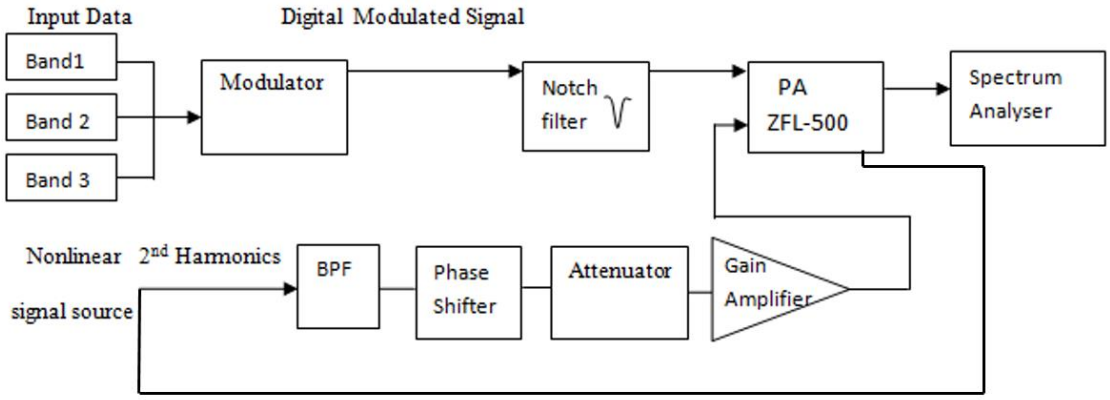

Figure 4-25: Proposed linearization technique for carrier aggregation.

Figure 4-25 shows how the notch filter is integrated with the proposed linearization circuit block diagram for carrier aggregation. In this architecture, aggregation is arranged with contiguous carrier components band 1 and band 2 as intra band contiguous and band 3 is allocated as their inter-band non-contiguous counterpart. Digital Modulated signals such as QPSK, 16 QAM and 64 QAM are used as input. 64 QAM is the modulation type used with LTE channel bandwidths such as 1.4 MHz, 3 MHz and 5 MHz. These signals are fed into the modulator. Band 1 and band 2 are the required bands and band 3 represents the interfering band which the notch is used to reject. The notch filter is used to reject the interfering band prior to amplification to obtain an output that will be easier to cancel out with the injection technique. The second order harmonics are then fed back into the input of the amplifier through the BPF after the interfering band has been rejected. As discussed earlier, the phase shifter and gain amplifier are used to carefully choose the amplitude and phase through optimisation and tuning techniques for cancellation of IM3 products.

The linearization circuit as shown in Figure 4-25 is designed as a hybrid microwave integrated circuit using the Advanced Design System (ADS) program. The notch filter designed in chapter 3 is used to reject the unwanted signals as shown in the block diagram.

A fabricated power amplifier is used for simulation purposes. Experimental data of this PA is used. The ZFL-500 amplifier is characterized by about 23 dB gain in the 500 MHz frequency range up to about 2.6 GHz but with input power 1-dB compression point (P_1dB) of 4.5 dBm.

In this simulation process, only the components in the second harmonics feedback path (BPF, phase shifters, gain amplifiers, variable attenuators) were used as ideal elements from ADS library meeting specifications and requirements.

The BPF is the first component in the feedback loop used to select only the second harmonics and second-order intermodulation (IM2) products from the PA's output and the variable

attenuator is used to control the attenuation of the second harmonics. The Gain amplifier and phase shifter are used simultaneously to adjust the amplitude and phase characteristics of the second harmonics and IM2 products to suppress the nonlinear distortions that occur at the PA's output.

In Theory, injecting the second harmonics into the input of the amplifier, should suppress nonlinear distortions by arranging for equal amplitude and opposite phase. In this architecture, the second harmonics are fed back into the amplifiers input and output using the components in the second harmonics feedback path (power splitter, phase shifters, band pass filters, gain amplifiers, variable attenuators etc.) are used to achieve this with the Notch filter incorporated to reject further bands substantially.

Using Figure 4-25, three digital modulated signals at 490 MHz, 500 MHz and 2.375 GHz represents band1, band 2 and band3 with band1 and band2 as intra-band and band 3 as the inter-band carrier component. For the Intra-band carrier aggregation process, the second harmonics at 960 MHz and 980 MHz are fed back into the input along with its IM2 products. The amplitude and phase are adjusted for equal amplitude and opposite phase characteristics which in theory should help cancel out third order inter-modulation products. The Notch filter helps to rejects unwanted signals at its resonant frequency of 2.375 GHz and contributes to reduction of nonlinear distortions.

Figure 4-26 shows the results of proposed technique on the real ZFL-500 PA being applied for intra-band carrier aggregation at 490 MHz and 500 MHz feeding back second harmonics into the input and output with notch to reject unwanted signals and suppress nonlinear distortions. The 64 QAM digital Modulated signal with LTE spectrum bandwidth of 1.4 MHz and carrier power of 3 dBm which is close to saturation as it is 1.5 dB below the 1 dB compression point.

Figure 4-26 shows the output spectrum obtained using Keysight/Agilent ADS spectrum analyser at the amplifiers output before and after applying the linearization technique was applied for the 3 dBm input power. As shown in Figure 4-26, the proposed technique has been able to reduce nonlinear distortions up to about 13 dB.

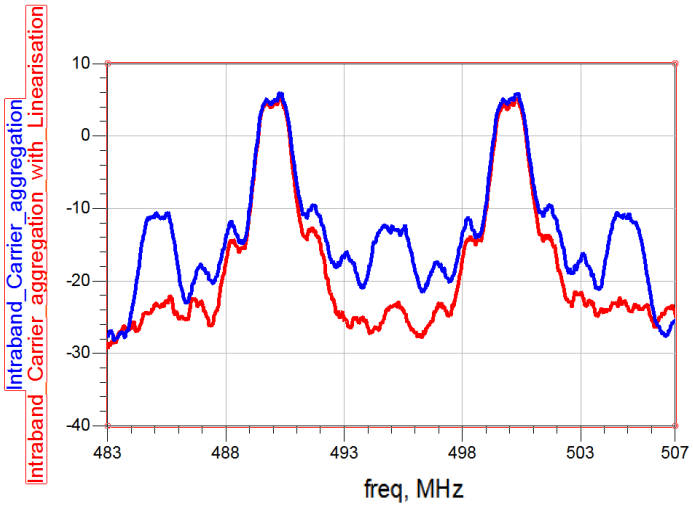

Figure 4-26: Reduction of nonlinear distortions for concurrent dual-band carrier aggregation.

The injection technique proposed has been effective in suppressing intermodulation products. However, the linearization technique has been modified to reduce nonlinear distortions in concurrent dual-band wireless transmitter has been considered. The technique used includes the injection of second harmonics into the input of the amplifier to reject inter-band nonlinear distortions and the use of an inter-stage notch filter to reject unwanted signals. Results show an improvement of about 13 dB in distortion performance. This proposed technique is very useful in concurrent dual-band wireless transmitters and could be used for modern day wireless communication applications such as WiMAX, LTE and LTE-Advanced applications.

4.3.2 Carrier Aggregation with 3 Component Carriers

LTE CA can support up to 5 component carriers up to a maximum of 20 MHz each. Carrier aggregation has been described with 2 carriers in the previous sub-chapter. In this section, 3-component carriers are investigated. Nonlinear distortions are evaluated, and the different proposed nonlinear suppression techniques are utilised. Three LTE component carriers at 480 MHz, 490 MHz and 500 MHz with bandwidth of 3 MHZ each are passed through the wireless transmitter. Figures 4-26 and 4-27 show the difference between the performance in the linear region and nonlinear region.

At the linear region, the 3 carriers are amplified equally when passed through the power amplifier (PA) in the transmitter system with the same amplitude. The output signal increase linearly with increasing input power spectra of each component carrier. All 3 carriers as seen in Figure 4-27 are at about -18 dBm each with intermodulation distortions about 60 dB away from the main signal thereby offering very little interference on the signal sensitivity and maintains linearity.

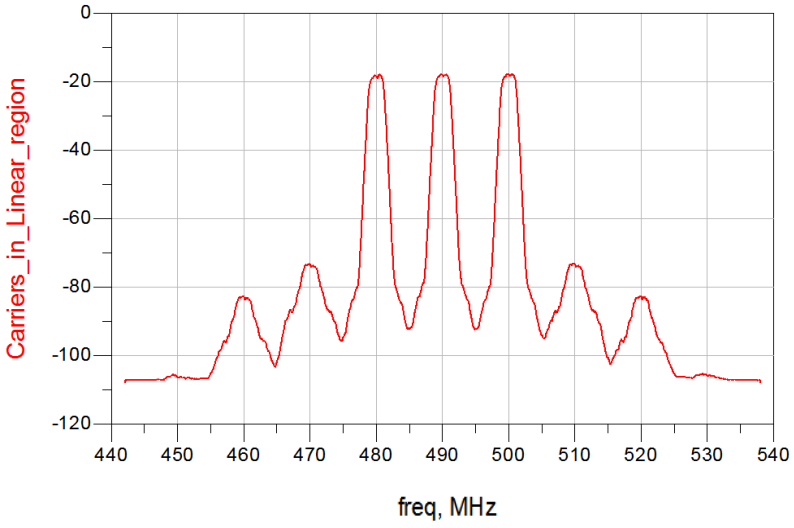

Figure 4-27: 3 Intra-band contiguous carriers in the linear region.

However, in Figure 4-28 where the system operates close to saturation, it could be observed that the behaviour of the carriers are no longer predictable and consistent as in the linear case as shown in Figure 4-27. The amplitudes of the three carriers are no longer the same and the nonlinearities of the carriers have become more obvious and have affected the performance of

the system. More notably, the third order inter-modulation distortions have now been raised to about 6 dB from the main signal compared to the linear case when it was about 60 dB.

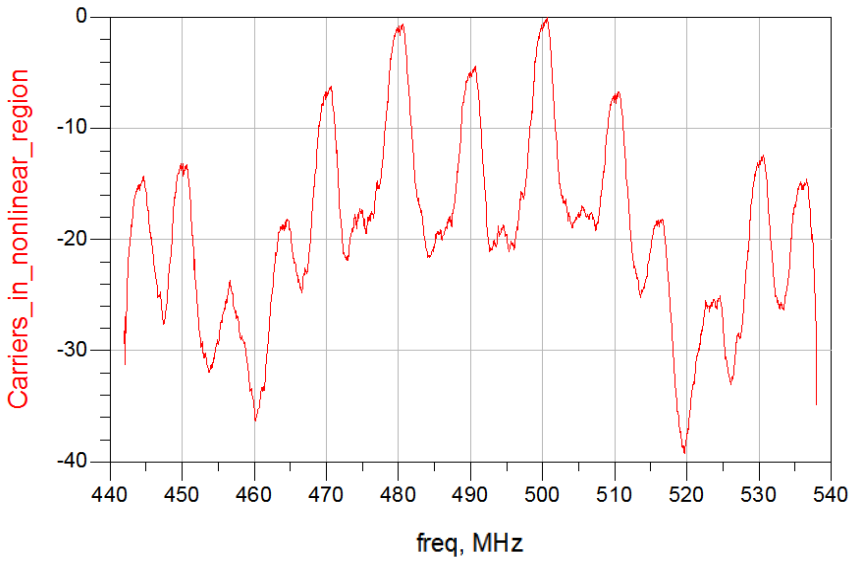

Figure 4-28: 3 Intra-band contiguous carriers in the nonlinear region.

To effectively suppress and reduce these kinds of nonlinear distortions, the injection technique is used. The second harmonic injection method is initially modified to suppress such nonlinear distortions. Because of the characteristics of these distortions, the notch filter will be integrated with the injection technique for inter and intra-band carrier aggregation wireless transmitters subsequently.

Figure 4-29 shows the schematic proposed to resolve the nonlinear problem observed when 3 component carriers operate at saturation.

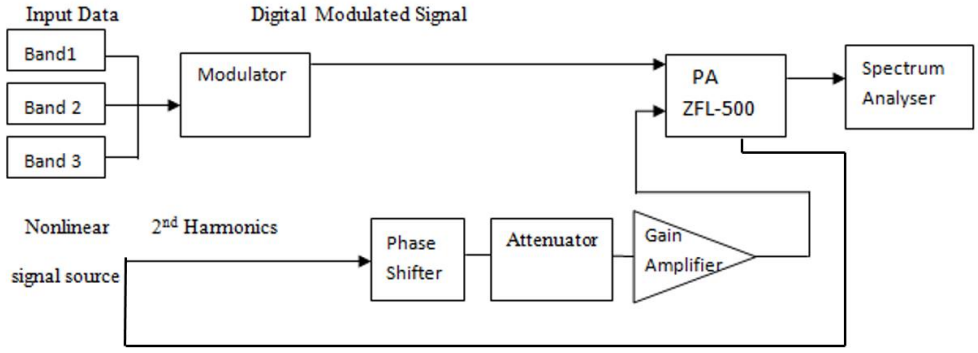

Figure 4-29: Injection technique for 3-carrier CA without notch filter.

The 3 intra-band carriers in Figure 4-29 are passed through a Modulator and then the PA. However, the 2nd harmonics of each carrier will be fed back to the input along with the signal to suppress the effect of the nonlinear components. Careful adjusting of the phase and amplitude will enable effective reduction with the aim to achieve not only reduction in the

distortions but also for the amplitudes of the main signals to become consistent and equal like in the linear case.

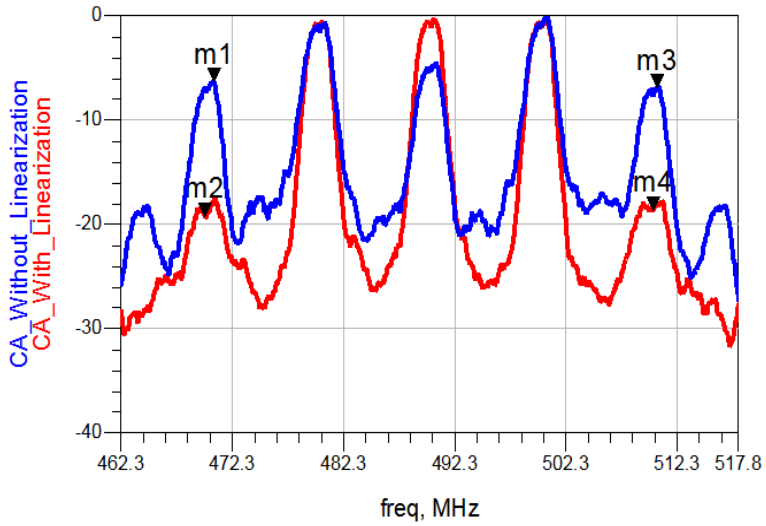

Figure 4-30: Distortion suppression for intra-band CA with 3 carriers.

As seen in Figure 4-30 above, the intermodulation distortion at saturation has been suppressed by about 15 dB restoring the carrier at 490 MHz which is now equal in amplitude with the other two carriers at 480 MHz and 500 MHz as well.

This technique works well and is effective for carrier aggregation that involves two or more carriers. However, the more the carriers, the bigger and complex the system architecture is and component tuning becomes more difficult to realise the necessary results.

As explained in chapter 3, other components in the wireless transmitter chain such as the filters can also play a very vital role both in interference suppression and in reducing the effects of nonlinear distortions.

In the inter-band case, we can reduce the overall system architecture as they do not directly impact on the signal and can be suppressed by a filter. Therefore, a very compact filter with good rejection abilities to reject unwanted signals could be designed. The injection technique could be used for the intra-band part thereby reducing the overall size of the system and also prevent the case whereby large chunks of the signal may be chopped off by the filter. A multiband or more flexible filter can also give further configurability for the design as it has its application in modern day networks that place emphasis on tunability and re-configurability that could make one design suitable at all frequencies.

Narrowband notch filter can be used before the PA to reject interference from other bands. The notch filter already designed in chapter 3 is used here and its signal rejection property is shown in Figure 4-31.

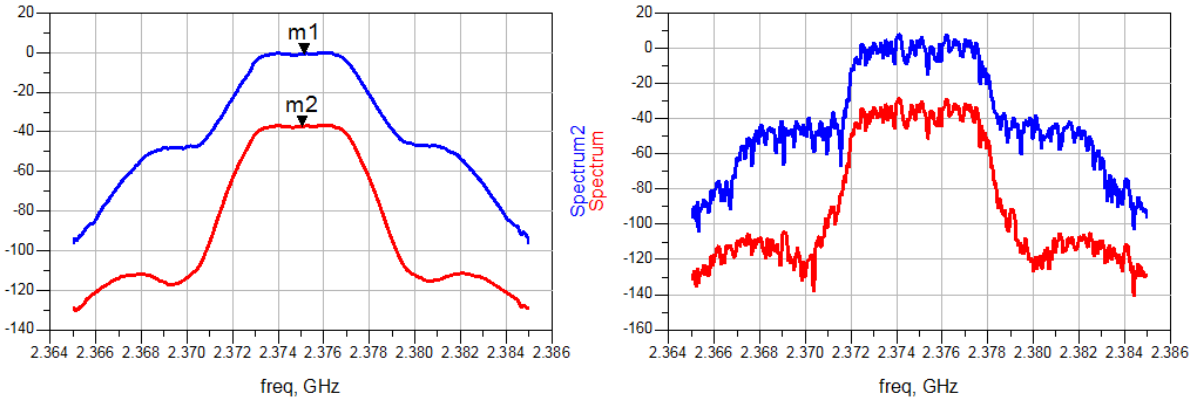

Figure 4-31: Notch filter rejection at center frequency of 2.375 GHz

Using Figure 4-25, two intra-band carriers (representing band 1 and band 2) of 3 MHz each at 2.14 GHz and 2.15 GHz band are sent through the transmitter along with a third inter-band component carrier (band 3) at 2.375 GHz. The aim of the notch is to reject the inter-band signal as much as possible alongside with the injection method. The result from using the proposed technique in Figure 4-25 is shown in Figure 4-32 below.

The notch filter rejected the interfering inter-band signal and the intra-band signal nonlinear distortions were also reduce by about 20 dB which is a very good improvement on the sensitivity of the system. The technique is far more effective than just using the injection technique. The injection technique on its own was only able to achieve about 10 dB improvement in nonlinear distortion. The proposed technique is successful in suppressing nonlinear distortions in Intra-band/Inter-band.

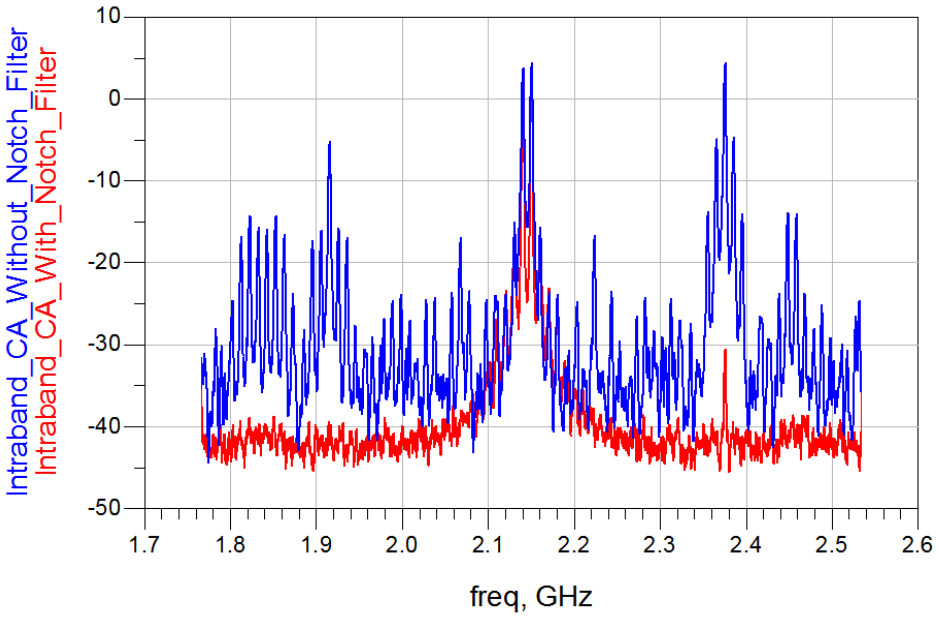

Figure 4-32: CA interference suppression and linearization using notch filter.

4.3.3 Inkjet-Printed Band-stop Filters for Interference Suppression in Multi-Standard Wireless Systems

With the rapid emergence of printed electronics, inkjet printing technology is becoming more prominent due to merits such as reduction in manufacturing costs, shorter fabrication time and aiding mass production flexibility [4.15]. Inkjet printing makes use of nanoparticle inks rather than conventional copper used in traditional techniques permitting the use of flexible substrates. Inkjet printing is preferred to conventional etching techniques owing to its adoption of low-cost processes such as the additive measures. The actual droplet is deposited only where it is needed reducing material usage and waste, making it more energy conservative and environmentally friendly [4.16].

A couple of RF/Microwave/mm-wave components and systems attributed to inkjet printing using different specific substrates have emerged in recent years. For instance, paper is an acceptable substrate used more often in the past decade due to its low cost and simplicity [4.17] but with high frequency absorption drawbacks and a range of humidity issues such as moisture absorption [4.18]. Due to this, other substrates have emanated such as Injected Printed Humidity Sensor on Kapton Substrate [4.19], Flexible Microwave filter on Liquid Crystal Polymer (LCP) Substrate [4.20] and LPDA antenna on PET (Polyethylene terephthalate) Substrate [4.21].

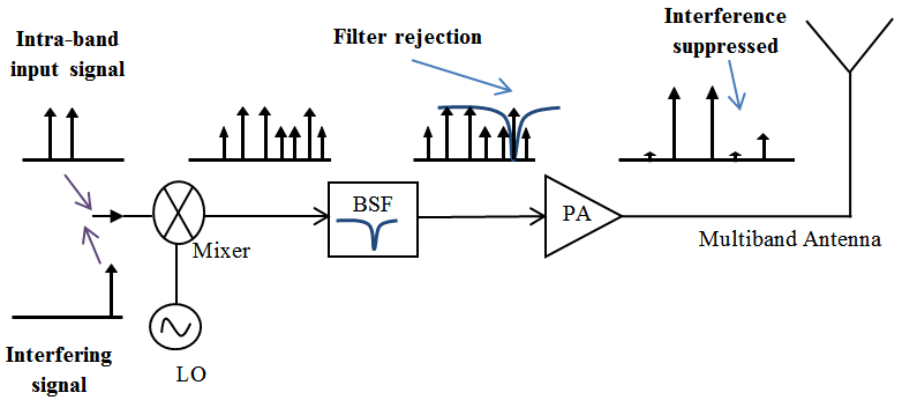

Figure 4-33: Block diagram of the wireless transmitter system for the application of the proposed BSF.

The advancement of flexible electronics, and the push for low cost and efficiency, led to the use of flexible materials for applications with ever keen interest such as wireless, cognitive radio and other high frequency applications have been critically investigated [4.20]. The flexible kapton polyimide film is considered in this paper because it is durable and maintains electrical and physical properties over a wide temperature range withstanding high temperature levels making it attractive for modern applications such as internet of things [4.19].

A novel BSF design using kapton substrate and its flexible polyimide film for inkjet printing is presented. The designed filter is very compact with reduced size and good stopband response characteristics when compared to other published BSFs.

Furthermore, the designed filter is also implemented in a Multi-standard wireless transmitter system. One of the main challenges facing the next generation networks is high data transmission and spectrum availability. Carrier aggregation (CA) is one of the techniques adopted for LTE-Advanced (Long Term Evolution) used by network operators to maximize spectrum availability, improve capacity and network performance, but with increasing levels of intra-band and inter-band interference [4.22].

The BSF can be used to reject such kinds of interference using the technique in Figure 4-33 above. The designed BSF was implemented in this paper and was able to effectively suppress interference in a Multi-band wireless transmitter system to improve performance and would be very useful for next generation networks such as 4G and 5G communication systems.

The filter design should be compact with good selectivity and enough attenuation at cut-off frequency to reject interfering and unwanted signals and improve performance. The narrowband BSF design aims to reject wireless (Wi-Fi) interference at about 2.4 GHz in wireless transmitter architectures

The BSF structure is a T-shaped stepped impedance microstrip configuration as shown in Figure 4-34 below designed in chapter 3. Modifying the defects on the main transmission line, creates different stopband characteristics at different frequencies which aids miniaturization as larger dimensions would normally be required for lower frequencies in such designs.

Using Quasi-TEM approximation equations, the width (W) of the microstrip line, effective dielectric constant (ε_{eff}) and guided wavelength (λ_g) can be obtained using empirical expressions described in chapter three.

For this kind of filter design to achieve compactness, very thin conductors are used. Silver is the metal type chosen for compatibility with the silver nanoparticles used for inkjet printing.

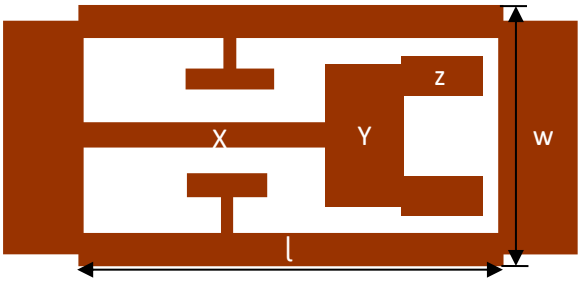

Figure 4-34: Structure of the band-stop filter.

The final dimensions of the filter structure shown in Figure 4-34 taken from its design in chapter 3 above are as follows: l = 15mm, W = 0.11 mm, X = 14.98 mm by 0.01 mm, Y = 0.6 mm by 0.05 mm and Z = 0.005 mm by 0.39 mm.

The structure is designed on a 50 µm thick kapton substrate of dielectric constant (ε_r) of 3.4 and loss tangent (tanδ) of 0.0021. Simulations are done using the *em Sonnet* commercial software. The simulated results of designed filter are shown in Figure 4-35.

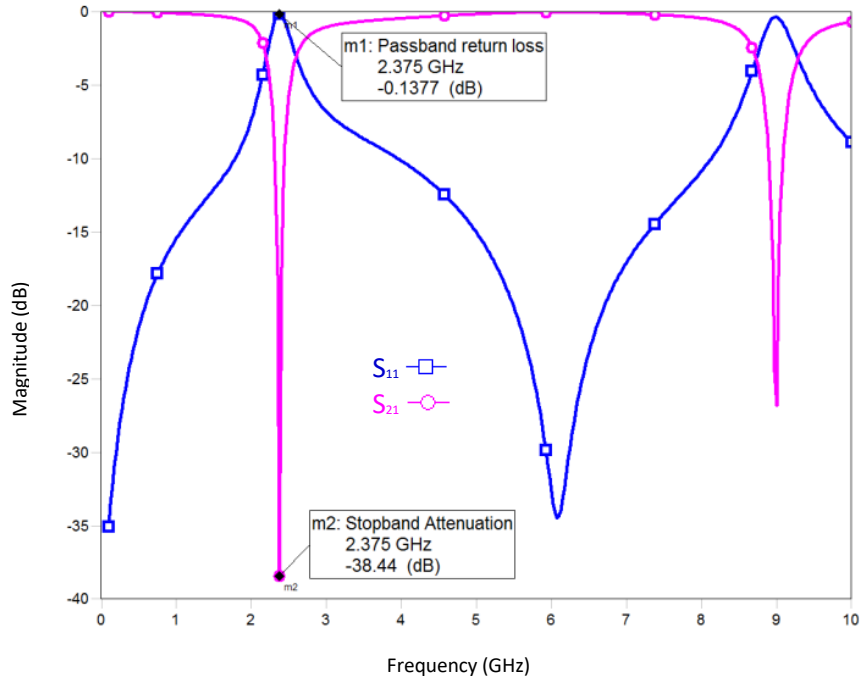

Figure 4-35: Interference Rejection at BSF cut-off frequency.

The structure produces good stopband rejection (S_{21}) of -38.44 dB, fractional bandwidth (FBW) of 6.25% and Q-factor of 16 at the resonant frequency of 2.375 GHz with its passband less than -0.14 dB exhibiting a very low loss. Figure 4-35 also presents excellent inter-band return loss performance properties (S_{11}> -30 dB up to 10 GHz).

The designed filter shows excellent band-stop properties such as attenuation and loss when compared to other filters as shown in Table 4-1.

Table 4-1: Size and performance comparison of BSF.

(BSF)	Dielectric Constant (ε_r)	Substrate thickness (mm)	Normalized area (λ_g x λ_g) (mm*mm)	Return Loss S_{11}(dB)	Attenuation S_{21} (dB)
[4.23]	3.48	0.508	0.28*0.062	> -15	> -30
[4.24]	2.2	1.54	0.35*0.065	> -10	> -45
[4.25]	2.55	1.5	0.201*0.101	> -10	> -25
[4.26]	2.65	1.6	0.22*0.11	> -15	> -25
[4.27]	2.5	2.63	0.17*0.07	> -5	> -35
This work	3.4	0.05	0.27*0.002	> -30	> -35

The proposed band-stop structure has rectangular area of 15 mm x 0.11 mm. By using equations (1) – (3), the normalized area of other similar band-stop filter structures has been calculated and compared in Table 4-1 below. The presented structure occupies the smallest rectangular area and records the least normalized area (0.27 λ_g x 0.002 λ_g).

4.3.3.1 BSF Implementation in Multi-Standard Wireless Systems

The designed BSF in chapter 3 and described above could be introduced into the wireless transmitter architecture. Figure 4-36 shows the implementation of the BSF (DUT) in a 4G wireless transmitter to investigate its rejection abilities.

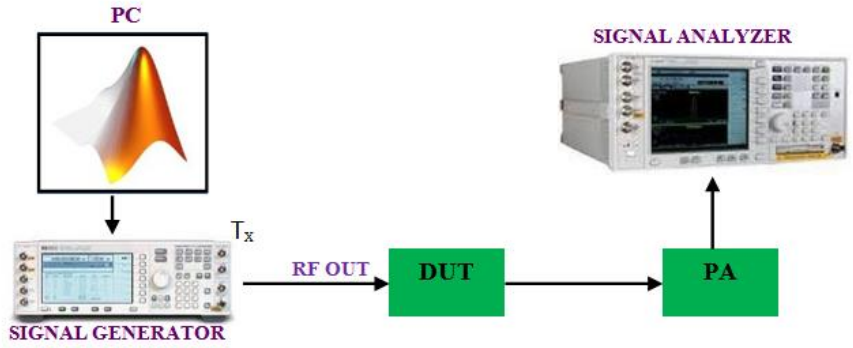

Figure 4-36: Band-stop filter implementation in a 4G wireless transmitter.

A 3 MHz LTE signal is generated in the signal generator. The signal is modelled, and measured results used in Agilent Keysight Signal Studio Kit. The DUT (Device under Test (BSF)) was fed by the 3 MHz LTE signal at the resonant frequency of the DUT (2.375 GHz). The signal passes through the DUT and then the Mini-circuits ZFL-PA. The results with and without the BSF could be seen in Figure 4-37 below. The BSF has been able to successfully suppress interference above 30 dB. However, for the BSF implementation in this paper, placing the DUT before the PA is preferred as it ensures that interference is suppressed prior to amplification. Figure 4-37 also shows the advantage of placing the DUT (BSF) at the input and output of the PA with the former giving a better overall output performance with good interference rejection abilities as well as increasing sensitivity and linearity as well.

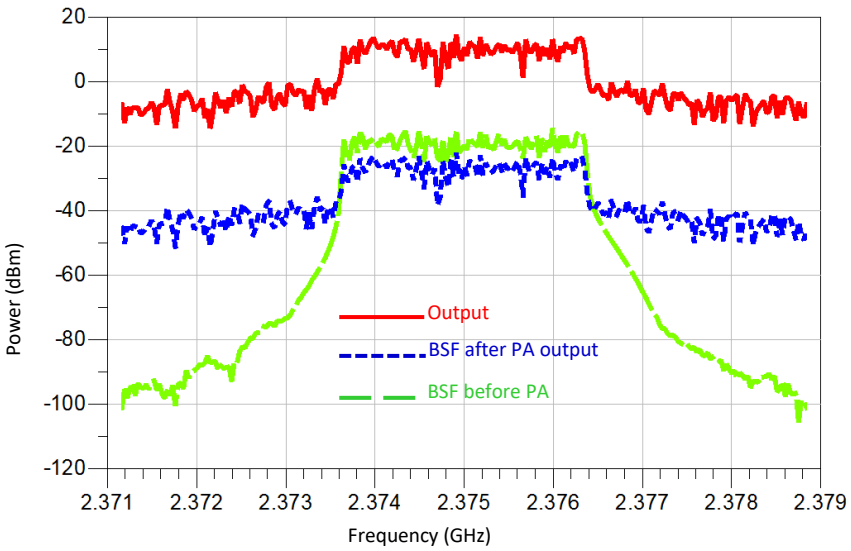

Figure 4-37: Interference rejection at BSF cut-off frequency

Furthermore, the BSF can be used useful to suppress interference in next generation Multi-standard systems such as LTE-Advanced and 5G communication systems. LTE-A carrier aggregation is becoming very prominent as the quest for higher data speeds increase. One of its major challenges' stems from reduced spectrum availability due to larger bandwidths applications. By aggregating carriers, higher data speeds could be achieved, but it comes at a cost of high levels of intra and inter-band interference. The BSF filter presented could be used to reject inter and intra-band interfering signals for such applications.

Figure 4-38 is the schematic for interference suppression with the BSF in such Multi-band wireless system. In this test setup, two 3 MHz LTE intra-band signals (f_1 and f_2) are transmitted along with a third interfering signal (f_{Int}) still using the multiband rejection technique described in Figure 4-33. The designed BSF rejects the interfering signal (f_{Int}) which reduces the noise level at the input of the power amplifier. When the PA amplifies the signal at its input, it gives a better output performance and interference is seen to be attenuated effectively.

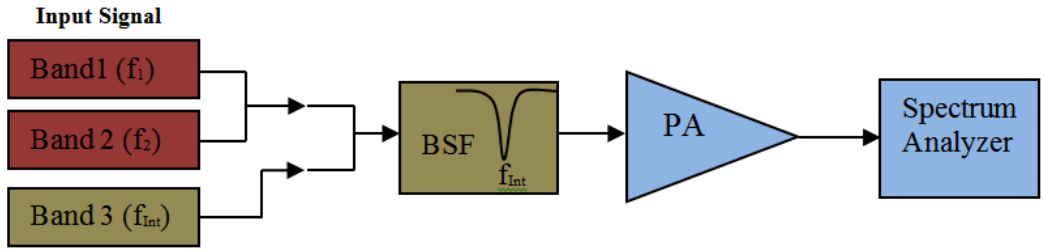

Figure 4-38: Block diagram of BSF implementation for the multi-standard transmitter system.

The effect of such interfering signal is shown in Figure 4-39 whereby the interfering signal reduces the gain of the signal by over 3 dB but most importantly, adds unwanted spurious responses thereby leading to a high increase in noise levels which reduced the sensitivity of the system. This impacts the system performance negatively. Rejecting the interfering signal with the BSF restores the two intra-band signals (as shown between 2 and 2.3 GHz in Figure 4-39) to its initial state without the interfering signal.

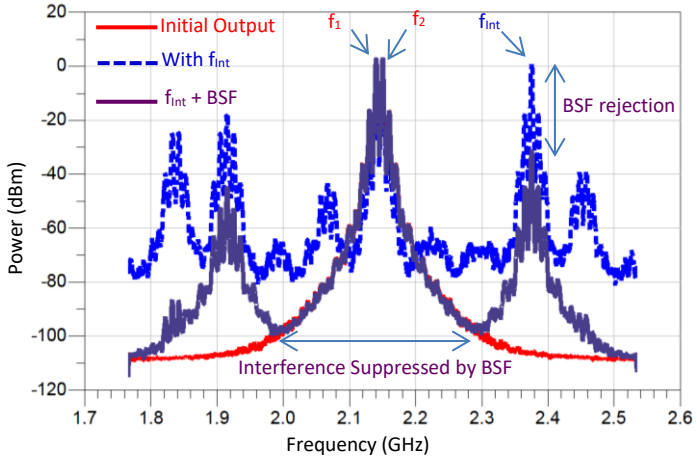

Figure 4-39: Multi-band interference suppression with BSF

The designed BSF has been able to reject the interfering signal (f_{Int}) by more than 30 dB and the effects of the interfering signal on the overall wireless transmitter system has been sufficiently suppressed thereby improving overall system sensitivity and performance.

4.4 Conclusions

In this chapter, nonlinear distortions in wireless transmitters have been evaluated and suppression techniques have been implemented. The second harmonic injection technique was successful for suppressing these distortions. However, as bandwidth increased (towards and more than 5 MHz) for evolving technologies, its suppression abilities reduced. Also, the technique had some limitations with nearby interference that may impact the IM3 products. This led to the integration of a narrowband BSF (notch) filter into the multiband system. The notch filter gave a more linear output when used prior to the PA's amplification process. This technique was adopted for LTE Advanced's intra-band and inter-band carrier aggregation involving 2 and 3 multi-carriers with significant nonlinear distortion suppression observed.

Also, the highly compact narrowband BSF designed in section 3.3 has been implemented in a Multi-standard wireless transmitter system to suppress nearby interference and nonlinear distortions. The BSF was able to maintain the IM3 reduction abilities as bandwidth increased from 1.4 MHz to 5 MHz which improved on the drawback noticed with the conventional second harmonic injection technique. In this technique, the BSF rejects interference prior to amplification achieving a better overall sensitivity and linearity performance than the case whereby it is used at the output of the PA. The BSF was successful in rejecting the interfering signal by about 30 dB whilst improving the sensitivity, linearity and improving the overall performance of Multi-standard wireless systems. This BSF is very compact and cheap which makes it useful for suppression of various kinds of interference in modern day networks that require miniaturisation and minimal complexity. The modified injection technique with BSF filter proposed in this section will be vital for LTE Advanced carrier aggregation and 5G networks that will even utilise higher bandwidths above 20 MHz.

4.5 References

[4.1] C.S. Aitchison, M. Mbabele, M.R. Moazzam, D. Budimir, and F. Ali, "Improvement of Third-Order Intermodulation Product of RF and Microwave Amplifiers by Injection", *in IEEE Trans. Microwave Theory Tech.*, vol. 49, no. 6, pp.1148-1154, June. 2001.

[4.2] S. P. Stapleton, "Adaptive feed forward linearization for RF power amplifiers", *in Proc. 55th Automatic RF Techniques Group Conference Digest- Spring*, vol. 37, pp. 1-7, June 2000.

[4.3] Y. Y. Woo, J. Kim, J. Yi, S. Hong, I. Kim, J. Moon, and B. Kim, "Adaptive digital feedback predistortion technique for linearizing power amplifiers", *IEEE Trans. Microw. Theory Tech.*, vol. 55, no. 5, pp. 932-940, May 2007.

[4.4] D. Bondar, and D. Budimir, "Digital baseband predistortion of wideband power amplifiers with improved memory effects", *Proc. IEEE Radio and Wireless Symposium*, Jan. 2009, pp. 284-287.

[4.5] N. Mizusawa, and S. Kusunoki, "Third- and fifth-order baseband component injection for linearization of the power amplifier in a cellular phone," *IEEE Trans. Microw. Theory Tech.*, vol. 53, no. 4, pp. 3327-3334, Apr. 2005.

[4.6] D.C. Cox, "Linear amplification with nonlinear components", *IEEE Transactions on Communication Technology*, vol. 22, no 12, pp 1942-1945, Dec. 1974.

[4.7] F. J. Casadevall, and A. Valdorinos, "Performance analysis of QAM modulations applied to the LINC transmitter", *IEEE Trans. Veh. Technol.*, vol. 42, no. 4, pp. 399-406, Nov. 1993.

[4.8] A. Grebennikov, "RF and Microwave Transmitter Design", *John Wiley & Sons, Inc.*, 2011.

[4.9] H. Uchida, H. Kamino, K. Totani, N. Yoneda , M. Miyazaki, Y. Konishi, S. Makino, J. Hirokawa, M. Ando, "Dual-band-rejection filter for distortion reduction in RF transmitters", *Microwave Theory and Techniques, IEEE Transactions on*, vol.52, no.11, pp.2550,2556, Nov. 2004.

[4.10] J.D. Rhodes and I.C. Hunter, "Synthesis of reflection-mode prototype networks with dissipative circuit elements", *IEEE Proc. Microwave Antenna Propagation*, Vol.144, No.6 December 1997, pp.437-442.

[4.11] N. Males-Ilic, B. Milovanovic, and D. Budimir, "Improvement in second harmonics linearization technique for multichannel amplifiers", *Microwave and Optical Technology Letters*, vol.38, no. 2, pp. 150-153, Jul. 2003.

[4.12] S. Dimitrov, "Iterative Cancellation of Non-Linear Distortion Noise in Digital Communication Systems," *Communications, IEEE Transactions on*, vol.63, no.6, pp.2325-2336, June. 2015.

[4.13] R. Ratasuk, D. Tolli, and A. Ghosh, "Carrier aggregation in lteadvanced", *in 2010 IEEE 71st Vehicular Technology Conf. (VTC 2010- Spring)*, pp. 1 –5, May 2010.

[4.14] Z. Shen, A. Papasakellariou, J. Montojo, D. Gerstenberger, and F. Xu, "Overview of 3gpp lte-advanced carrier aggregation for 4g wireless communications", *IEEE Commun. Mag.*, vol. 50, pp. 122 –130, February 2012.

[4.15] H. Saghlatoon, L. Sydänheimo, L. Ukkonen, and M. Tentzeris, "Optimization of Inkjet Printing of Patch Antennas on Low-Cost Fibrous Substrates", *IEEE Antennas Wireless Propag. Lett.*, vol. 13, no. 1, pp. 915-918, May 2014.

[4.16] B. Ando, S. Baglio, C. O. Lombardo, and V. Marletta, "A Low-Cost Accelerometer Developed by Inkjet Printing Technology", *IEEE Trans. on Instrum. Meas.*, vol. 65, no. 5, pp. 1242-1248, May, 2016.

[4.17] R. Vyas, V. Lakafosis, A. Rida, N. Chaisilwattana, S. Travis. J. Pan and M. Tentzeris, "Paper-Based RFID-Enabled Wireless Platforms for Sensing Applications", *IEEE Trans. on Microwave Theory and Techniques*, vol.57, No.5, part 2, pp.1370-1382, May 2009.

[4.18] H. L. Kao, C. L. Cho, X. Dai, C. S. Yeh, X. Y. Zhang, L. C. Chang and H. C. Chiu, "Hairpin Bandpass Filter on Liquid Crystal Polymer Substrate using," *IEEE MTT -S Int. Microwave Sym, Seattle, W A*, pp. 1-4, June 2013.

[4.19] J. Virtanen, L. Ukkonen, T. Bjorninen, A. Z. Elsherbeni, and L. Sydänheimo, "Inkjet-printed humidity sensor for passive UHF RFID systems," *IEEE Trans. on Instrum. Meas*., vol. 60, no. 8, pp. 2768–2777, Aug. 2011.

[4.20] Y. Lan, Yuehang Xu, C. Wang, Z. Wen, Y. Qiu, T. Mei, Y. Wu, and R. Xu, "Flexible Microwave filters on Ultra-Thin Liquid Crystal Polymer substrate", *IEEE MTT-S Int. Microw. Symp.*, Phoenix, Arisona, pp. 1-3, May 2015.

[4.21] G. A. Casula, G. Montisci, P. Maxia, G. Valente, A. Fanti and G. Mazzarella, "A Low-Cost Dual-Band CPW-Fed Printed LPDA for Wireless Communications", *IEEE Antennas Wireless Propag. Lett.*, vol. 15, no. 1, pp. 1333-1336, April 2016.

[4.22] S. Dimitrov, "Iterative Cancellation of Non-Linear Distortion Noise in Digital Communication Systems," *IEEE Transactions on Comm*., vol.63, no.6, pp.2325-2336, June 2015.

[4.23] W. Y. Sam, Z. Zakaria, M. A. Mutalib, M. F. M. Fadhli, A. R. Othman, and A. A .M. Isa, "A Compact DMS Triple-Band Band-stop Filter with U-slots for Communication Systems", *Proc. IEEE Int. Conf. on Electronic Design*, Penang, Malaysia, pp. 383-386, August 2014.

[4.24] K. Chakrabarty, and D. Budimir, "Compact tunable bandstp filters using Defected Microstrip Structure for multi-standard wireless systems", *Proc. 43rd Eur. Microw. Conf*., Nuremberg, Germany, pp. 1031-1034, October 2013.

[4.25] J. Wang, H. Ning, L. Mao, and M. Li, "Miniaturized Dual-Band Band-stop Filter Using defected Microstrip Structure and Defected Ground Structure", *IEEE-MTT-S Int. Microw. Symp. Dig.*, Montreal, Canada, pp. 1-3, June 2012.

[4.26] D. La, Y. Lu, and S. Sun, “Novel Band-stop Filter Using Dual-U Shape Defected Microstrip Structure”, *Proc. Int. Symp. Signals, Systems and Electronics*, Nanjing, China, pp. 400-402, September 2010.

Chapter 5: Compact Microstrip Coupler Design and its Next Generation Wireless Transceiver Applications

Hybrid couplers are very vital passive circuits for microwave and mm-wave applications. The quadrature hybrid coupler (QHC) also known as the Branch line coupler (BLC) is a common example of such couplers which provides equal amplitude with quadrature (90^0) phase difference between the output ports (S_{21} and S_{31}) at the desired frequency. They are also known as directional couplers. Directional couplers are designed to split power equally between two ports. They are 4 port networks designed to divide and distribute power.

These devices are very important for microwave systems and can be used in a variety of practical and system applications such as in wireless transmitter power amplifier configurations such as balanced power amplifier and Doherty amplifiers. Their application is also found in image-rejection mixer, antenna array feed networks and phase-shifters. The conventional branch line coupler is implemented as a single ended design with four quarter wavelength transmission lines.

It has been observed that the conventional coupler occupies a very large area, especially when considering lower frequencies of interest which makes it too bulky for practical use. Several techniques and technologies have been proposed over the years to reduce the size of the coupler such as the use of the defected ground structure (DGS) [5.1], the use of stubs [5.2] and different kinds of resonators such as the meander shaped slots complementary single split ring resonators (CSSRRs) [5.3] and meta-material based complementary split ring resonators (CSRRs) [5.4-5.5].

One main challenge for the couplers is the large size at low frequencies mainly below 4 GHz. Hence techniques for microwave couplers seem to be a continuous area of interest. Recently, the composite right/left hand (CRLH) TL to design compact couplers has been explored broadly [5.6]. However, some of these CRLH could be complex and even though overall area is reduced, there seems to be an increase in the overall width of the structure. To improve on drawbacks such as complexity and width size increase, a new transmission line is proposed.

In the next section, a compact coupler is presented to maintain high performance whilst reducing size, circuit area and complexity. One of such structures is fabricated in this section 5.1 with a total reduction of about 64% in its occupied size when compared to its conventional equivalent. The structure also gives good return and insertion loss performance. Another USTL coupler was later designed in section 5.2 and fabricated to achieve further size reduction and improve on the performance of the previous coupler at 1.5 GHz which happens to be one of the bands of consideration for 5G below 6 GHz. This USTL QHC coupler achieved 70% size reduction with better transmission and isolation properties giving good match between simulation and measured results.

Inkjet printing technology is ever becoming more in demand for microwave components due to its good flexible properties, size reduction and ease of fabrication. Other advantages include reduction of waste and material quantity over the conventional etching techniques. Inkjet-printed couplers will also be considered in this thesis. This can achieve further size reduction,

with better performance. One of such couplers was designed in section 5.3 using the inkjet printing technology achieving a total reduction of about 78% which is about 14% more than its PCB (printed circuit board) equivalent with the added advantage of better coupling, isolation and multiband properties.

5.1 Compact Microstrip Branch-line Couplers based on U-shaped Transmission lines

The branch-line couplers (BLC) are four-port network device with a 90^0 phase difference between the output ports (2 and 3) at the desired frequency [5.7]. The BLC could be used for a single transceiver (Transmitter/Receiver) system or could even acts as splitters/combiners for I/Q signal signals. The conventional BLC is implemented as a single-ended design with four quarter wavelength transmission lines ($\lambda_g/4$) having two peculiar impedances (Z_0 and $Z_0/\sqrt{2}$) which are usually 50 and 35.35 Ω as shown in Figure 5-1. These designs occupy a considerable large size which affects its implementation in compact systems.

Different microstrip transmission line concepts have been proposed to effectively reduce the overall size of the conventional 3 dB branch-line couplers by replacing the $\lambda_g/4$ transmission lines ($\lambda_g/4$ TL) of the conventional BLC [5.8].

Such methods include the use of planar transmission lines [5.9], T-shaped transmission lines [5.10], coupled transmission line concept [5.11] and Pi-Shaped transmission line [5.12] achieving a total size reduction of about 53 %, 54%, 58% and 60% respectively. Furthermore, a substrate integrated suspended line technology [5.13] achieved a 62% reduction and a T-shaped transmission line structure [5.14] embedded within a fractal shaped geometry has also achieved about 67% reduction and the CRLH TL obtained a 63.6% size reduction [5.15]. To achieve further miniaturisation with lesser complexity, this thesis presents a U-shaped transmission line (USTL) coupler.

In this section, a novel compact branch-line coupler based on novel U-shaped transmission line (USTL) is proposed. When compared to other presented microstrip branch-line coupler designs in [5.10] – [5.15], the USTL design achieves a good size reduction and maintains outstanding coupling/splitting properties. The next section explains the design and concept of the coupler design.

5.1.1 Proposed Branch-line Couplers Structure Design

The conventional 3-dB branch-line coupler is a 4-port device. It consists of four quarter wavelength ($\lambda_g/4$) transmission line segments. The geometry of the branch-line coupler is shown in Figure 5-1 consisting of two adjacent characteristics impedance Z_0 (50 Ω) and the other two with $Z_0/\sqrt{2}$ (35.33 Ω).

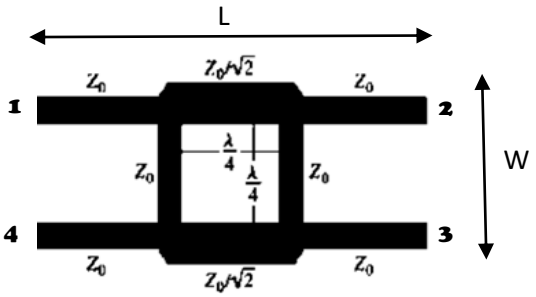

Figure 5-1: Conventional BLC with four quarter wavelength TL.

The quadrature hybrid coupler (QHC) shown in Figure 5-1 was designed using electromagnetic software (*em* sonnet) giving a large size (L X W) of 108.9 x 40.4 mm^2 at center frequency of 1.725 GHz. Due to this, a compact coupler must be designed whilst maintaining/improving performance.

The U-shaped transmission line (USTL) model is assumed to have distributed circuit inductance along the line and a distributed capacitance across the line. This design is used to reduce the large size of the quadrature hybrid couplers. However, the reduction in length leads to shorter distributed circuit elements. The loss in inductance and capacitance are compensated for by the characteristics impedance and using shunt capacitors respectively. The conventional case of quarter wavelength ($\lambda_g/4$) transmission line segments with electrical length Ø and characteristics impedance Z_0 can be expressed using the ABCD parameters in matrix form as follows [5.16]:

$$\begin{bmatrix} a & b \\ c & d \end{bmatrix}_{\lambda_g/4} = \begin{bmatrix} \cos Ø & jZ_0 \sin Ø \\ j/Z_0 \sin Ø & \cos Ø \end{bmatrix} \tag{5.1}$$

The phase difference is designed to be around 90 (π /2) degrees and so by setting the electrical length to π/2 and inserting into equation (1), it becomes:

$$\begin{bmatrix} a & b \\ c & d \end{bmatrix}_{\lambda_g/4} = \begin{bmatrix} 0 & jZ_0 \\ j/Z_0 & 0 \end{bmatrix} \tag{5.2}$$

For the unit cell equivalent circuit, it is initially assumed to be asymmetrical and the matrices can further be expressed as:

$$\begin{bmatrix} a & b \\ c & d \end{bmatrix}_{U} = [U_1]\,[U_2]\,[U_3] \tag{5.3}$$

Each individual matrix is defined in equations (5.4) – (5.6)

$$[U_1] = \begin{bmatrix} a & b \\ c & d \end{bmatrix}_{U_1} = \begin{bmatrix} \cos Ø_1 & jZ_1 \sin Ø_1 \\ j/Z_1 \sin Ø_1 & \cos Ø_1 \end{bmatrix} \tag{5.4}$$

$$[U_2] = \begin{bmatrix} a & b \\ c & d \end{bmatrix}_{U_2} = \begin{bmatrix} 1 & 0 \\ j\tan Ø_2/Z_2 & 1 \end{bmatrix} \tag{5.5}$$

$$[U_3] = \begin{bmatrix} a & b \\ c & d \end{bmatrix}_{U_3} = \begin{bmatrix} \cos Ø_3 & jZ_3 \sin Ø_3 \\ j/Z_3 \sin Ø_3 & \cos Ø_3 \end{bmatrix} \quad (5.6)$$

Where $Ø_1$, $Ø_2$, $Ø_3$, are the electrical lengths and Z_1, Z_2, Z_3 are the characteristics impedance of the unit cell. For the U-shaped TL to be equivalent with the quarter wavelength ($\lambda g/4$) TL, the abcd matrices parameters for both must be equal. The two RH-TLs shown in Figure 5-2 are taken to be the same and so equations (5.4) and (5.6) can be merged.

$$[U_1] = [U_3] = \begin{bmatrix} a & b \\ c & d \end{bmatrix}_{U_1} = \begin{bmatrix} \cos Ø_1 & jZ_1 \sin Ø_1 \\ j/Z_1 \sin Ø_1 & \cos Ø_1 \end{bmatrix} \quad (5.7)$$

Hence, $Ø_1 = Ø_3 = Ø_{RH}$ whilst $Ø_2 = Ø_{LH}$ and $Z_1 = Z_3 = Z_{0RH}$ whist $Z_2 = Z_{0LH}$ according to Figure 5-2. The phase responses of the RH and LH TLs are in equations (5.8) and (5.9) [5.15]. The principle used for the proposed USTL coupler design is like the CRLH transmission line (TL) concept. The unit cell of the CRLH TL is shown in Figure 5-2. Equations are derived from the unit cell for the design. The values from the equations then determine the CRLH TL equivalent of the conventional design. The inductance and capacitance of a U-shaped defect can be modified by altering the structure until it matches the CRLH values. Once this is determined, the conventional ($\lambda_g/4$) transmission section is then substituted for a discontinuous U-shaped transmission line (USTL) as shown in Figure 5-3. The RH TL part of the branch line coupler represents the standard microstrip line. The LH TL part is then replaced with the U-Shaped discontinuity. The discontinuities modify the inductance and capacitance which help reduce the TL and circuit size.

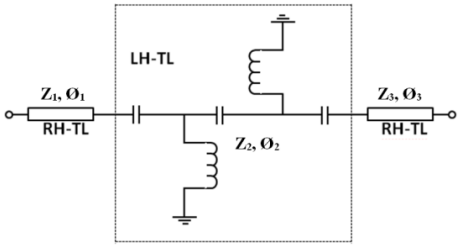

Figure 5-2: The u-shaped equivalent circuit.

$$Ø_{RH} = -2\pi f N\sqrt{L_{RH}C_{RH}} \quad (5.8)$$

$$Ø_{LH} = \frac{N}{2\pi f\sqrt{L_{LH}C_{LH}}} \quad (5.9)$$

The phase response could be determined by altering the values of L_{RH}, C_{RH}, L_{LH} and C_{LH}. The characteristics impedance of the RH (Z_{0RH}) and LH transmission lines (Z_{0LH}) are respectively denoted by equation (5.10) and (5.11) below.

$$Z_{0RH} = \sqrt{\frac{L_{RH}}{C_{RH}}} \quad (5.10)$$

$$Z_{0LH} = \sqrt{\frac{L_{LH}}{C_{LH}}} \quad (5.11)$$

From equations (5.8) – (5.11), inductance and capacitance values for L_{RH}, L_{LH}, C_{RH} and C_{LH} can be determined [5.6]. Figure 5-3 is the block diagram of the transformation concept used. The inductance and capacitance (L-C) values of the LH section of each CRLH unit cell as shown in Figure 5-2 are matched to the L-C equivalent for each arm of the USTL and converted to its microstrip transmission line equivalent.

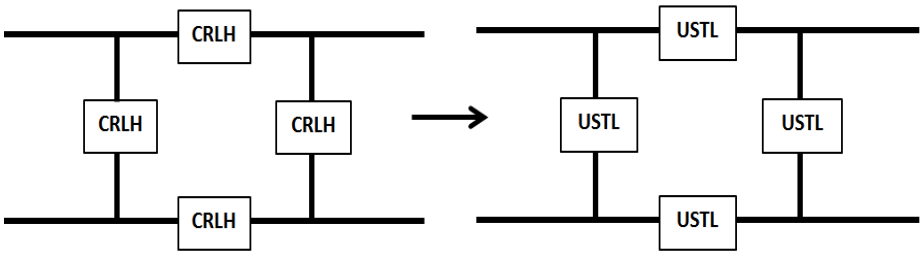

Figure 5-3: Proposed line transformation concept.

The CRLH inductance and capacitance values obtained using [5.17] are used as initial values to design the USTL. By adjusting the inductance and capacitance values, the hybrid coupler could be designed at different frequencies. With further optimization techniques, the right USTL dimensions are obtained by converting the L-C values into its microstrip transmission line equivalent. Instead of replacing the $\lambda_g/4$ TLs with CRLH TLS, they are replaced with the final optimized USTL which had been obtained based on the initial inductance and capacitance values obtained as illustrated in Figure 5-4.

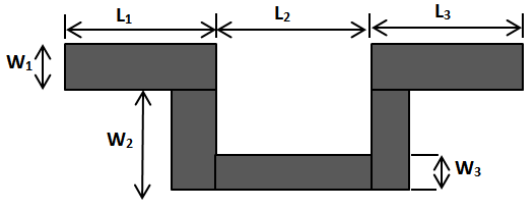

Figure 5-4: The USTL structure.

These values help determine the dimension of the U-shaped structure as any changes in the structure alters the combined inductance and capacitance within the structure. With the aid of mathematical expressions in (5.1) – (5.11) and optimization techniques, the dimensions of the coupler's structure are shown in Table 5-1 below. The USTL parameter values in Table 5-1 are then used to complete the dimensions of the USTL structure in Figure 5-4.

Table 5-1: USTL parameters in main line and branch line.

Characteristic impedance (Ω)	**W_1** (mm)	**W_2** (mm)	**W_3** (mm)	**L_1** (mm)	**L_2** (mm)	**L_3** (mm)
50 (Z_0)	2.4	9.1	2.4	11	5	11
35.35($Z_0/\sqrt{2}$)	3.9	6.2	3.9	6.5	8	6.5

Figure 5-5 gives the layout of the USTL coupler. The values obtained in Table 5-1 are used to form each of the four arms of the coupler structure as shown in Figure 5-4. The corresponding USTL now takes the place of the conventional ($\lambda_g/4$) segments as shown in Figure 5-1. The two $Z_{0\ and}$ $Z_0/\sqrt{2}$ adjacent impedance sections in Figure 5-1 are now replaced with the equivalent calculated using Table 5-1 and Figure 5-4 forming the new coupler design in Figure 5-5. The bended U-shape was observed to possess reduced overall circuit area when compared with the conventional case in Figure 5-1.

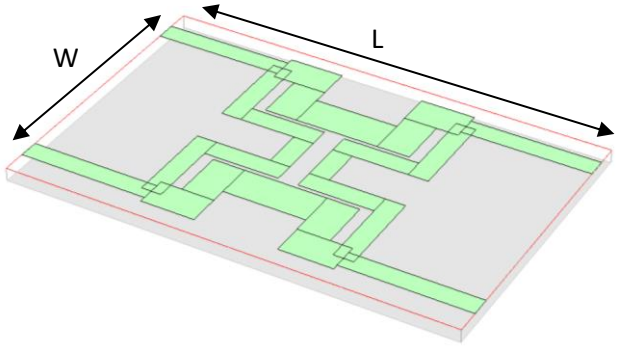

Figure 5-5: The layout of proposed USTL hybrid coupler structure.

Figure 5-5 shows the three-dimensional (3D) view of the proposed USTL hybrid coupler. The structure is simulated using Rogers 5880 with thickness of 0.79 mm, dielectric constant (ε_r) of 2.2 and loss tangent of 0.0021. The metal type used for the structure is copper with thickness of 17 µm. The structure is designed to operate at 1.725 GHz. Figure 5-6 gives the simulated s-parameter response of the proposed BLC.

The scattering transmission parameter (S_{11}) as shown in Figure 5-6 is around −20 dB at the center frequency (1.725 GHz) with good isolation (S_{12}) also lower than −20 dB. The transmission and coupling properties (S_{12} and S_{13}) at the required frequency also give good results hovering as expected around -3 dB.

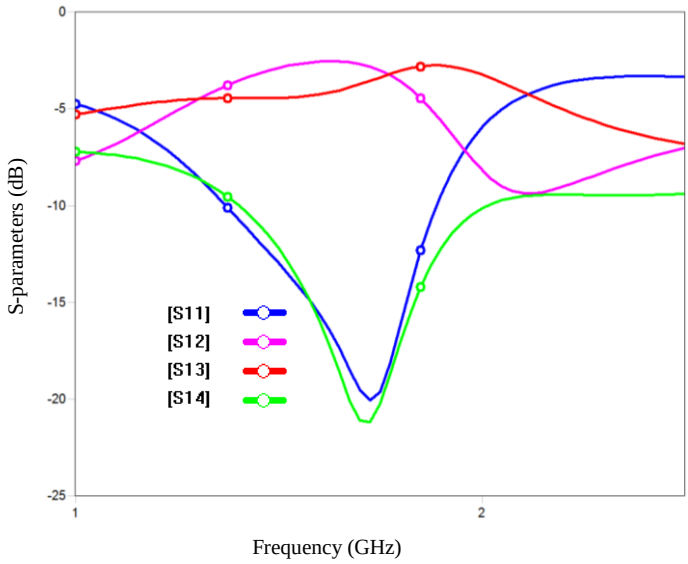

Figure 5-6: Simulated s-parameter results of the proposed BLC.

Figure 5-7 also gives the phase results. The Phase difference ($Ø_{31} - Ø_{21}$) of the simulated branch-line coupler between the transmitted and coupled ports (ports 2 and 3) at the center frequency also satisfies specifications as it is around 90 degrees (48.52 + 42.63 = 91.15) .

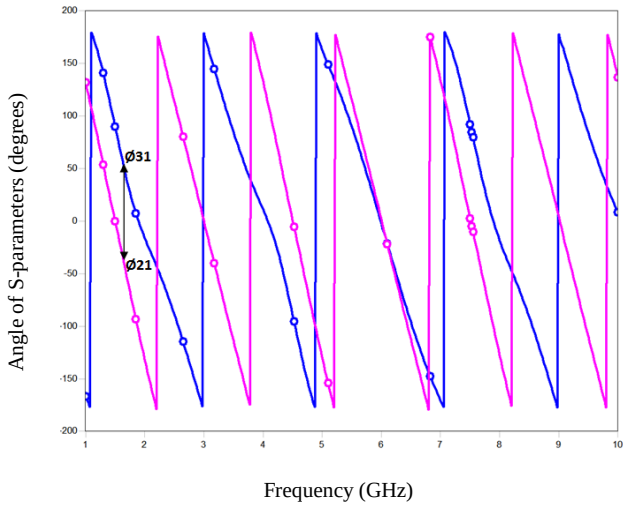

Figure 5-7: Simulated phase of the proposed BLC.

Figure 5-8 shows the photograph of the proposed fabricated USTL branch-line coupler with the size of 52 x 31 mm^2. The coupler was fabricated in microstrip technology using RT/Duroid 5880, with dielectric constant (εr) of 2.2 and substrate thickness of 0.79 mm. The proposed design achieves compactness with a size of 52 x 31 mm^2 which shows considerable compactness as compared to the conventional design using Figure 5-1 which had a size of 108.9 x 40.4 mm^2 at the same center frequency. Simulated and measured results are presented in Figure 5-9.

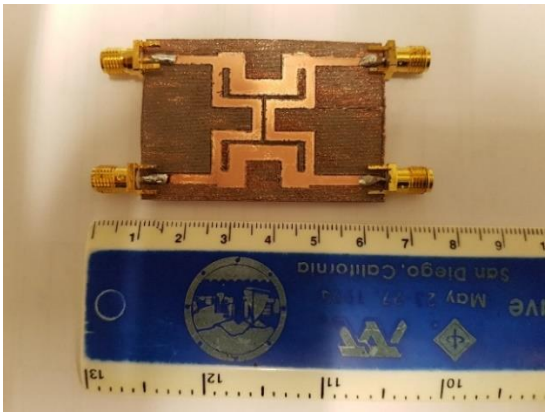

Figure 5-8: Photograph of the fabricated BLC.

Figure 5-9 presents the measured and simulated scattering parameters of the proposed coupler versus the frequency. It was noticed that there is a slight shift in center frequency from 1.725 GHz to about 1.8 GHz. At the center frequency of the fabricated structure, the S_{21} parameter is about -3.36 dB and the coupling S_{31} parameter is about -3.48 dB. The loss (S_{11}) and isolation (S_{41}) are better than -15 dB, respectively.

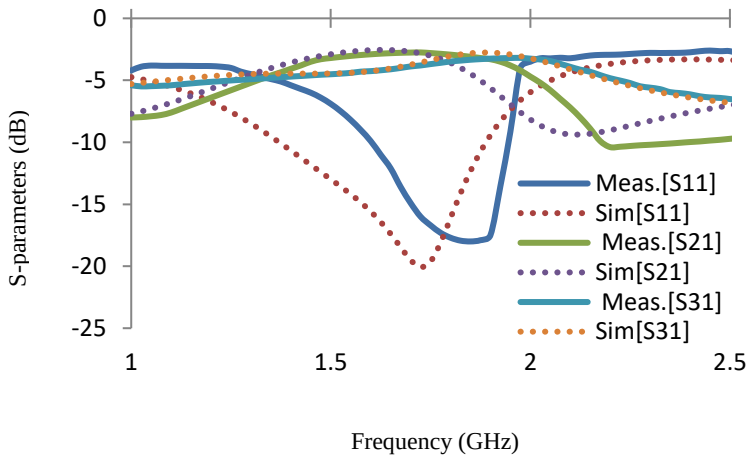

Figure 5-9: Measured and simulated s-parameter vs frequency results of BLC.

Furthermore, at the same frequency, the size/circuit area (LXW) of the conventional hybrid coupler shown in Figure 5-1 is 108.9 x 40.4 mm^2. It is noted that the size reduction of the proposed USTL BLC of 52 x 31 mm^2 is about 64%.

Table 5-2 gives further comparison between the conventional and the proposed BLC. The couplers were compared in simulations and from the table it could be observed that apart from the proposed coupler achieving a significantly reduced size, other results such as return loss, isolation, coupling and phase also gave relatively good matches with its conventional equivalent thereby maintaining performance.

Table 5-2: Conventional and proposed BLC comparison.

Specifications	**Designs**	
	Conventional BLC	**Proposed BLC**
Frequency (GHz)	1.725 GHz	1.725 GHz
Total Circuit Area (mm^2)	4470	1610
Size	100%	35.8 %
Return Loss (S_{11} in dB)	-20.5	- 17.8
Isolation (S_{14} in dB)	-22.8	-21.5
Coupling (S_{13} in dB) Coupling (S_{12} in dB)	-3.2 -3.2	-3.48 -3.36
Phase difference ($Ø_{31}$-$Ø_{21}$ in degrees)	89.56	91.15

A novel compact U-shaped microstrip branch-line coupler has been proposed in this thesis chapter. The coupler structure was designed, simulated and fabricated. The simulated and

measured results have been presented. The measurement results of the fabricated branch-line coupler using U-shaped transmission lines at 1.725 GHz demonstrate size reduction of 64%. The structure is very useful for balanced amplifier configurations, mixers, phase shifters, beam-forming networks and antenna arrays.

5.2 Miniaturized USTL 3 dB Quadrature Hybrid Couplers

In this section, a 3dB quadrature hybrid coupler based on a novel U-shaped transmission line (USTL) technique is proposed to maintain high performance whilst reducing size, circuit area and complexity. This coupler is aimed to improve on the size and performance of the coupler designed in section 5.1. One of such structures is presented in this paper with a total reduction of about 70% in its occupied size when compared to the same conventional coupler. When compared to other presented microstrip QHC designs in [5.10] – [5.15], the USTL design achieves a good size reduction with better performance. The measured results of the fabricated structure also give good return and insertion loss performance matching with the simulated results and could easily be incorporated in modern wireless communication systems. The next sub-chapter paper consists of the design of the proposed coupler structure. Simulated and measured results for the coupler are also presented.

5.2.1 Proposed Miniaturised Quadrature Hybrid Structure

This section focuses on achieving better results in terms of size and performance which would be suitable for balanced power amplifiers. For lesser RF frequencies, it is expected that the size of the coupler should increase. One of the 5G bands below 6 GHz is at 1.5 GHz. Hence, the coupler will be designed for a center frequency of 1.5 GHz to achieve further size reduction and even better performance properties than the coupler in section 5.1. This design is used to reduce the large size of the quadrature hybrid couplers/ branch line couplers. The same USTL design method in section 5.1.1 is utilized in this section but for another design at a different center frequency of 1.5 GHz.

However, by carefully choosing the gaps between each USTL lines, improved coupler results and size reduction is achieved. Also, more importantly, the dimensions L_3 and W_1 are chosen carefully to provide immunity against load insensitivities for the isolation port 4. By considering the theoretical expressions and equations from (5.1) – (5.11), the coupler dimensions for each side of the four USTL structures in Figure 5-4 are obtained. The USTL parameter values then obtained are used to complete Table 5-3. Figure 5-10 gives the final dimensions of the structure using Table 5-3.

Table 5-3: USTL QHC design parameters.

Characteristic impedance (Ω)	**W_1** (mm)	**W_2** (mm)	**W_3** (mm)	**L_1** (mm)	**L_2** (mm)	**L_3** (mm)
50 (Z_0)	2.44	8	4	12	2.44	12
35.35($Z_0/\sqrt{2}$)	3.96	8.2	3.96	10	3.96	10

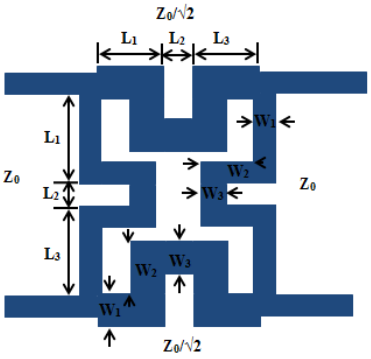

Figure 5-10: The layout of proposed quadrature hybrid coupler structure.

Figure 5-11 compares the proposed quadrature hybrid coupler structure with its conventional equivalent. There is a considerable size reduction with a size of 41.96 x 31.84 mm^2 as compared to the conventional design which had a size of 108.86 x 40.8 mm^2 at the same center frequency of 1.5 GHz. The four arms of the transmission line have been optimised to obtain the significant miniaturisation of the conventional circuit.

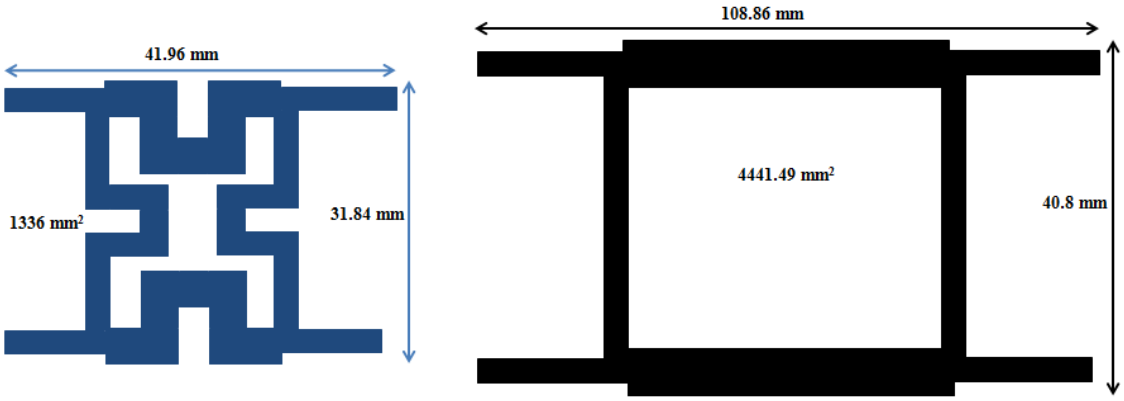

Figure 5-11: Comparison of miniaturized coupler with conventional coupler.

The relative circuit area of the proposed coupler and other designs are compared in Table 5-4. The proposed USTL structure was able to achieve the least relative area of about 30% of the total area of the conventional coupler design. The conventional design is very large at such low RF/microwave frequencies manily below 6 GHz and it is very vital to achieve good reduction whilst maintaining or even achieving better performance.

The coupler is fabricated in microstrip technology using RT/Duroid 5880, with dielectric constant (ε_r) of 2.2 and substrate thickness of 0.79 mm. Figure 5-12 shows the photograph of the proposed fabricated coupler under measurement with its measured results are presented in Figure 5-13.

Table 5-4: Comparisons of properties with proposed coupler.

Reference	Technique	Relative Area (%)	Freq (GHz)	$\|S_{11}\|$ (dB)	$\|S_{14}\|$ (dB)	Phase (degrees)
Conventional	Conventional Design	100	1.5	> 35	> 35	89.56
[5.10]	T-shaped transmission line	46	1.0	> 22	> 22	87
[5.11]	Coupled transmission line	42	1.87	> 12	> 12	93
[5.12]	Pi-Shaped transmission line	40	2.0	> 26	> 26	87
[5.14]	Fractal Shaped transmission line	33	1.0	> 28	> 28	88
This Work	U-Shaped Transmission Line	30	1.47	> 30	> 35	91.15

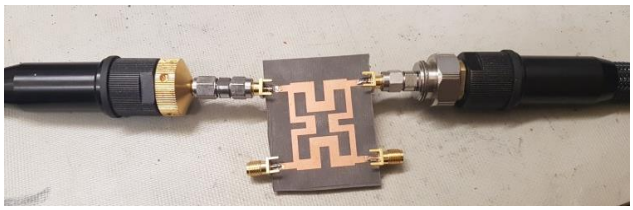

Figure 5-12: Fabricated coupler under measurement.

Figure 5-13 shows a comparison between the simulated and measured S-parameters for the coupler structure. The structure was designed and simulated using em sonnet software and compared with measured results after fabrication. The results obtained by measurements and those obtained by simulations show a relatively good match; we attribute the minor disagreements to be mainly due to the fabrication tolerances and lesser frequency points in measurement. Namely, a slight center frequency shift, from 1.5 GHz to 1.47 GHz, has been noticed for the measured coupler, with a slight deviation in *S*-parameter values over its simulation equivalent.

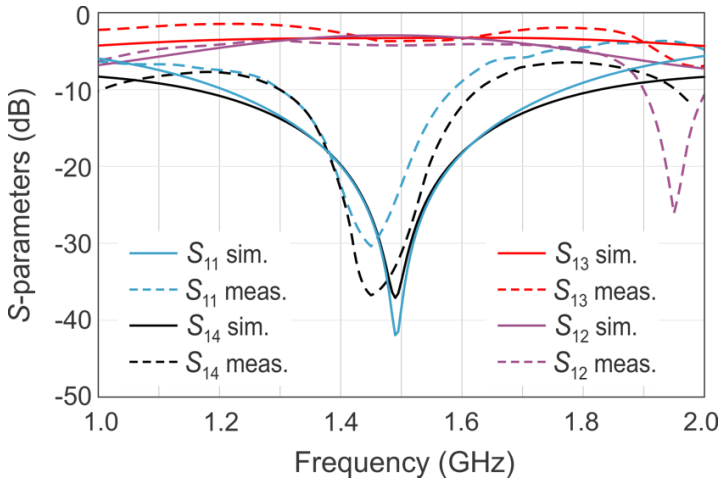

Figure 5-13: Simulated and measured s-parameters for the proposed coupler.

Return loss, S_{11}, at the center frequencies for simulations and for the measured data are both below 30 dB, which is excellent. Isolation (S_{14}), obtained by measurements, is slightly better, with two groups of results being very close and both below 35 dB. The coupling and transmission coefficients (S_{12} and S_{13}) are both near 3 dB at the center frequency range. Phase was observed to be 91.2^0.

The proposed 3 dB quadrature hybrid coupler (QHC) is very compact achieving a size reduction of 70% which is just 30% of the conventional coupler. The design does not only achieve a much-reduced size but gives good performance. The performance of the coupler makes it a good candidate for different power amplifier configurations for 5G wireless communication systems as it is compact and its good isolation results are very attractive as they boost immunity against load insensitivity characteristics.

5.3 Miniaturised Inkjet-printed Quadrature Hybrid Couplers for Multiband Wireless Systems

Quadrature Hybrid Couplers (QHCs) or branch-line couplers are commonly used in are widely used in numerous Sensing, RFID, wireless systems, RF and micro-/mm-wave circuits such as mixers, amplifiers, phase shifters, antenna array feed networks and beam-forming networks [5.18]. Conventional quadrature hybrid couplers with quarter wavelength transmission lines operate at a fundamental frequency and its odd harmonics. Inkjet printing technology is excellent candidate for low-cost circuit realization.

Using inkjet printing technology, several advantages such as faster fabrication, waste decrease and low fabrication costs, reduction in material quantity can be achieved over conventional etching technology. In last few years several inkjet-printed couplers have been implemented in a wide range of applications [5.19] - [5.20]. To overcome the problem of complexity and increase in size, a U-shaped transmission line is proposed to replace the four quarter wavelength transmission lines of the conventional couplers.

In this thesis, a novel U-shaped transmission line (USTL) is proposed for the quadrature hybrid coupler to maintain high performance whilst reducing size. One of such structures is proposed in this paper with a total reduction of about 78% in its occupied size when compared to its conventional equivalent. The structure also gives good return and insertion loss performance at multiband frequencies.

5.3.1 Inkjet-Printed Quadrature Hybrid Coupler Design

The 3D schematic of the conventional inkjet quadrature hybrid coupler designed using sonnet is shown in Figure 5-14. This design will be based on inkjet-printing technology with flexible substrate. The conventional structure's dimensions are based on the characteristic impedances and electrical length of all transmission lines as depicted earlier in Figure 5-1.

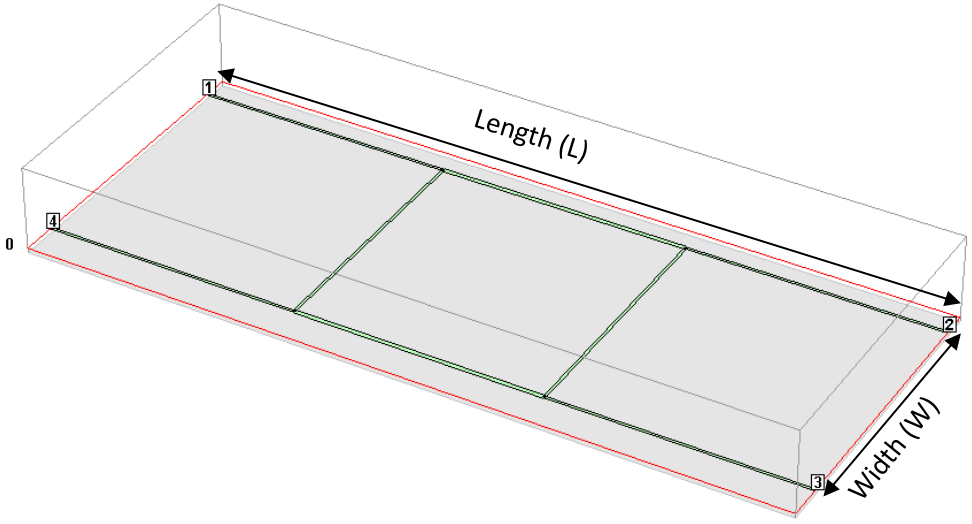

Figure 5-14: 3D view of the conventional QHC design.

Table 5-5 gives physical dimensions of the transmission lines in the branch line coupler.

Table 5-5: Inkjet QHC design parameters

Characteristics impedance (Ω)	**Width (W)** (mm)	**λ_g** (mm)	**Length (L) (λ_g/4)** (mm)
50 (Z0)	0.11	122.28	30.57
35.35(Z0/√2)	0.19	119.52	29.88

The conventional coupler has a total size (L x W) of 91.10 x 31.14 mm^2 and its simulated results are shown in Figure 5-15 below.

The main difference between the inkjet coupler and other couplers is the substrate and metallization used in designs, simulations and fabrication. The branch line coupler or QHC is designed as a microstrip structure using the inkjet printing technology with the aid of flexible kapton polyimide substrate. Metal lines of the inkjet-printed QHCs are printed on substrate foil of 50 µm thickness and relative dielectric permittivity of ε_r = 3.4. Kapton polyimide is chosen because it fulfils the required properties and has a low loss factor of 0.0021. Silver nanoparticles thickness of 1 µm for inkjet printing is chosen to reduce losses in metal.

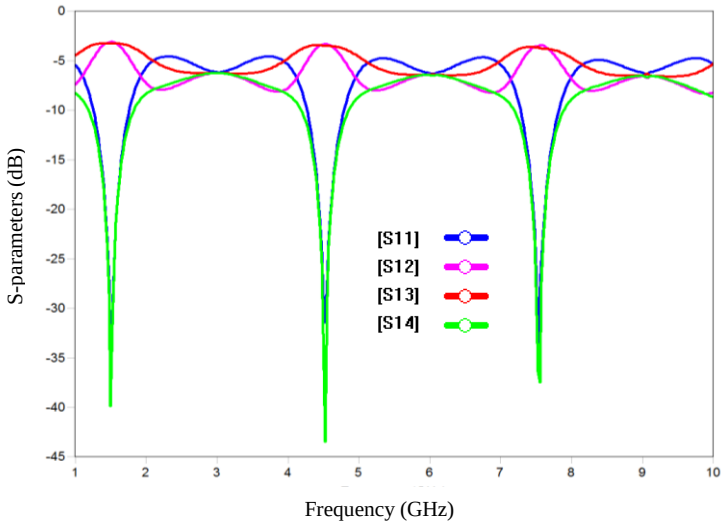

Figure 5-15: Simulated results of conventional inkjet QHC.

To reduce the size of the coupler, U-shaped transmission line units shown in Figure 5-4 are used instead of λ/4 transmission lines. The $\lambda_g/4$ Transmission lines are replaced with USTL shown in Figure 5-16. The dimensions of the proposed coupler structure are shown in Table 5-6.

Table 5-6: USTL inkjet design parameters

Characteristics impedance (Ω)	**W1 (mm)**	**W2** (mm)	**W3** (mm)	**L1** (mm)	**L2** (mm)	**L3** (mm)
50 (Z0)	0.32	8.7	0.32	6.0	5.3	6.0
35.35(Z0/√2)	0.54	5.2	0.54	5.5	7	5.5

Figure 5-16 shows the structure of the proposed compact quadrature hybrid coupler. It is implemented with inkjet printing technology using the same mathematical equations as in (5.1) – (5.11). The proposed coupler was simulated using full 3D electromagnetic simulation software, *em* Sonnet as shown in Figure 5-16.

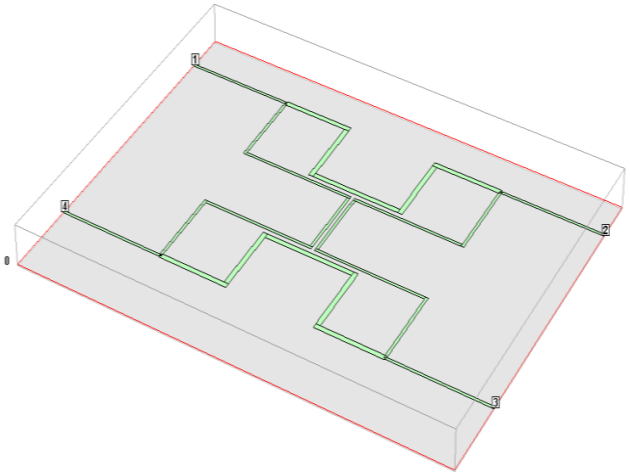

Figure 5-16: Proposed inkjet QHC 3D structure.

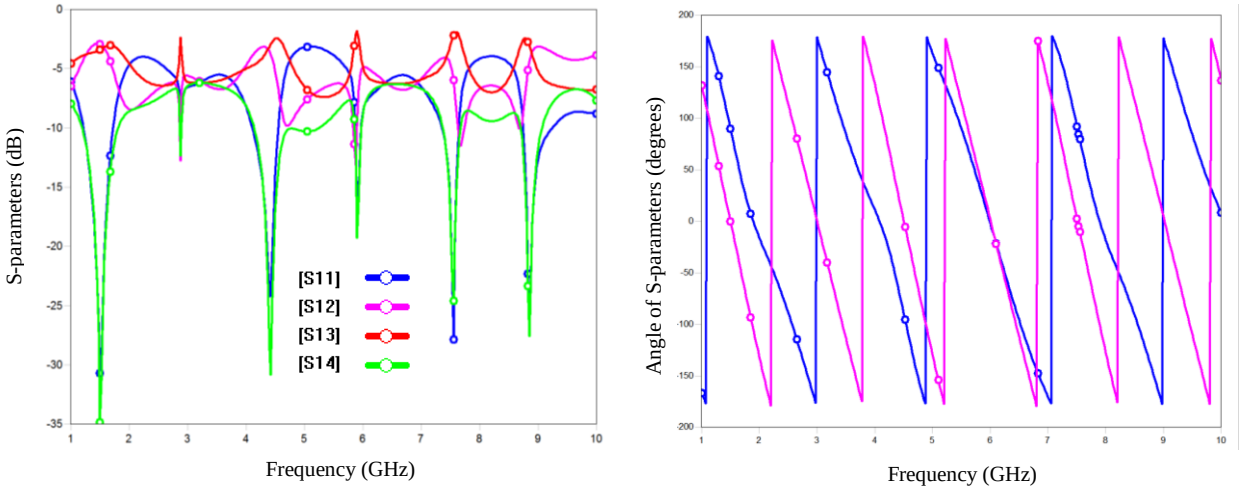

(a) (b)

Figure 5-17: (a) Simulation s-parameters of the proposed QHC coupler. (b) Simulated results of angles of S_{21} (red) and S_{31} (blue) parameter of the proposed coupler.

The proposed multiband inkjet-printed quadrature hybrid coupler was designed and simulated using *em* Sonnet software. The coupler has a total compact size (L x W) of 34x.4 x 17.84 mm^2 as compared to 91.10 x 31.14 mm^2 achieving a 78% reduction in total area. The simulated S-parameters are shown is given in Figure 5-17a. The scattering parameter S_{11} is lower than −20 dB at all bands. Even better results are with isolation parameter S_{14} is lower than −25 dB at all bands. Also, the transmission parameter S_{12} and coupling parameter S_{13} are close to −3 dB. The phase difference of a branch line coupler between ports 2 and 3 at both bands is around 90 degrees (89.93 + 0.02 = 89.96), as shown in Figure 5-17b.

By comparing the results of the conventional coupler in Figure 5-15 with the proposed coupler in Figure 5-17a, it could be observed that the proposed coupler has improved the multiband properties by 50% as there are now 6 bands between 1 and 10 GHz as compared to the conventional case with only 3 bands. The proposed coupler now has resonance at 1.5 GHz, 2.75 GHz, 4.5 GHz, 6.0 GHz, 7.5 GHz and 9.0 GHz, respectively whilst the conventional only maintains the ones at 1.5 GHz, 4.5 GHz and 7.5 GHz. The coupler also maintains good s-parameter performance whilst improving its multiband properties and reducing size significantly.

A miniaturised multiband inkjet-printed Quadrature Hybrid Coupler has been proposed and designed. The design of an inkjet-printed coupler on a flexible 50 µm Kapton substrate is simulated. The 3 dB S_{21} and S_{31} targets were achieved. At the main center frequency of interest, the return loss and isolation values were about -30 and -35 dB respectively giving good power splitting properties. The simulated reflection coefficients and isolation loss results were better than −15 dB and −20 dB, respectively at at 1.5 GHz, 4.5 GHz, 6.0 GHz, 7.5 GHz and 9.0 GHz, respectively. The proposed inkjet-printed QHC size is 78% smaller than the conventional inkjet-printed QHC.

5.4 High-Efficiency Rectifier based on Inkjet-printed Quadrature Hybrid Coupler

The emergence of microwave power transmission (MPT) plays a vital role in wireless powered circuits such as RF identification (RFID) and other low-power wireless sensor applications such as internet of things [5.21]. The total efficiency of the microwave wireless system depends mainly on the RF-dc conversion efficiency of the rectifier circuits which has made high efficiency rectifier design very important.

Recent research has focused on different topologies to improve RF-dc conversion efficiency performance [5.22]. Some of such topologies and models have been proposed in [5.23] – [5.26]. It was found that the electromagnetic energy is generally not constant due to the varying input power and operating frequency which leads to input impedance variation. The impedance variation degrades the rectifier performance due to the nonlinearity of the rectifying device. Another drawback from some of these improvements was due to load variation at the output of the rectifier which also leads to input impedance modification that can cause efficiency to deteriorate. To overcome the drawbacks and boosts robustness against the input power and output load variations, some further techniques were developed. Some of those solutions included resistance compression networks [5.27] which helped to improve the input impedance variation issue but still had bandwidth efficiency issues.

Recent work has now focused on performance of rectifiers under different signal types rather than just considering the matching network and device selection. Previous work had considered single and two-tone modes of operation. It has been observed when investigating multi-tone signals that high peak-to-average power ratio (PAPR) may lead to a higher RF-dc conversion efficiency than its equivalent signal with the same input power [5.28]. This work optimizes the RF-dc efficiency performance by identifying the optimal load resistance that could be stabilized by the QHC using digitally modulated signals. In this paper, a compact inkjet-printed quadrature hybrid coupler (QHC) is used alongside a novel rectifier design to improve efficiency over a wider range of input power, output load and frequency bandwidth. The isolation property of the coupler helps to provide better stability for output load variations and robustness against input impedance modification which boosts efficiency. This proposed coupler will be tested and compared using multi-tone analog, digitally modulated signals and 4G LTE signals for RF-dc conversion efficiency and PAPR verification.

The proposed design is made of a 3 dB QHC with a grounded isolation port whose outputs are feeding two sub rectifier circuits. Any change in input power (Pin) and output load (R_L), leads to varying input impedance which distorts the impedance. The reflected waves which ensue from both sub-rectifiers can be introduced back to each sub-rectifier with the aid of the coupler. This re-injection leads to improved efficiency as the reflected power can be utilised again. With this, the proposed rectifier design will be able to sustain high efficiency over a wider range of Pin, frequency and load (R_L).

This section presents a novel rectifier with enhanced efficiency based on a compact inkjet-printed quadrature hybrid coupler (QHC). The aim is to improve efficiency over a wider range of input power level and output load. The input matching network and output load of the rectifier are optimized for optimal RF-dc conversion efficiency. However, in the proposed topology, the output ports of the QHC are connected to the input matching networks of two

sub-rectifying circuits. The aim of the QHC is to improve RF-dc conversion efficiency by re-using the power in the rectifying circuits. The rectifier was designed at 1.5 GHz and the proposed equivalent also operates in the same frequency and performance comparison was done. The proposed topology was able to achieve a higher efficiency over a wider input power level and load dynamic ranges than the single rectifying circuit without the coupler. The input level range for a maximum RF-dc conversion efficiency increased from about 3 dBm to over 8 dBm for a two-tone input signal. Improvement of over 7 dBm input power range was also achieved using digital signals such as QPSK, 16 QAM and 64 QAM. A 4G LTE signal is also used to evaluate the ACPR performance of the rectifier.

5.4.1 Inkjet-printed Coupler Application in a Rectifier Circuit

Figure 5-18 gives the schematic of the proposed rectifier design.

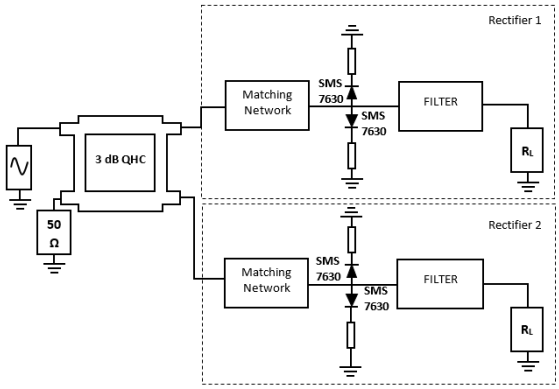

Figure 5-18: The block diagram of the proposed rectifier topology.

The compact inkjet-printed multiband coupler described in section 5.3 is used in this section as the main input splitter as shown in Figure 5-18.

The design of the rectifier circuit was essential to achieve the best RF-DC conversion efficiency, for this purpose a single stage, full wave; peak to peak rectifier has been used [5.29]. At the input of the rectifier, the coupler's matching network was used to ensure the highest power transfer between input power and output power through converting the 50 Ω input impedance of the antenna to match the conjugate input impedance of the rectifier. The coupler's robustness against load insensitivities will also help improve the efficiency of the rectifier circuits for each individual load R_L.

Multi-tone such as two-tone and digitally modulated 4G QPSK, 16 QAM and 64QAM signals are used to evaluate the efficiency for varying loads and selected input power levels. The RF-dc conversion efficiency versus input power and output load is shown in Figure 5-19 and Figure 5-20 respectively. The two proposed rectifiers based on the coupler are compared with the rectifier without the coupler. The proposed topology gives a better bandwidth efficiency performance than the rectifier without the coupler. Figure 5-19 shows the RF-dc conversion efficiency of the proposed rectifier topology versus input power for a two-tone input power. At the same input power (Pin) of 15.5 dBm, they have almost the same peak values. However, the proposed design with the coupler achieves a higher efficiency over the one without the coupler.

Also, the efficiency is improved over a wider input power range as compared to the rectifier itself. The efficiency over 70% for the rectifier is between 12.5 dBm and 15.4 dBm whilst for the proposed design; it gives a wider input power level range between 10.1 dBm and 18.5 dBm over 70%. For efficiency results above 60%, improvements of over 5 dBm on the input power level is also noticed (3 to 20 dBm for proposed and 5 to 17 dBm for single rectifier).

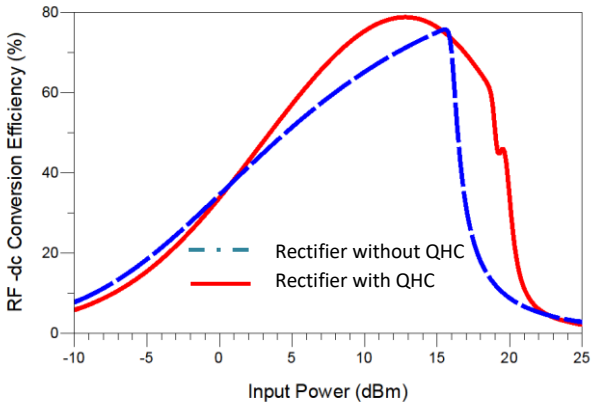

Figure 5-19: Simulated results for load R_L = 5k at 1.5 GHz.

Figure 5-20 gives the RF-dc conversion efficiency of the proposed rectifier topology versus output load (R_L) for a two-tone input power. The efficiency of the rectifier has been enhanced by the proposed rectifier plus coupler configuration over the load range of 1 to 15 kΩ. The Figure 5-20 shows that the performance of the proposed rectifier with the coupler has also effectively improved the performance of the coupler over a wider output load range.

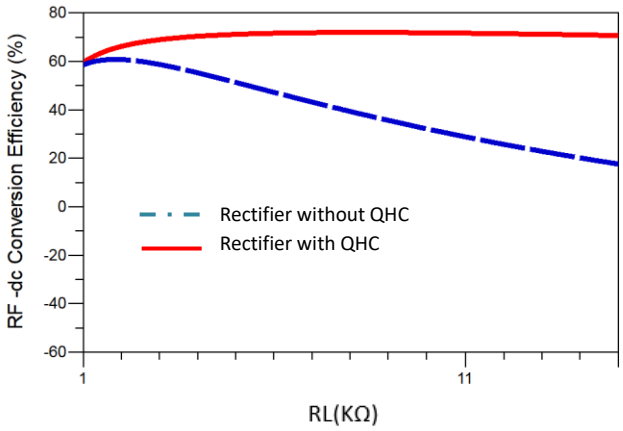

Figure 5-20: Simulated Results for Pin of 12.2 dBm at 1.5 GHz

To further evaluate the efficiency performance, the proposed rectifier topology is tested with QPSK, 16 QAM and 64 QAM digitally modulated signals and an improvement of over 7 dBm was observed for all 3 cases as seen in Figure 5-21, Figure 5-22 and Figure 5-23 with a higher efficiency over a wider bandwidth.

The QPSK, 16-QAM and 64-QAM signal transmits 2 bits, 4 bits and 6 bits per symbol respectively. For QPSK, the signal shifts among phase states that are separated by 90 degrees. Data into the modulator is separated into two channels I and Q. Two bits are transmitted simultaneously, one per channel. Each channel modulates a carrier and the amplitude of the two carrier frequencies are the same, but their phase is offset by 90 degrees. The two carriers are then combined and transmitted. The same idea is used for 16-QAM and 64-QAM. For 16-QAM signals, four I values, and four Q values are used yielding four bits per symbol and for 64 QAM, six I values and 6 Q values yielding six bits per symbol. QPSK, 16-QAM and 64-QAM are all quadrature meaning that the phase is offset by 90 degrees. The changing amplitude and phase for different symbols are set in the LTE signal generator for QPSK, 16-QAM and 64-QAM respectively.

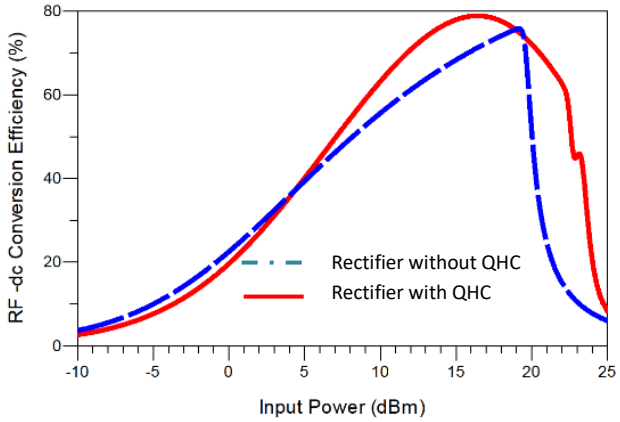

Figure 5-21: Simulated efficiency results with QPSK digital signals.

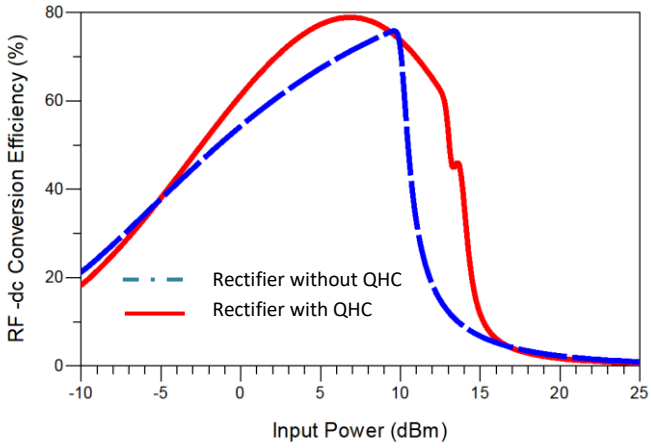

Figure 5-22: Simulated efficiency results with 16 QAM digital signals.

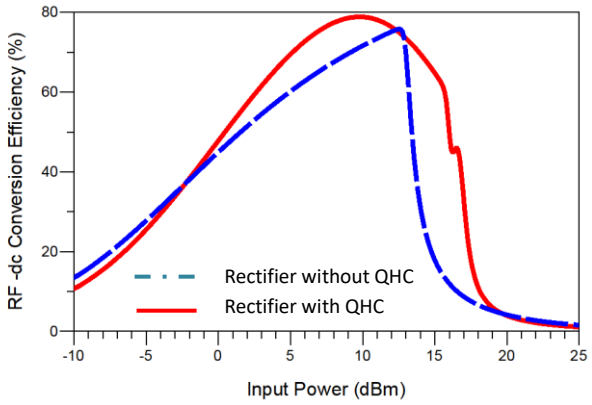

Figure 5-23: Simulated efficiency results with 64 QAM digital signals.

The wider bandwidth efficiency observed in the 3 consecutive Figures above (Figure 5-21, Figure 5-22 and Figure 5-23) is due to the properties of the inkjet-printed coupler whereby it maintains its good performance (good isolation) over a wide band. To evaluate the peak-to-average power ratio (PAPR), a 3 MHz digital 4G LTE signal is used. The block diagram for the test set up is shown in Figure 5-24a. The experiments are conducted using Figure 5-24. The 3 MHz LTE signal is generated from the LTE signal generator which is then sent through the QHC that splits the outputs to both rectifiers before being analysed at the spectrum analyser where the power spectral density is observed as seen in Figure 5-24b.

The in-band PAPR for proposed rectifier with and without coupler is evaluated and compared based on output power spectral density. RF-dc conversion efficiency conclusions from the PSD results are also described. Figure 5-24b depicts the output power spectra result for the proposed rectifier with and without QHC.

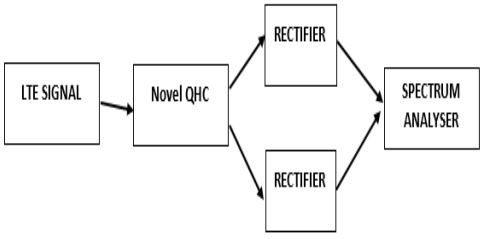

(a)

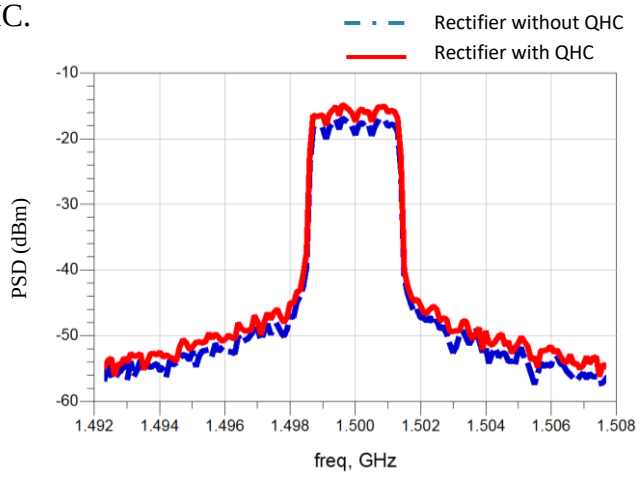

(b)

Figure 5-24: (a) Block diagram of PAPR test circuit. (b) Output power spectra for proposed rectifier.

To evaluate the output power spectral density performance of the proposed circuit, 3MHz LTE 64-QAM signals were utilized. Fig. 10 shows the output power spectra density for the LTE

signal at the center frequency of 1.5 GHz. The output power spectral density (PSD) results for both rectifier cases are depicted in the figure.

LTE input signals of 10dBm are fed into the normal and proposed rectifier design and the rectifier's output spectral density is evaluated as shown in Figure 5-24b. The output power spectral density of the proposed circuit shows a slightly higher peak PSD value whilst maintaining spectral efficiency. This implies that for the same power at the rectifier's input, higher peak PSD was achieved which is a sign of improved efficiency which was already presented in Figure 5-19 – Figure 5-23.

This section has successfully presented a new effective topology for developing high-efficiency rectifiers to improve efficiency over a wider input power and output load range. The proposed circuit has been implemented with over 8 dBm improvement in input power level for efficiency above 70% at the center frequency of 1.5 GHz. Performance comparison has been done for the rectifier with and without the coupler (QHC) and compared with literature.

These results illustrate that the proposed rectifier with QHC design will improve efficiency as it has demonstrated higher peak output PSD for the same output power and improved RF-dc conversion efficiency over a larger bandwidth thereby improving the overall performance of the system. These improved properties make the design very useful for energy harvesting.

5.5 Evaluation of 5G Waveform Candidates

It is predicted that the mobile broadband traffic will be increased by 1000-fold during the next decade [5.29]. The rising popularity of bandwidth-hungry applications such as high-definition video streaming and multimedia file sharing calls for faster data rates with low latency connection. Once 5G is up and running, development of the IoT will accelerate until IoT applications such as smart cars and smart home appliances are a part of everyday life which will drive artificial intelligence (AI) and virtual reality (VR). The increase in internet traffic will require constant connectivity, efficient management systems and an architecture that is able to handle the number of devices. With capability objectives for 5G, such as 20 Gbps peak data rate, 106 devices/km^2 connection densities and 1 ms latency, improvements must be made upon the current 4G cellular technology [5.30]. One improvement at the heart of this advancement is the use of alternative waveforms that can achieve better spectral efficiency for various input power levels and increasing bandwidth.

Orthogonal frequency-division multiplexing (OFDM) has been the major waveform used for 4G with good robustness against multi-path propagation but with drawbacks such as large side-lobes which leads to high adjacent channel interference (ACI) and inter-carrier interference (ICI) which should be avoided for 5G networks. Its cyclic prefix technique (CP-OFDM) reduces spectral efficiency significantly [5.31]. The spectrum efficiency of 5G is expected to be three times higher than CP-OFDM as the 10% of the bandwidth reserved as guard bands needs to be reduced enormously [5.30]. The reduction of these guard bands should ensure that the spectral efficiency is maintained over larger bandwidths.

Currently, there are several multicarrier waveform candidates that are being considered for 5G to address these limitations. The two leading candidates at the moment are FBMC and UFMC.

Filter-bank multicarrier (FBMC) implements subcarrier filtering to achieve better spectral efficiency and overcomes the strict synchronization specifications of OFDM whilst Universal Filter MultiCarrier (UFMC) has comparable spectral efficiency to FBMC, but has reduced filter length requirement and is achieved by performing filtering operation per sub-band instead of per subcarrier [5.32]. Recently, the 5G waveform candidates have been evaluated in different ways but none have considered the spectral efficiency over increasing bandwidths up to 50 MHz or more.

This section represents evaluation of the nonlinear behaviorur of a nonlinear power using 4G CP-OFDM signal in comparison with 5G FBMC and UFMC signal. The two leading 5G waveform candidates were evaluated and compared for bandwidths up to 50 MHz at different input power levels. Experiments were also carried out to evaluate the spectral efficiency performance for the 4G (CP-OFDM) and 5G waveform candidates (FBMC, UFMC) at different input power levels for different bandwidths. The next considers the waveform candidates characteristics that form the basis of this paper and then simulation and experimental results for CP-OFDM, UFMC and FBMC are presented and investigated. Future work and conclusions are also presented.

5.5.1. Improved Nonlinear Distortion Performance with new 5G Waveforms

In this section, various waveform candidates are considered and compared based on their implementation in wireless transmitters. The 5G waveform candidates FBMC and UFMC and CP-OFDM are evaluated in simulations and experimentally for different input power levels at saturation and different bandwidths.

5.5.1.1 ZFL-500 Nonlinear Evaluation for the 5G Wireless Transmitters

Highly efficient power amplifiers will reduce power consumption and increase the battery life of the 5G wireless transmitter. The signals for 5G should be able to maintain high linearity even at saturation and for high bandwidths as the signal will mostly operate close to saturation of the power amplifier (wireless transmitters) to maximise efficiency. In this sub-chapter, CP-OFDM, UFMC and FBMC signals are evaluated and compared close to saturation and at different frequency bandwidths to evaluate the spectral performance of each signal and deduce the best waveform candidate for 5G. The centre frequency of 700 MHz was chosen as it is one of the main 5G bands below 6GHz for Europe. Figure 5-25 shows the test set up with the mini-circuits ZFL-500 PA.

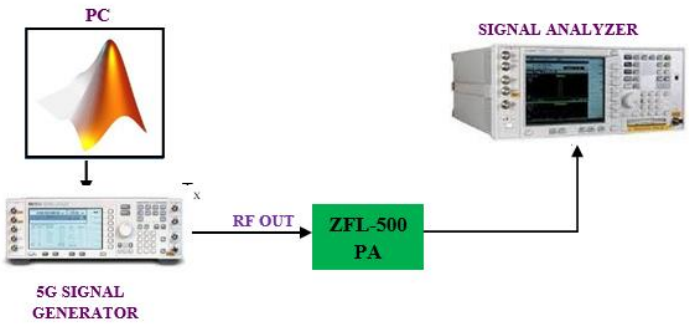

Figure 5-25: 5G transmitter test setup.

In Figure 5-25, all three signals with 3 and 10 MHz channel bandwidth are passed through the baseband equivalent wireless transmitter model at 700 MHz. The system level simulations were performed using Keysight's Agilent design software. Experimental model for the Mini-Circuits ZFL-500 PA was used in simulations. These signals are sent throught the ZFL-500 PA with the outputs observed in the signal analyzer. Using Figure 5-25, power spectra of CP-OFDM, 5G FBMC and UFMC signals at the output of the PA are presented in Figure 5-26 and Figure 5-27 to evalautae the nonlinear distortions.

Figure 5-26 and Figure 5-27 show the effect of nonlinear distortion of the PA on all three signals. As can be seen from Figure 5-25, the ACPR for 5G FBMC signal is about 16 dBc more when compared to CP-OFDM and about 10 dBc for UFMC. For Figure 5-27, a 16 dBc improvement in CP-OFDM ACPR and 8 dBc for UFMC. For higher bandwidth of 10 MHz, whilst the linearity of UFMC increases with respect to FBMC, CP-OFDM still maintains its poor spectral performance.

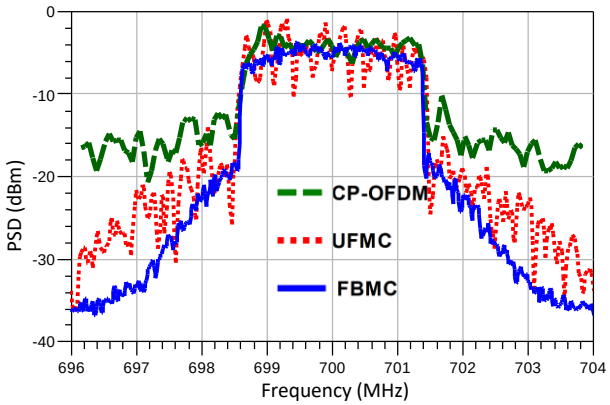

Figure 5-26: Simulated output power spectra for 3MHz bandwidth.

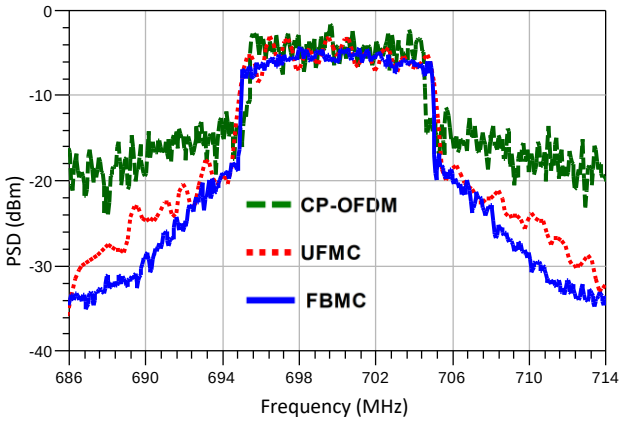

Figure 5-27: Simulated output power spectra for 10 MHz bandwidth.

LTE can only support a maximum of 20 MHz. For channel bandwidths greater than 20 MHz which is the maximum for 4G, only 5G Signals such as UFMC and FBMC will be considered. Figure 5-28 evaluates the nonlinear distortion performance for the PA close to saturation for a 50 MHz channel bandwidth with the two leading 5G candidates (UFMC and FBMC).

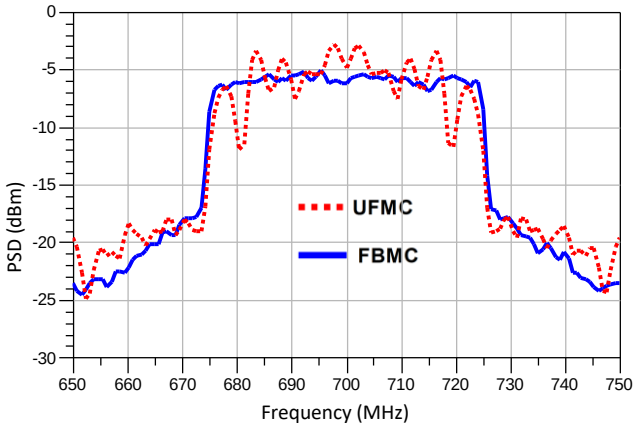

Figure 5-28: Simulated output power spectra for 50 MHz bandwidth.

Figure 5-28 shows that for a 50 MHz channel bandwidth, FBMC and UFMC are becoming more comparable in ACPR improvement compared to lower frequencies like in the 3MHz and 10 MHz cases in Figure 5-26 and Figure 5-27 respectively. The linearity of the spectrum for both signals are much similar with UFMC still achieving higher power spectral density as well. As the channel bandwidth becomes larger (say above 20 MHz), the performance of UFMC improves and becomes more comparable to FBMC whilst still achieving a higher power spectral density.

The subcarrier grouping of UFMC allows the filter length to be reduced when compared to FBMC. It uses a finite impulse response (FIR) filter whose impulse response can be of a shorter finite duration (short filter length). Spectral efficiency relates to how linear the digital signals (such as OFDM and FBMC) are at the same input power. As seen in Figure 5-26, Figure 5-27 and Figure 5-28, UFMC has good linear performance like FBMC. FBMC and UFMC will both play a vital role as the proposed 5G candidate for linearity when the wireless transmitter is maximising efficiency by operating close to saturation and for higher channel bandwidth above 20 MHz.

Experiments were carried out using all three 5G waveform candidates. Figure 5-29 gives the 5G measurement set up for the signal evaluations. It consists of Keysight MXG N5182A signal generator which is the Laboratory equivalent of the wireless transmitter. The Mini-Circuits ZFL-500 PA was used as device under test (DUT) for measurement. This DUT was fed by a CP-OFDM and then with 5G FBMC and UFMC signals. All signals were tested at 5G's 700 MHz band with the same input power and measurements were taken. The input power was varied at saturation to observe the effect of nonlinear distortion introduced by PA. The signal was down-converted by Keysight VSA and captured by 89600 VSA software running on the PC.

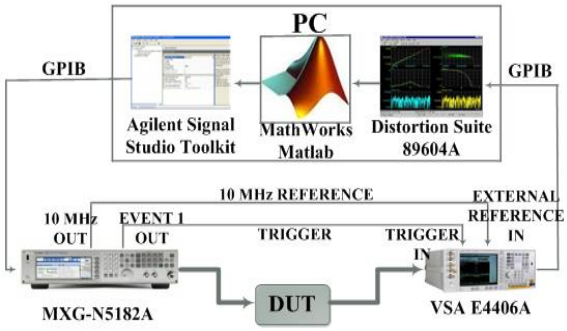

Figure 5-29: 5G measurement setup.

Even though simulations have tested up to 50 MHz, for the purpose of mesurements, channel bandwidths of 1.4 MHz and 3 MHz will be used in this analysis as its the maximum that the signal generator could support. In order to evaluate the level of the nonlinear distortion introduced by the ZFL-500 PA to the wireless transmitter, the output power spectra of the CP-OFDM, FBMC and UFMC signals for the 1.4 MHz LTE bandwidth at input power level of –15 dBm is shown in Figure 5-30.

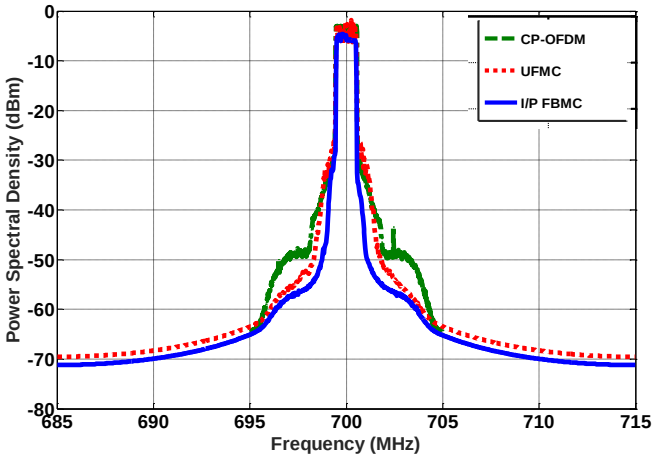

Figure 5-30: Measured output power spectra of the PA for 1.4 MHz bandwidth.

As depicted in the measured results shown in Figure 5-30 above, 1.4 MHz CP-OFDM signals have larger side-lobes in comparison with 5G FBMC and UFMC signals. 5G FBMC signals have the best spectrum of the 3 signals for the same input power as it has steep slopes at its edges. While CP-OFDM relies on the CP to prevent ISI and to convert the channel into a set of flat-gain subcarriers, FBMC exploits the fact that narrow and numerous subcarriers can be characterized by a flat gain to achieve better spectral efficiency. CP-OFDM and UFMC both possess high PAPR characteristics that increases sensitivity to nonlinear distortion. This high PAPR characteristic is due to the overlapping of multi-carrier signal. However, even at low frequency bandwidth of 1.4 MHz, the spectral shape of UFMC is still better than CP-OFDM as its filtering operation leads to a reduced out-of-band leakage which makes UFMC respond better to distortion. Also, UFMC is more spectrally efficient than CP-OFDM as it reduces the

guard bands in adjacent channels and avoids the use of CP as well. Due to the poor performance of CP-OFDM, this paper then focuses on comparing the two leading candidates for 5G communications. Figure 5-30 already shows ACPR improvement of 15 dB (PSD of -40 dBm and -55 dBm) for FBMC over UFMC.

The measured results of FBMC and UFMC signal operating at different input power levels close to saturation are subsequently compared. To observe how FBMC and UFMC respond to different levels of distortion, two saturation input power levels of the PA (-15 dBm and -10 dBm) are utilised. Figure 5-31 and Figure 5-32 gives the measured results of the ZFL-500 PA for a 3MHz channel bandwidth of the 5G UFMC and FBMC signals utilising input power of -15 dBm and -10 dBm respectively at the same centre frequency of 700 MHz.

It has been observed from the analysis of both measured results in Figure 5-31 and Figure 5-32 that even though FBMC still maintains a better spectral efficiency and linearity performance, its response to nonlinear distortions is similar to UFMC in relation to the input power level change. The ACPR for both increased by 10 dB for both signals when the input power level changed from -15 dBm to -10 dBm. This is partly due to the fact that UFMC also reduce the OOB emissions in CP-OFDM as FBMC does. However, the level of distortion in FBMC is still lower with a 10 dB (PSD of -30 dBm for UFMC and -40 dBm for FBMC) difference over UFMC.

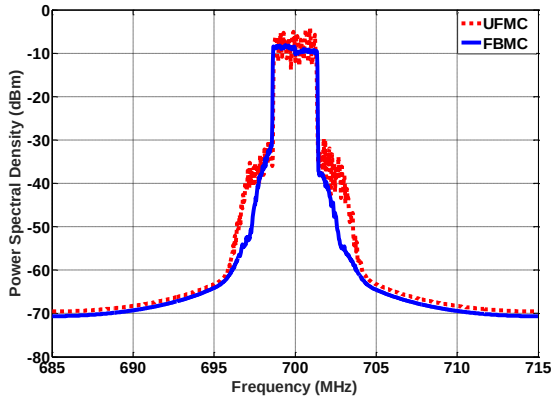

Figure 5-31: Measured PA Output Power Spectra for 3 MHz Bandwidth and -15 dBm Pin

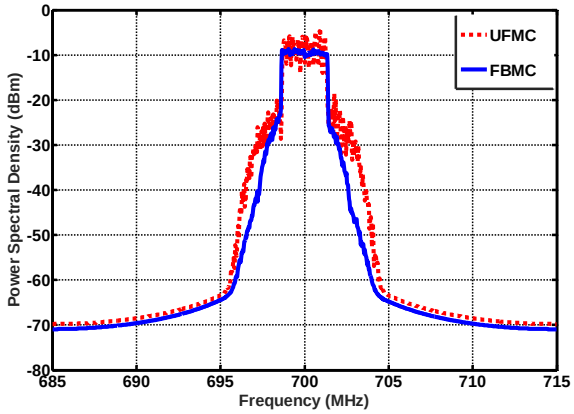

Figure 5-32: Measured PA Output Power Spectra for 3 MHz Bandwidth and -10 dBm Pin

FBMC outperforms other 5G candidates with regards to spectral efficiency at different channel bandwidths and has the best sensitivity to nonlinear distortions in the 5G wireless transmitters. Whilst FBMC is very promising for 5G, it may be more complex to implement in practice when compared with UFMC. This is because UFMC is a direct improvement on the draw backs of the already deployed and successful OFDM technology for LTE. Further advancements in UFMC can still compare to FBMC especially for larger bandwidths above and below 6 GHz.

Different single and multi-carrier waveforms are being investigated as prospective candidates for the 5G radio interface. In this section, the waveform of 4G's cyclic prefix CP-OFDM in comparison with the two leading 5G waveform candidates (FBMC and UFMC) have been evaluated. These signals are evaluated and compared for different input power levels up to saturation and for increasing bandwidth. Simulated results show that UFMC gained about 6 dBc ACPR improvements over FBMC for 3 MHz and 10 MHz bandwidth whilst CP-OFDM maintained its poor performance. For 5G bandwidth of 50 MHz, spectral efficiency of UFMC further improved and was comparable to FBMC whilst UFMC still achieved higher power spectral density which improves the case for adopting UFMC as a leading 5G waveform candidate.

Measured results for 1.4 MHz and 3 MHz bandwidth show FBMC ACPR improvements of 15 dBc and 10 dBc over UFMC. This reduction shows that for larger bandwidths above 20 MHz, UFMC could match FBMC's spectral efficiency performance. Experimental results match with simulations with FBMC outperforming other candidates for spectral efficiency and nonlinear distortion performance in the 5G wireless transmitter. However, UFMC is matching FBMC for bandwidths above 20 MHz which implies that both signals will be vital for 5G wireless communication infrastructure.

The performances of 5G waveform candidates in comparison with its 4G equivalent have been evaluated. CP-OFDM, UFMC and FBMC were all evaluated at different channel bandwidths and different power levels for nonlinear distortions at 5G's 700 MHz frequency band. Measured and simulated results give a good match for 3 MHz signals and show that for higher bandwidths, the spectral efficiency of UFMC improves with respect to FBMC whilst CP-OFDM still maintains its poor spectral performance. Both FBMC and UFMC are worthy candidates for 5G. Even though FBMC is very promising, it may be easier to implement UFMC as it is a direct improvement on the draw backs of already deployed CP-OFDM and further advancements in UFMC can compete with FBMC at lower and higher channel bandwidths.

5.6 Balanced Power Amplifier Designs with the aid of USTL microstrip couplers for 5G Applications

High speed data transmission is becoming more in demand for applications such as wireless personal area network and LTE-Advanced applications. Because of the shift towards higher power and more bandwidth applications, the flexibility of adapting to traffic and carrier aggregation (CA) is a dire need for next generation networks [5.33]. Because of such high data throughput rate, power and spectral efficiency over the whole bandwidth should be improved to maintain good signal quality [5.34].

Important PA characteristics such as high power, high efficiency, linearity, gain flatness, and good input and output matching over the whole bandwidth has become more stringent to match the needs of such advanced networks.

Due to the ever-growing demand for battery life extension, it is highly essential that the efficiency of the PA is significantly improved at both low output and peak power levels [5.35]. However, recent spectrum efficient modulation schemes such as OFDM and this day multiple access techniques result into signals with large peak-to-average power ratio (PAPR). Poor efficiency has been observed in conventional PAs operating with such signals, when operated at output power back-off (OPBO) region at saturation [5.35]. In such case other PA amplifier configurations such as Doherty and balanced PA could be used to improve efficiency.

In a balanced PA configuration, by taking advantage of the multi-mode operation of the coupler and the balanced topology, load-insensitivity characteristics could be accommodated thereby enhancing efficiency [5.35]. Similar balanced PA design techniques have been used in [5.35], [5.36] and [5.37] to increase the power aided efficiency (PAE) of the PA.

However, the size of the balanced PA architecture could be very large when using conventional coupler designs that operate at frequencies below 4 GHz.

In the next chapters, a highly linear and efficient balanced PA is presented. The compact quadrature hybrid coupler using a novel USTL concept designed and fabricated in chapter 5.2 has been used here. Small signal measurements show good gain flatness over the frequency band match with improvements of over 20 dB in input (S_{11}) and output (S_{22}) matching performance of the balanced PA with coupler as compared to the individual PA due to the absorption of the reflected power in the coupler terminations.

More importantly, large signal measurements of the proposed design gave an increase in maximum saturated output power and PAE in simulations and for measurement results in chapter 5.6.2. When tested for 5G applications, the proposed design with USTL coupler achieved better efficiency and improved linearity even as the bandwidths become larger. The proposed balanced PA with coupler is highly efficient, linear and will be very useful for next generation 5G networks.

5.6.1 Balanced Power Amplifier Design with USTL QHC and GaN CGH40010 PA

The emergence of new technologies need for faster speeds and reliable connection for the growing millions of subscribers are the drivers for next generation mobile networks such as 4G LTE, LTE-Advanced and 5G networks. The ever-growing data rate expectations and number of end users for mobile communications has had a direct impact on the future of mobile wireless communications. Currently, the wireless communication frontier is shifting from the current fourth generation (4G) to the forthcoming 5G networks as higher speed data transmission with low latency has become more popular [5.38]. To achieve higher data rates, LTE requires more bandwidth and can combine up to 5 component carriers to achieve the higher speeds required. The increased bandwidth can achieve better throughput but should maintain good efficiency, power and linearity over the whole bandwidth to meet the stringent requirements for next generation networks. Because the PA is a vital component in the wireless transmitter, it is highly essential that the efficiency of the PA is significantly improved at low and saturation

power levels [5.39]. A very effective way of maintaining high PA efficiency is by operating the amplifier in the class J mode [5.40]. Hence, a highly efficient amplifier could be used but its efficiency and linearity will still be affected at its peak power levels.

PA configurations such as balanced PA have been utilized to increase the power aided efficiency of the power amplifier by improving the load variations. Integrated quadrature hybrid couplers in the balanced topology help to achieve robustness against load insensitivities which then boosts efficiency [5.41] - [5.43]. However, it has been observed that the conventional coupler occupies a very large area especially when considering lower RF frequencies below 4GHz which makes it too bulky for practical use [5.44]. Various microstrip line concepts have been utilized to reduce the overall size of the quadrature hybrid couplers by replacing its conventional transmission line.

In this section, the coupler designed in section 5 is used in conjunction with a class-J GaN [5.45] power amplifier in a balanced PA architecture to achieve better efficiency and linearity at saturation. The proposed balanced PA design also achieved better input and output matching. It also achieved encouraging spectral efficiency improvements when implemented in a carrier aggregated system with two component carriers and for different bandwidths. The proposed balanced PA is highly linear, efficient and will be play a vital role for next generation wireless communications such as 5G.

5.6.1.1 Balanced GaN CGH40010 PA Design with USTL QHC

The balanced PA circuit consists of two identical power amplifiers (PA) and couplers each. The couplers and PAs are chosen to operate at identical frequencies. Figure 5-33 shows the balanced PA schematic. The coupler acts as a splitter at the input to divide the signals out of phase by 90^0 and then recombines the signals at the output after it has been amplified by the PAs.

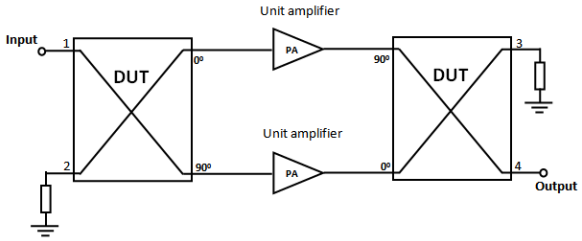

Figure 5-33: Balanced PA schematic.

The DUT is the USTL QHC designed in section 5.2. Simulation results of the USTL coupler are used in the architecture. The coupler is optimized to operate wideband with centre frequency of 1.5 GHz.

The PA under test is the class-J GaN PA. The PA was designed using Cree's CGH40010 transistor. The operating frequency is f =1 .5 GHz, Vb = 20V, and Im =1A. The gate voltage is set to Vg = −2.8 V, which positions the quiescent drain current to about 10% of its maximum. [8]. Simulated results of the GaN CGH40010 PA are also used.

The balanced PA has been designed using the USTL quadrature hybrid coupler and PA into Figure 5-33 above. Simulated results are presented for the balanced PA in section III and

compared with the single GaN CGH40010 PA in terms of matching, efficiency, linearity and for different bandwidths at saturation. The simulated results of the designed balanced PA with coupler and the individual GaN class-J PA are presented and compared in this section. Small and Large signal measurements were made.

Figure 5-34 shows that the simulated gain of the balanced PA almost matches with the gain of the single GaN CGH40010 PA from 1.4 to 1.7 GHz even though it is slightly higher for the GaN PA as expected. The maximum gain is about 20 dB at the centre frequency of 1.5 GHz and both results match well from the frequency range between 1.4 GHz and 1.7 GHz before it starts to drop considerably in relation to the single GaN case. The bandwidth of the balanced PA is slightly narrower due to the characteristics of the USTL QHC.

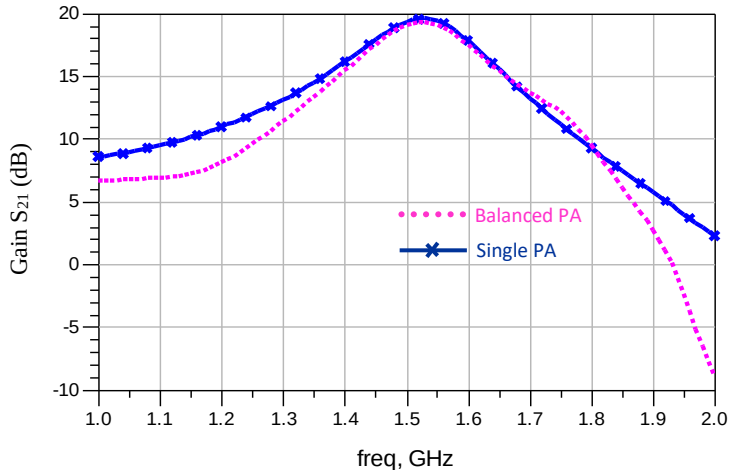

Figure 5-34: Simulated s-parameter (S_{21}) results.

Other small signal measurements for input and output gave better matching results for the proposed configuration. The input and output return reflection coefficient (S_{11} and S_{22}) GaN PA has been improved by the balanced PA design as seen in Figure 5-35 and Figure 5-36 respectively. The S_{11} result for the single GaN PA is around -32 dB whilst the measured and simulated S_{11} results for the proposed balanced PA at the required frequencies are lower than -38 and -42 dB respectively.

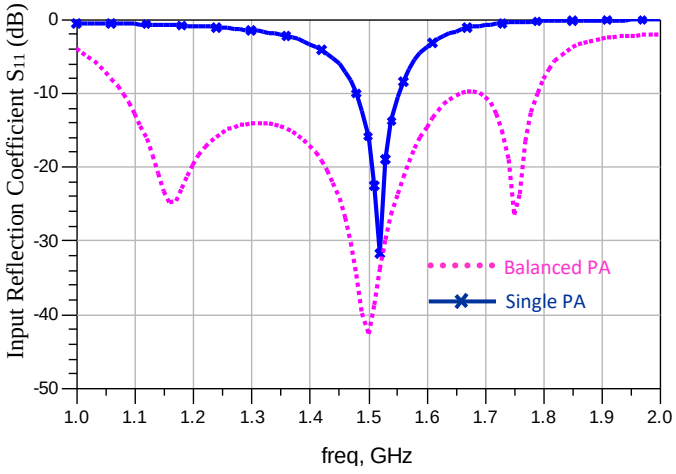

Figure 5-35: Simulated s-parameter (S_{11}) results.

Similarly, for the output S_{22} in Figure 5-36, the results of the balanced PA design showed better matching over its GaN PA equivalent. Figure 5-36 shows about -32 dB for the single PA whilst both simulated and measured results for the balanced PA are both below – 35 dB at the same operating frequencies.

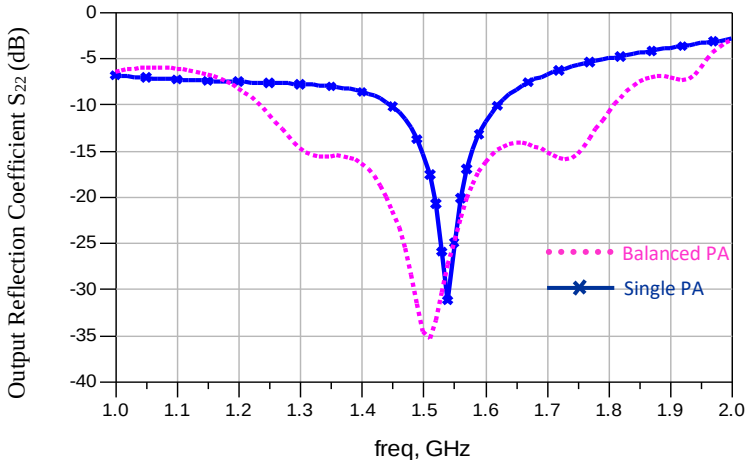

Figure 5-36: Simulated s-parameter (S_{22}) results.

For linearity and efficiency measurements, the centre frequency of the QHC at 1.5 GHz is targeted for input power levels just above the 1 dB compression. Due to this, the power aided efficiency for the balanced PA is considered at the input power of 23 dBm for the frequency range (1.2 – 1.8 GHz) due to the properties of the QHC. Figure 5-37 gives the efficiency for the PA and balanced PA with about 10% improvement over the whole frequency band.

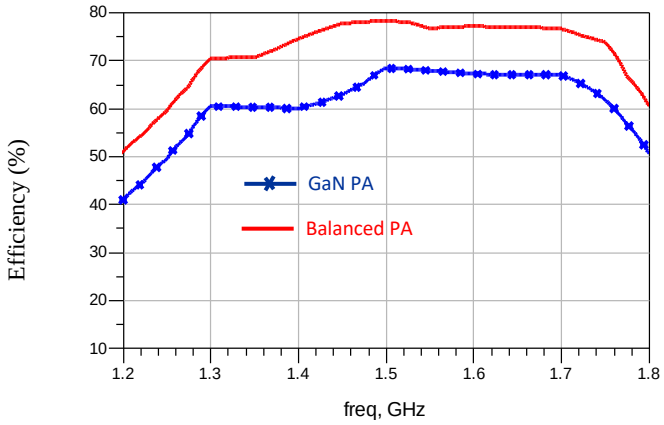

Figure 5-37: PAE against frequency at saturation.

Other measurements such as output power, gain and drain efficiency (DE) at the QHC centre frequency of 1.5GHz were obtained and compared. These measurements were obtained by power sweeps (Pin) from -10 to 30 dB. Figure 5-38 shows the graph combining the gain, output power and drain efficiency for the above input power (Pin) range up to saturation. The balanced PA utilizes the isolation port (port 4) of the USTL QHC as its signal path. GaN CGH40010 PA under test delivers a maximum saturated output power (Pout) of 37.41 dBm and the implemented balanced PA achieved higher maximum Pout of 42.92 dBm.

The drain efficiency (DE) for both single and balanced were similar until the GaN power amplifier moved above its 1 dB compression point. For input power of 25 dBm, the PAE of the GaN PA is 74.5 % whilst the implemented balanced PA with incorporated QHC showed a good improvement with highly enhanced drain efficiency (DE) of 83.8 % thereby boosting efficiency by about 10%.

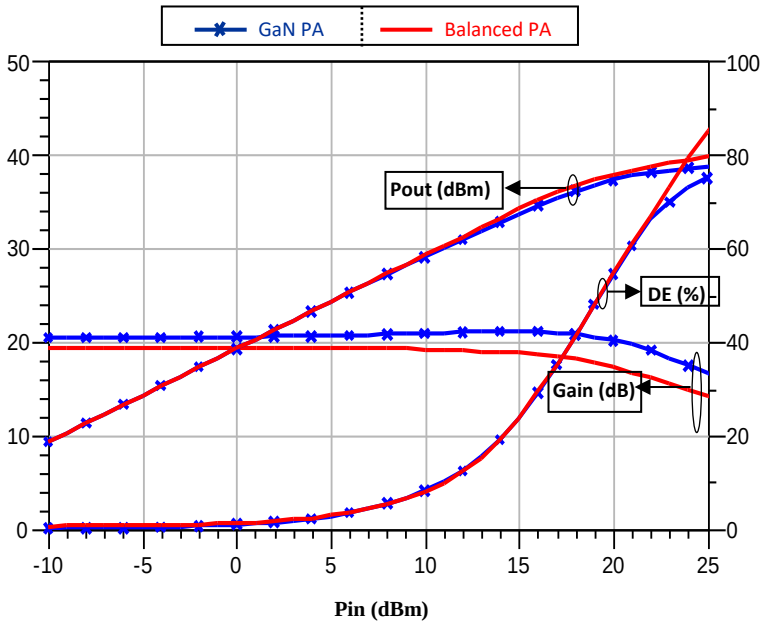

Figure 5-38: Gain, output power and drain efficiency at 1.5 GHz.

These power aided efficiency improvements ensure the PA performs highly efficient for high power levels above the 1 dB compression point of the PA. These results show that the balanced PA would positively affect the battery life of mobile phones. The spectral performance of balanced PA design will be evaluated in 4G and 5G wireless transmitters to observe linearity improvements at saturation (good efficiency) due to the improved output power and efficiency results.

5.6.1.2 Balanced GaN PA Application in Next Generation Wireless Transmitters

The proposed balanced PA has been observed to deliver better efficiency in section 5.6.1.1. However, efficiency and linearity are trade off characteristics at saturation which means that its linearity would ideally degrade at saturation. The designed balanced PA can achieve better linearity than its single PA equivalent. This proposed architecture with the aid of the USTL QHC will be tested in 4G LTE and 5G wireless transmitters. The configuration will be investigated for linearity and spectral efficiency improvements at different frequency bandwidths and different power levels close to and at saturation. Figure 5-39 gives the balanced power amplifier measurement setup.

LTE signals of 3 MHz and 10 MHz are sent through the DUT. The signal used is generated in the MXG signal generator through Agilent Keysight Signal Studio Kit. The signal passes through the USTL QHC coupler which splits the signal to both gallium nitride (GaN) CGH40010 transistor PAs and are then recombined. The centre frequency of 1.5 GHz will be used as it's the operating frequency for the coupler and GaN PA.

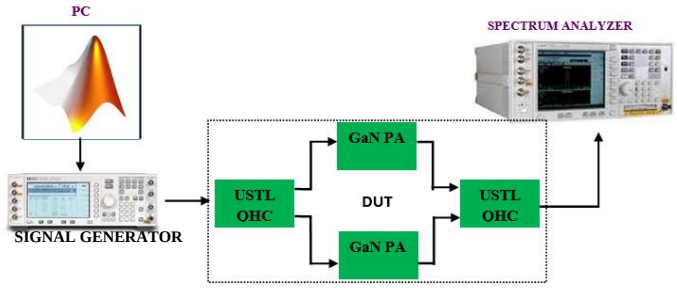

Figure 5-39: Balanced power amplifier test setup

The wireless transmitter test will be performed for 10 MHz channel bandwidth at three different power levels close to saturation of the GaN PA. Figure 5-40, Figure 5-41 and Figure 5-42 give the output spectra of the balanced PA when compared to the its single GaN equivalent at input power levels of 15, 20 and 25 dBm (Back-off levels from saturation (23 dBm)) respectively.

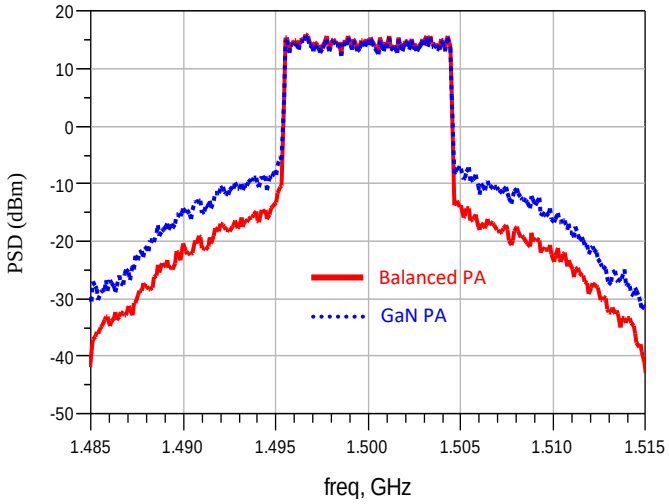

Figure 5-40: Simulated PA output spectra for 10 MHz LTE signal and Pin of 15 dBm.

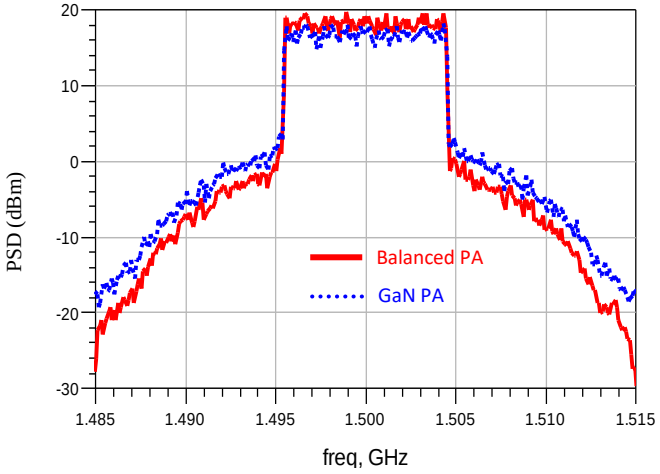

Figure 5-41: Simulated PA output spectra for 10 MHz LTE signal and Pin of 20 dBm.

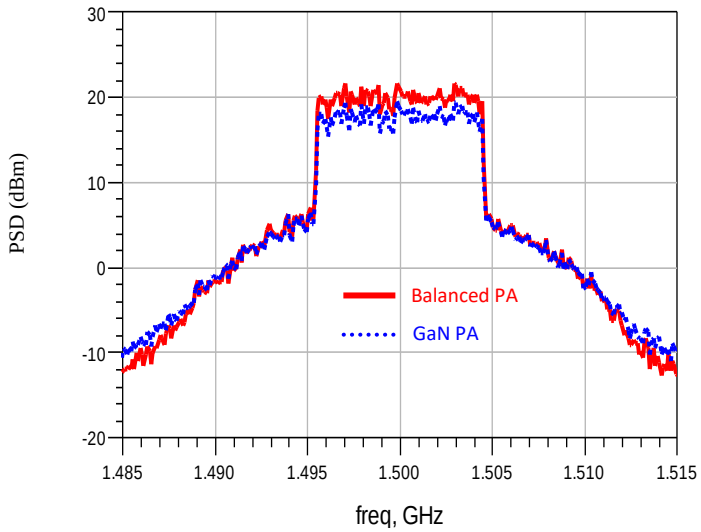

Figure 5-42: Simulated PA output spectra for 10 MHz LTE signal and Pin of 25 dBm.

As can be seen from the results above, for Pin of 15 dBm in Figure 5-40, the GaN PA is still in its linear region as its 1 dB compression point (P_1dB) is at 17 dBm input signal and so the PSD peaks are the same for the balanced PA and single GaN PA. The nonlinear distortion (IM3) point for the 10 MHz signal bandwidth with centre frequency of 1.5 GHz is 1.491 GHz for all 3 cases. However, the balanced PA is still more linear as its ACPR is better by 6.2 dB (-15.294- (-21.527)).

However, as the PA operates in its nonlinear region, the balanced PA shows better efficiency as its PSD starts becoming higher. In Figure 5-41, the peak PSD is higher by 3.136 dB (19.563-16.427) and its IM3 point is better by 3.372 (-1.541 - (- 4.913)). This gives a 6.5 dB ACPR improvement for 20 dBm Pin. This implies that the balanced PA was able to simultaneously improve efficiency and linearity. Also, for a higher saturation input power of 25 dBm, the peak PSD of the balanced PA continues to rise faster than the single GaN case. The peak value for the balanced PA at the centre frequency is now 21.451 dB and 16.276 dB giving ACPR improvement of 5.175 dB. In this case, this implies that efficiency and linearity has been enhanced by 5.2 dB. The proposed balanced PA has shown great improvements on the efficiency and linearity performance for the PA at saturation and for different power levels. This design will be very useful for next generation 5G networks.

The excellent performance of the balanced PA in comparison to its single equivalent implies that it would be a very promising candidate for 5G networks. The next set of results will compare the 4G OFDM and 5G FBMC results when used with the proposed balanced PA. Still using the set up in Figure 5-39, more results are obtained. 4G and 5G balanced PAs will be compared using 3 MHz and 10 MHz channel bandwidth for two saturation input power levels of 20 dBm and 25 dBm of the GaN CGH40010 PA. Figure 5-43 and Figure 5-44 give the output power spectral density for the case of 3 MHz signal whilst Figure 5-45 and Figure 5-46 are for the 10 MHz channel bandwidth for Pin of 20 dBm and 25 dBm respectively.

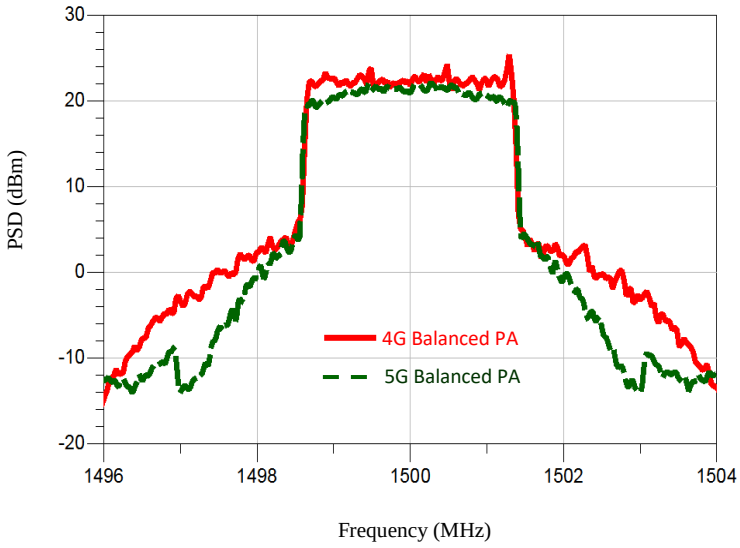

Figure 5-43: Simulated PA output spectra for 3 MHz LTE and FBMC signals with Pin of 20 dBm.

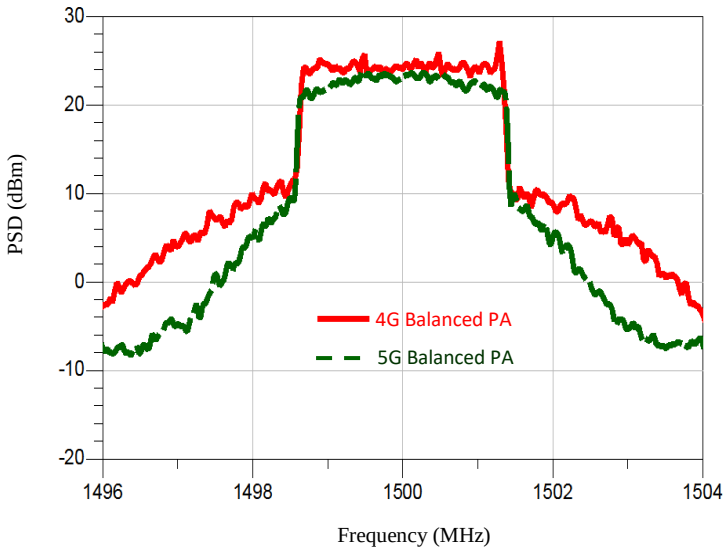

Figure 5-44: Simulated PA output spectra for 3 MHz LTE and FBMC signals with Pin of 25 dBm.

For the input power level of 20 dBm and channel bandwidth of 3 MHz, 4G balanced PA with OFDM has ACPR of 23.971 dB (21.763 dBm – (-2.208 dBm)) and 5G balanced PA with FBMC has ACPR of 34.313 dB (20.920 – (-13.393)). The nonlinear distortion (IM3) point for the 3 MHz signal bandwidth with centre frequency of 1.5 GHz is 1.497 GHz Therefore, the 5G balanced PA gave ACPR improvement of over 10.34 dB for the 3 MHz bandwidth for input power level of 20 dBm. Also, for higher saturation powers of 25 dBm, the 5G balanced also gave ACPR of 28.263 (22.670- (-5.593)) and 4G balanced had ACPR of 18.573 (23.971-(5.398)). Hence, 5G balanced also improved ACPR by about 9.7 dB.

The same calculations as above are done for 10 MHz channel bandwidth at the same input power levels. The nonlinear distortion point is the same at about 1.491 GHz. The ACPR for 10 MHz Pin of 20 dBm as seen in Figure 5-45 is about 35.855 dB for 5G balanced and 26.638 dB for 4G balanced with 5G having a 9.22 dB ACPR improvement over 4G. For Pin of 25 dBm, the ACPR improvement is 8.78 dB from the figure 5-46.

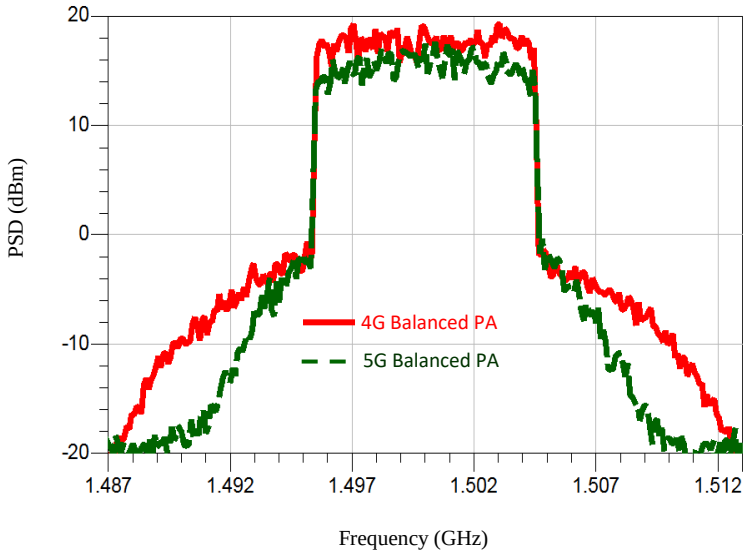

Figure 5-45: Simulated PA output spectra for 10 MHz LTE and FBMC signal with Pin of 20 dBm.

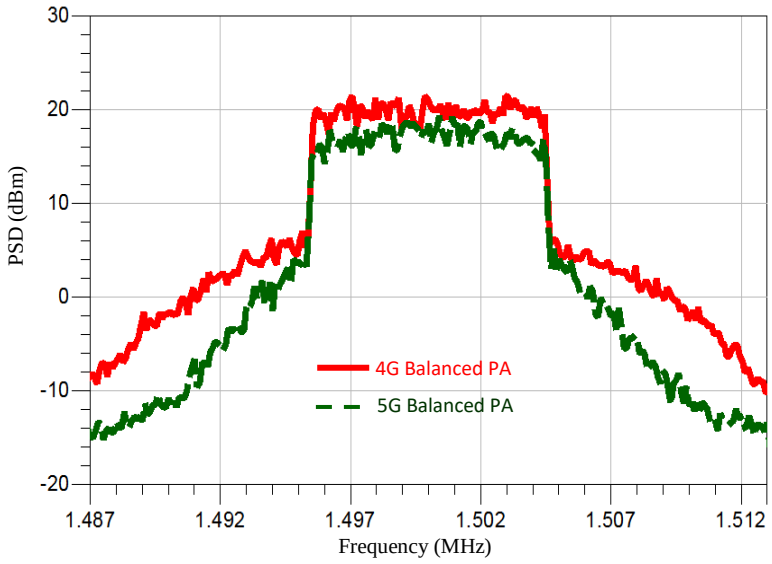

Figure 5-46: Simulated PA output spectra for 10 MHz LTE and FBMC signals and Pin of 25 dBm.

From these results, it is easy to conclude that the balanced PA was able to improve efficiency and linearity over its single PA equivalent. Not only was the balanced PA able to reduce the nonlinear distortions, it was able to maintain it over a higher bandwidth without loosing too much compensation abilities like in the case of other RF linearization methods like the second harmonic injection technique. The fact that the 5G balanced PA also outshined the 4G balanced PA makes it a potential candidate to be deployed massively for upgcoming 5G networks.

The balanced PA is linear (at back-off level before saturation) and efficient. Through this section, it has shown improved matching abilities as the input and output reflection coefficients are both less than -35 dB respectively. The proposed balanced PA also reaches a maximum saturated power from 37.41 dBm to 42.92 dBm with max PAE increasing by about 10% at saturation. The proposed balanced PA configuration improved linearity considerably at different input power levels and its 5G nonlinear distortion performance also outshined its 4G equivalent by about 10 dB. The balanced PA was able to maintain good linearity and efficiency even for larger bandwidths (from 3 MHz to 10 MHz). The proposed balanced PA will be very useful for 5G wireless transmitters as its characteristics mean it will contribute positively to battery life and data throughput.

In the next session, a real power amplifier (ZHL 4240W) would be used for practical verification of the proposed balanced configuration.

5.6.2 Balanced ZHL4240 W PA for 5G Applications

Efficiency and linearity are becoming vital in modern day networks with the aim to meet the ever growing demand of mobile end-users. 5G comes with great prospects and challenges on delivering the data rates promised in reality. The balanced PA has been designed and tested in section section 5.6.1.1. The PA used was used mainly for simulations. In this section, a real PA model (ZHL-4240W) is used for measurements.

In this section, the balanced PA configuration is used to achieve better efficiency and linearity with the aid of the novel microstrip quadratic hybrid coupler designed and fabricated in chapter 5.2. The proposed configuration achieved improved s-parameter performance and achieved better efficiency and linearity. The proposed balanced PA is highly efficient, linear and will be very useful for next generation networks.

5.6.2.1 Balanced ZHL-4240W PA Design with USTL QHC

The same balanced power design that was used in simulations in chapter 5.6.1 is used here. Howvever this time, a measure coupler and measured PA are both used to compare with the simulation and single-ended results. The designed coupler is designed to operate between 1.2 and 1.8 GHz with maximum performance at 1.5 GHz. Phase difference of 90 degrees between the transmitted and coupled ports was achieved for the coupler design so it could be used in the proposed balanced topology in Figure 5-33. The printed circuit boards (PCB) of the coupler were fabricated in microstrip technology using RT/Duroid 5880 0.79 mm laminates with 4 port-50 ohms impedance terminations as shown in Figure 5-47.

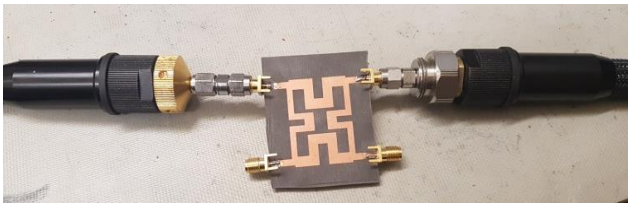

Figure 5-47: Photograph of fabricated QHC under test.

The unit PA used is the ZHL-4240W Mini-circuits PA. The real ZHL PA in conjunction with the USTL coupler is used for the balanced PA configuration. The input signal is split into two signals which are 90^0 out of phase by the first QHC and then passed through the unit PA and then combined again by the second QHC as shown in Figure 5-33. It was optimized through the band to obtain improved PAE. Measured results from the fabricated coupler with the real PA will also be introduced for experiments. This section will examine the impact of the proposed configuration with its single equivalent. Simulated and measured responses of the designed balanced PA and the single ZHL-4240W PA are presented and compared in this section.

Figure 5-48 shows the simulated and measured gain S_{21}. The simulated and measured gain of the balance PA show a good match around 45 dB with the single PA from 1.3 GHz and 1.6 GHz with the peak of the balanced architecture slightly lower than the single-ended PA. At other frequencies, the gain reduces. The gain bandwidth of the balanced PA is slightly narrower due to the characteristics of the USTL which acts as both the splitter and the combiner. The slight deviation from the simulation results could be caused by tolerances in the components and the milling of the PCBs.

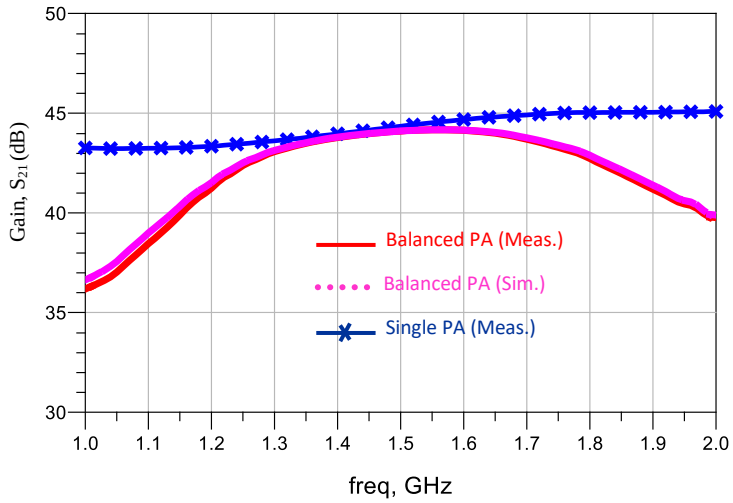

Figure 5-48: Measured and simulated s-parameter (S_{21}) responses.

Figure 5-49 and Figure 5-50 give the input and output matching results for the balanced PA respectively. The input and output reflection coefficients (S_{11} and S_{22}) for the ZHL-4240W PA have been enhanced for better matching and stability by the balanced PA design. Figure 5-59 shows that the S_{11} results for the PA is around -16 dB and the measured and simulated balanced

PA S_{11} results at the required frequencies are lower than -45 dB giving a very good matching improvement. The lower the results, the better the matching. Hence, the coupler was able to achieve a better input matching. The measured and simulated S_{22} results of the balanced PA were able to show good improvement than the single PA under test as well. The S_{22} results are around -35 dB at the required operating frequencies for both the balanced PA in comparison to about -10 dB for the single PA as shown in Figure 5-50. This good output reflection matching property also ensures that the design will boost robustness against instabilities and load insensitivities. Overall these excellent small signal s-parameter results show a more stable PA with improved matching for signals at the input and output of the PA which improves reliability. This stability is because each branch of the balanced PA is terminated with a fixed load of 50 ohms whilst the single-ended PA is loaded with actual loads. There termination of this load at each branch of about 50 ohms as shown in Figure 5-33 with the aid of the isolation port of the high Q performance USTL coupler explains why the coupler is more stable with better matching properties.

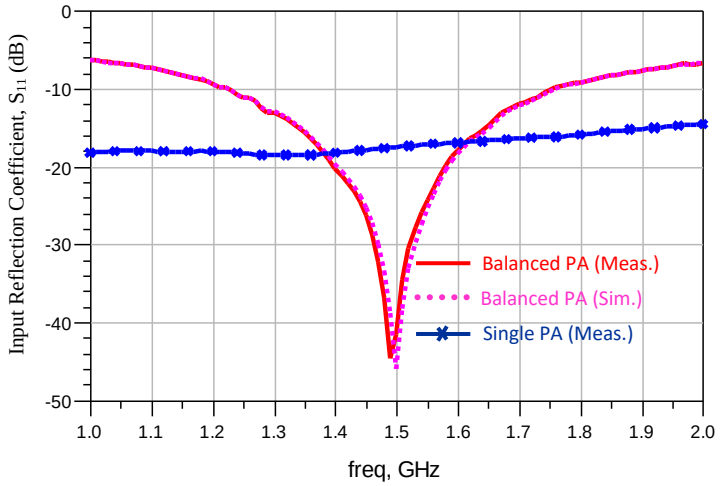

Figure 5-49: Measured and simulated s-parameter (S_{11}) responses.

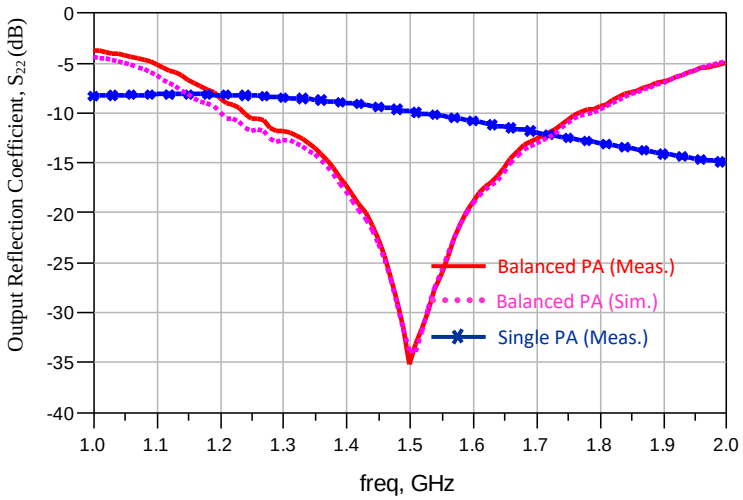

Figure 5-50: Measured and simulated s-parameter (S_{22}) responses.

Large-signal measurements were then obtained by power sweeps at several frequency points and the PA in the balanced topology uniquely uses the isolation port of the microstrip USTL branch line coupler as its signal path. Figure 5-51 compares the output power and gain at different input powers leading to saturation for the balanced PA and the single-ended case. The ZHL-4240W Mini-circuits PA under test delivers a maximum saturated output power (Pout) of 31 dBm. The maximum gain is around 46 dB and then it reduces as the input power reaches saturation as shown in the figure. However, it is observed that the balanced PA shows a large signal improvement delivering a maximum Pout of 35 dBm with maximum gain around 45 dB which also reduces as the input and output power moves towards saturation. This steady reduction of gain is an indication that the PA is starting to operate in its nonlinear region.

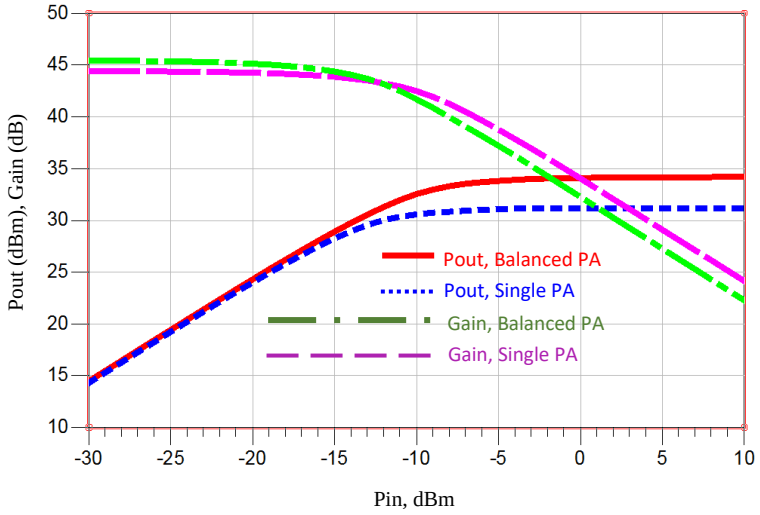

Figure 5-51: Output power and gain vs input power.

Figure 5-52 and Figure 5-53 give the power aided efficiency (PAE) results against input power and frequency respectively. Unlike the simulation case, the power aided efficiency is calculated from input and output ports rather than the gate and drain that were used in simulations. PAE improvement of about 13.5 % was noticed as the PAE for balanced PA is 66.8% and that of the single-ended ZHL-4240W PA. Figure 5-52 also showed that for lower input powers in the saturation region, the efficiency is similar but as it moved towards the saturation region, the balanced PA starts to become better and improves steadily until saturation. This is important as the efficiency is mainly needed at saturation where both efficiency and linearity requirements are high.

The PAE was also investigated over the frequency band. There was improvement of about 10 dB at the centre frequency with a gradual reduction through the whole frequency band as shown in Figure 5-53. This is because the coupler and balanced PA design has optimum performance at the centre frequency. As it moves through to other bands, the PAE will steadily reduce depending on the operating bands of the balanced PA design over the whole frequency band from 1.2 GHz to 1.8 GHz as shown in Figure 5-53. This efficiency result will also be discussed further when the balanced PA is implemented in a wireless transmitter.

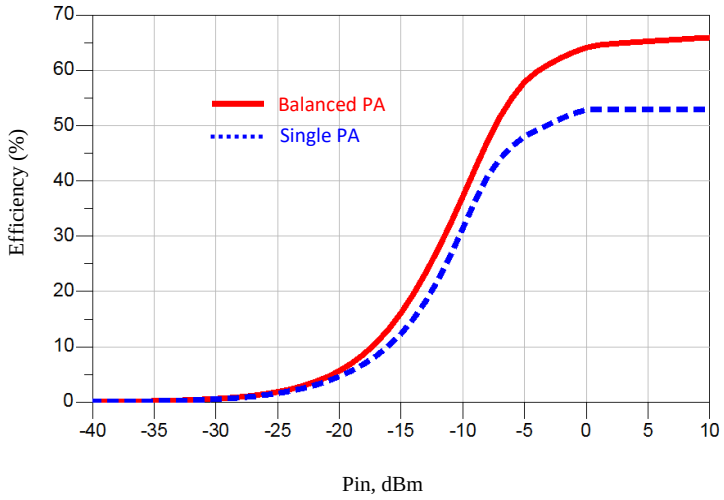

Figure 5-52: PAE against input power.

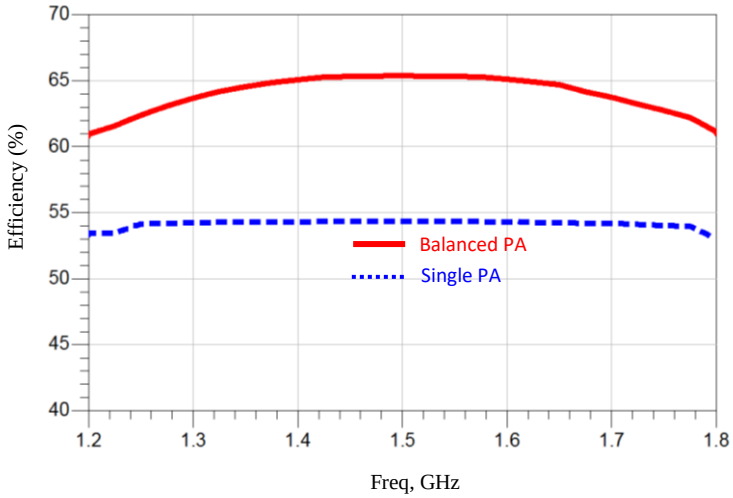

Figure 5-53: PAE against frequency at saturation.

Due to the great Pout and PAE performance at saturation, the spectral performance of balanced PA design will be evaluated in a 5G wireless transmitter to observe linearity improvements at saturation due to the encouraging measurement results described above. The balanced configuration aims to achieve both good efficiency and linearity at saturation at the same time unlike other techniques that trades-off both vital transmitter requirements.

5.6.2.2 Proposed USTL coupler for 5G Applications

Figure 5-54 shows the application of the proposed USTL coupler in a 5G wireless transmitter system. In this setup, 5G FBMC signal is generated in the signal generator and is sent through the DUT (Device under test). The USTL QHC designed in section 5.2 is integrated into the balanced PA architecture with single-ended ZHL -4240W mini-circuits PA. Experimental data for ZHL-4240W PA is used with the proposed USTL coupler to achieve better spectral efficiency.

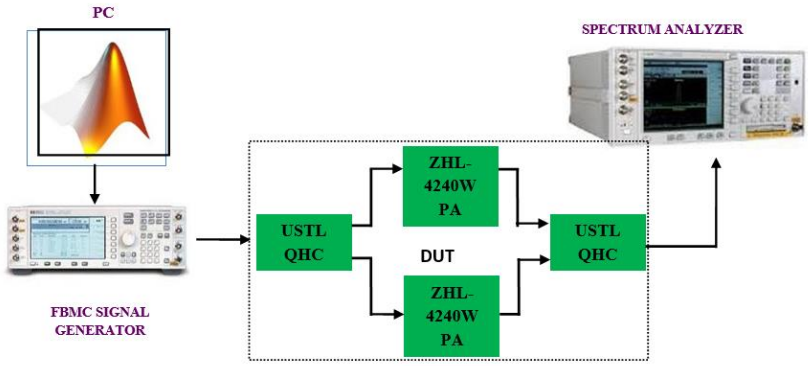

Figure 5-54: Proposed coupler application in 5G wireless transmitters.

The FBMC signal is modelled, and measured results used in Agilent Keysight Signal Studio Kit. The USTL quadrature hybrid coupler designed and fabricated in section 5.2 as in Figure 5-47 was fed by 3MHz, 5 MHz and 10 MHz FBMC signal at the centre frequency of the coupler 1.5 GHz. The signal passes through the USTL coupler which splits the signal to both Mini-circuits unit PAs before combining the signal again. The experiments were taken at 3 strategic input power levels close to saturation. The power levels of -20 dBm, -15 dBm and -10 dBm were used as they were the power levels just before and after the 1-dB compression point (P_1dB) to analyse the output spectra performance in terms of efficiency and linearity for the proposed balanced PA design. The output saturation point for the PA depends on the bandwidth. The more the bandwidth increases, the lower the quicker the PA reaches saturation for the corresponding input power level. Figure 5-55, Figure 5-56 and Figure 5-57 give results for the proposed coupler using a 3 MHz bandwidth for the 3 input power levels of -20 dBm, -15 dBm and -10 dBm.

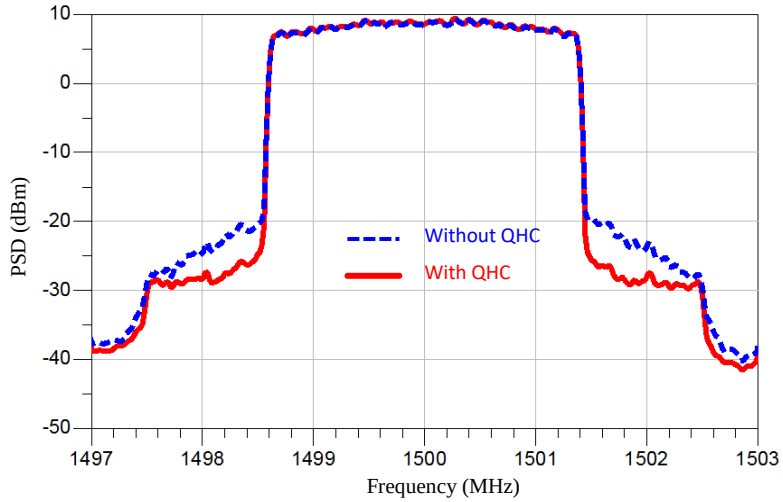

Figure 5-55: Measured PA output spectra for 3 MHz 5G FBMC signal and Pin of -20 dBm.

The output power spectral density results for 3 MHz bandwidth show that at this stage in Figure 5-55 before the compression point, the PA is still linear and the balanced PA with coupler peak results still macth with the single-ended PA. The ACPR improvement according to Figure 5-

55 is -4.5 dB (-28.594 – (-24.096) dB). However, for the same 3 MHz bandwidth as it moves into saturation for input power of -15 dBm, the balanced PA with coupler starts to become more efficient as it has higher PSD maximum values for the same input power.

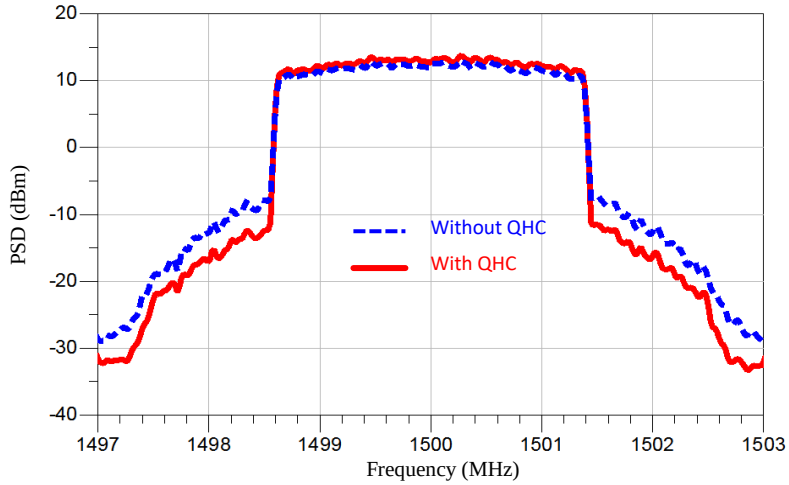

Figure 5-56: Measured PA output spectra for 3 MHz 5G FBMC signal and Pin of -15 dBm.

From Figure 5-56, the ACPR for the PA without the coupler is now 27.97 dB (11.34 – (-16.63) and the PA with the coupler is 34.85 (13.25 – (-21.6)) giving ACPR improvement of about 7 dB. Hence, at this stage, efficeincy and linearity have both been increased by the PA with the coupler which is a very encouraging result. To investigate further, higher pin of -10 dBm is used as shown in Figure 5-57. At this level, the efficiency has been improved further by 2.6 dB (16.635-14.002) for the PA with coupler over the single PA. The ACPR for PA with coupler is now 28.641 (16.635 – (-12.006)) and the PA without coupler is 22.254 (14.012 – (-8.242) giving overall ACPR reduction of about 6.4 dB. These results for 3 MHz FBMC signal for PA with coupler are very encouraging.

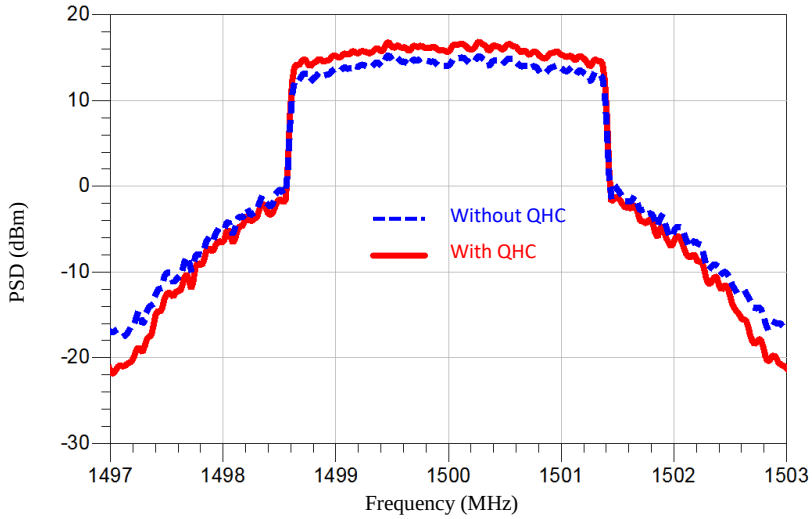

Figure 5-57: Measured PA output spectra for 3 MHz 5G FBMC signal and Pin of -10 dBm.

To further understand the peformance of the PA with coupler, it will be tested with higher bandwidths of 5 MHz and 10 MHz to observe how it responds to the nonlinear distortions at

saturation in terms of efficiency and linearity. Figure 5-58, Figure 5-59 and Figure 5-60 show the measured output spectra for 5 MHz 5G FBMC signal for the same 3 input power levels of -20 dBm, -15 dBm and -10 dBm respectively.

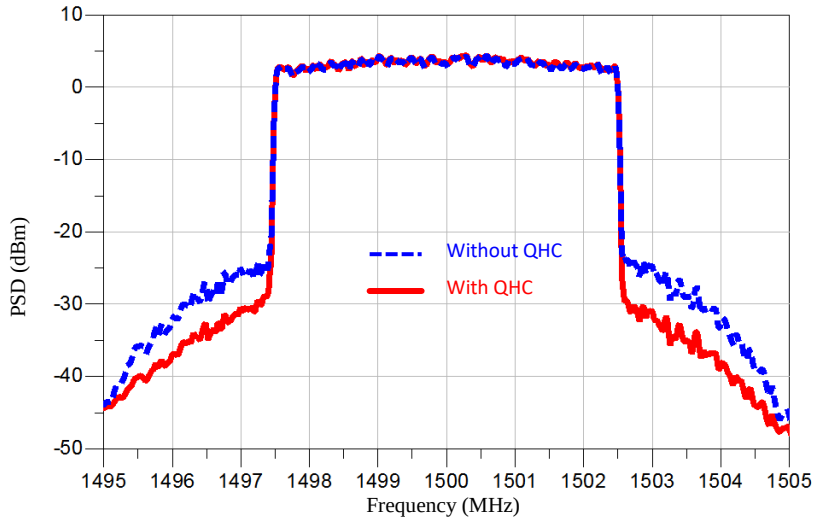

Figure 5-58: Measured PA output spectra for 5 MHz 5G FBMC signal and Pin of -20 dBm.

For Figure 5-58, the input power level is still in the linear region and the PSD maximum values are the same at this point which is the same result that was observed for the 3 MHz case in Figure 5-55.

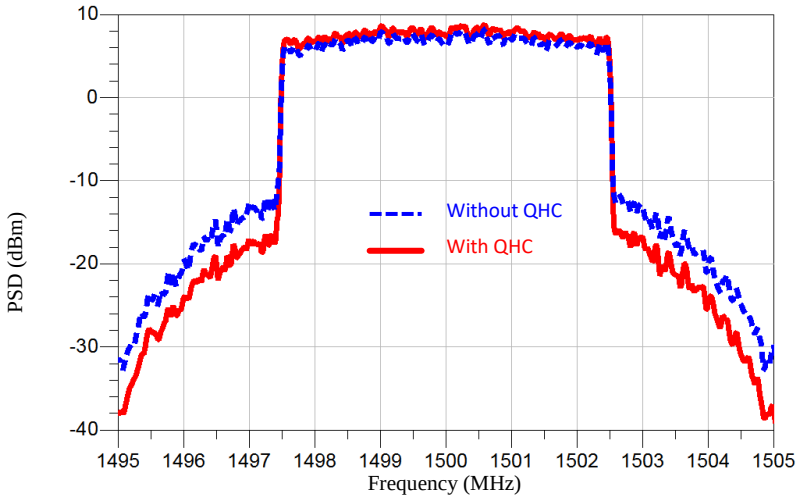

Figure 5-59: Measured PA output spectra for 5 MHz 5G FBMC signal and Pin of -15 dBm.

Using the same ACPR graph analysis like in the 3 MHz, the ACPR calculations are obtained for 5 MHz. For 5 MHz FBMC signal and -20 dBm input power, the ACPR improvement between the PA with and without the coupler is 5.6 dB (-27.247 – (-32.856)) as obtained from Figure 5-58. For the same 5MHz bandwidth, Figure 5-59 also gives ACPR improvement of about 7.8 dB (29.95 – 22.15). As the PA moves deeper into saturation, efficiency improves further with a 2.4 efficiency improvement for the PA with coupler whilst also achieveing ACPR improvement of about 6.6 dB (22.775 – 16.158) is achieved.

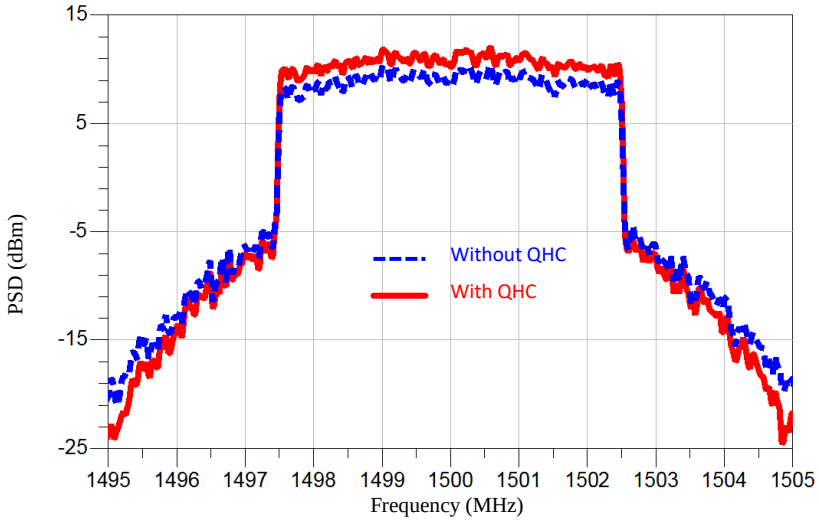

Figure 5-60: Measured PA output spectra for 5 MHz 5G FBMC signal and Pin of -10 dBm.

Finally, the same calculations for 3 MHz and 5 MHz are also used for the 10 MHz case. Figure 5-61, Figure 5-62 and Figure 5-63 give the measured output spectra for 10 MHz FBMC signal.

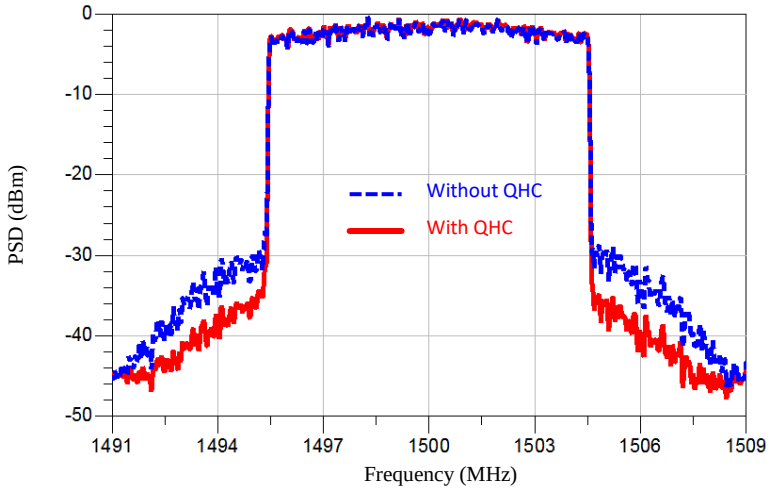

Figure 5-61: Measured PA output spectra for 10 MHz 5G FBMC signal and Pin of -20 dBm.

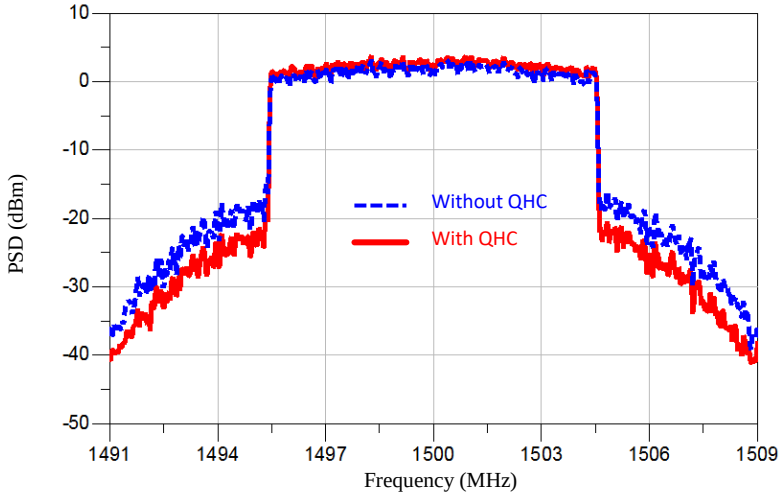

Figure 5-62: Measured PA output spectra for 10 MHz 5G FBMC signal and Pin of -15 dBm.

ACPR improvement of 5.8 dB (-30.707+36.503) is observed for the linear input case of -20 dBm as seen in Figure 5-62. The ACPR for pin of -15 dBm for the PA without coupler is 29.782 dB whilst for PA without coupler, ACPR is 18.836 dB, The ACPR improvement is therefore 10.946 dB. Also for pin of -10 dBm, ACPR improvements of 9.83 dB (24.817 – 14.987) is observed.

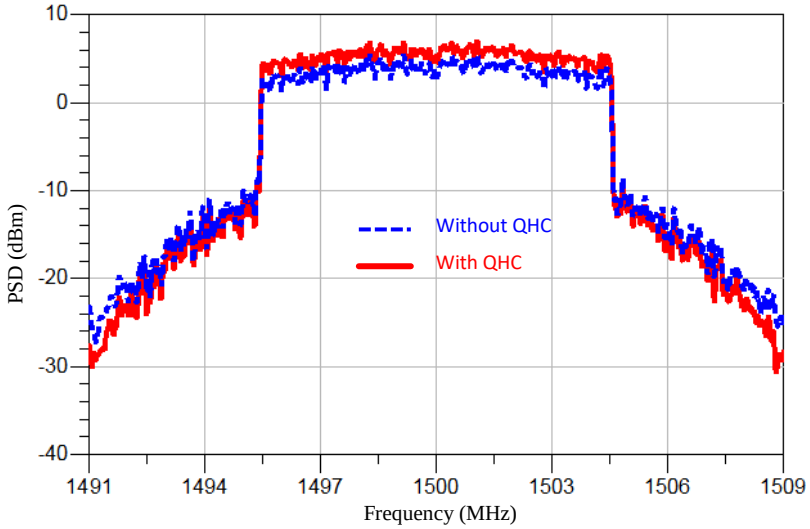

Figure 5-63: Measured PA output spectra for 10 MHz 5G FBMC signal and Pin of -10 dBm.

These results show that for higher bandwidths, the proposed PA with USTL QHC design (in the balanced configuration) is giving satisfactory results. For the Pin before saturation, the output power levels for all cases were the same. As it gets above saturation, the output PSD of the PA with coupler starts to become higher as it becomes more efficient. That is seen in all cases from 3 MHz to 10 MHz with maximum efficiency improvements of about 3.5 dB for all cases. Most importantly, it was observed that as the bandwidth increased from 3 MHz to 10 MHz, the maximum ACPR improvement observed were 7 dB, 7.8 dB and 10.946 dB for the 3 MHz, 5 MHz and 10 MHz bandwidth respectively. This result is very important for next generation 5G networks that require higher bandwidths. Many other RF and baseband linearisation techniques like injection have really been limited in the compensation of nonlinear distortions for higher bandwidth applications most notably from 3 MHz upwards but the proposed design has been able to not only maintain but improve on the nonlinear distortion performance for such high bandwidths. Further work will involve testing for higher bandwidths above 100 MHz for 5G. Integrating the coupler in the balanced configuration at transistor level will give better efficiency results and improved linearity at the output power back-off region.

The power output of the PA with the USTL coupler gives better overall output performance with increasing sensitivity, better linearity and better spectra efficiency.The coupler was able to maintain a better spectral efficiency performance over higher bandwidths when implemented in the 5G wireless transmitters. This is due to the USTL maintaining its high performance over a larger bandwidth. Many linearity techniques such as harmonic injection and DPD have achieved reduced ACPR improvements for higher channel bandwidths which makes the

improved ACPR improvements for larger bandwidths a very good contribution towards next generation mobile wireless transceivers.

5.7 Conclusions

This chapter has sucessfully presented compact microstrip branch line coupler (BLC) designs and implemented in wireless transceiver applications. A novel U-shaped transmission line has been proposed for compactness by creating a U-shaped defect on the transmission line. The initial BLC design using PCB technology was able to achieve a 64 % area reduction when compared to its conventional equivalent and further improved for a 70% size reduction. This same design is also implemented in inkjet printing technology thereby improve the compactness to about 78% reduction in overall circuit area. These BLC designs also give good coupling and isolation properties with the inkjet equivalent giving good multiband properties.

The BLC has been implemented in different transceiver applications in this thesis. One of such applications was for energy harvesting. A noverl rectifier with enhanced efficiency based on the compact inkjet BLC was proposed. By identifying optimal load resistance, the grounded isolation ports of the BLC helps to improve efficiency by reducing input impedance, output load variations and reinjecting reflected waves. This proposed topology was able to improve efficiency over a wide range of input power level and output load without compromising the linear properties of the output. The RF transceiver implementation also demonstrates higher peak output PSD for the same output power and improved RF-dc conversion efficiency over a larger bandwidth thereby improving the overall performance of the system. These outstanding properties makes the proposed design very useful for energy harvesting.

Another application of the BLC was to be used in the wireless transmitter in a balanced power amplifier configuration. Since, the balanced configuration is very similar to the proposed rectifier configuration, it is expected to improve power aided efficiency as the balanced PA cinfiguration takes advantage of the coupler properties to boost robustness against load-insensitivity characteristics. These balanced configurations were also tested with modern day 4G and 5G signals. LTE CP-OFDM and 5G UFMC and FBMC have been compared and utilised in this paper. 5G FBMC has proven to be a good candiddate for better linearity for bandwidths up to 10 MHz for simulations and experiments while UFMC has matched FBMC for good linearity as bandwidths get above 10 MHz. One major observation was that the coupler was able to maintain its linear performance for higher bandwidths which is a major issue that current linearization techniques have struggled with. The balanced topology could be integrated with improved linearization techniques such as DPD to improve the compensation of nonlinear distortions even for higher bandwidths that will be above 100 MHz for modern day 5G wireless communication systems.

5.8 References

[5.1] M. Khoubroo Eslamloo, P. Mohammadi, S. Demir, and M. Khoubrou, "Miniaturized Wideband branch-line hybrid coupler with Capacitive effect and defected ground structure (DGS)," *Indian Journal of Science and Technology*, vol. 8, no. 35, Dec. 2015.

[5.2] R. Ghatak, M. Pal, and B. Sarkar, "Realization of Miniaturized Quadrature Hybrid Coupler with Reduced Length Branch Arms Using Recursively Loaded Stubs," *Progress In Electromagnetics Research Letters*, vol. 43, pp. 45–54, 2013.

[5.3] B. M. Sa'ad, S. K. A. Rahim, and R. Dewan, "Compact wide-band branch-line coupler with Meander line, cross, and Two-Step stubs," *Microwave and Optical Technology Letters*, vol. 55, no. 8, pp. 1810–1815, May 2013.

[5.4] Y.-B. Jung, "Wideband branchline coupler using symmetrical four-strip interdigitated coupler," *Electronics Letters*, vol. 50, no. 6, pp. 452–454, Mar. 2014.

[5.5] K. Y. Liu, C. Li, and F. Li, "A new type of Microstrip coupler with complementary split-ring Resonator (CSRR)," *PIERS Online*, vol. 3, no. 5, pp. 603–606, 2007.

[5.6] Q. Wang, J. Lim, and Y. Jeong, "Design of a compact dual-band branch line coupler using composite right/left-handed transmission lines," *Electronics Letters*, vol. 52, no. 8, pp. 630–631, Apr. 2016.

[5.7] P. Kurgan and S. Koziel, "Design of high-performance hybrid branch-line couplers for wideband and space-limited applications," *IET Microwaves, Antennas & Propagation*, vol. 10, no. 12, pp. 1339–1344, Sep. 2016.

[5.8] C.-F. Chen, S.-F. Chang, and B.-H. Tseng, "Compact Microstrip dual-band Quadrature coupler based on Coupled-Resonator technique," *IEEE Microwave and Wireless Components Letters*, vol. 26, no. 7, pp. 487–489, Jul. 2016.

[5.9] V. Iran-Nejad, A. A. Lotfi-Neyestanak, and A. Shahzadi, "Compact broadband quadrature hybrid coupler using planar artificial transmission line," *IET Electronics Letters*, vol. 48, no. 25, pp. 1602–1603, Dec. 2012.

[5.10] A. R. Hazeri and T. Faraji, "Miniaturisation and harmonic suppression of the branch-line hybrid coupler," *International Journal of Electronics*, vol. 98, no. 12, pp. 1699–1710, Dec. 2011.

[5.11] J. Shi et al., "A balanced filtering branch-line coupler," *IEEE Microw. Wireless Compon. Lett.*, vol. 26, no. 2, pp. 119–121, Feb. 2016.

[5.12] M. A. Maktoomi, M. S. Hashmi, and F. M. Ghannouchi, "Systematic design technique for dual-band branch-line coupler using T- and pi-networks and their application in novel Wideband-Ratio crossover," *IEEE Transactions on Components, Packaging and Manufacturing Technology*, vol. 6, no. 5, pp. 784–795, May 2016.

[5.13] Y. Wang, K. Ma, and S. Mou, "A compact branch-line coupler using substrate integrated suspended line technology," *IEEE Microwave and Wireless Components Letters*, vol. 26, no. 2, pp. 95–97, Feb. 2016.

[5.14] S. Reshma and M. K. Mandal, "Miniaturization of a 90° hybrid coupler with improved bandwidth performance," *IEEE Microwave and Wireless Components Letters*, vol. 26, no. 11, pp. 891–893, Nov. 2016.

[5.15] Q. Wang, J. Lim, and Y. Jeong, "Design of a compact dual-band branch line coupler using composite right/left-handed transmission lines," *IET Electronics Letters*, vol. 52, no. 8, pp. 630–631, Apr. 2016. C. Gai, Y.-C. Jiao, and Y.-L. Zhao, "Compact dual-band branch-line coupler with dual transmission lines," *IEEE Microwave and Wireless Components Letters*, vol. 26, no. 5, pp. 325–327, May 2016.

[5.16] S. Babale and S. Rahim, "Miniaturized quadrature coupler using low-cost instant inkjet printing technology," Microwave and Optical Technology Letters, vol. 59 no.8, pp.1819-1824, Jan. 2017.

[5.17] I-Hsiang Lin, M. DeVincentis, C. Caloz and T. Itoh, "Arbitrary dual-band components using composite right/left-handed transmission lines," in IEEE Transactions on Microwave Theory and Techniques, vol. 52, no. 4, pp. 1142-1149, April 2004.

[5.18] W-C Lee; B-W. Min; C-Y. Kim, J. C. Kim, J-M. Yook, A compact switched beam-orming network using silicon IPD technology for low-cost 5G communication, in *International Microwave Symosium (IMS)*, 22-27 May 2016.

[5.19] S.Kim, H. Aubert, M. M. Tentzeris, An Inkjet-printed Flexible Broadband Coupler in Substrate Integrated Waveguide (SIW) Technology for Sensing, RFID and Communication Applications, in *International Microwave Symosium (IMS)*, 1-6 June 2014.

[5.20] Modeling and Characterization of Copper Tape Microstrips on Paper Substrate and Application to 24 GHz Branch-Line Couplers, in *Proceedings of the 43rd European Microwave Conference*, pp. 794-797, October 2014.

[5.21] F. Bolos, J. Blanco, A. Collado and A. Georgiadis, "RF Energy Harvesting From Multi-Tone and Digitally Modulated Signals," IEEE Microwave and Wireless Components Letters, vol. 64, no. 6, pp. 1918–1927, June 2016.

[5.22] X.Y. Zhang, Z.-X. Du and Q. Xue, "High-Efficiency Broadband Rectifier with Wide Ranges of Input Power and Output Load based on Branch-Line Coupler," IEEE Trans. Circuits and Systems, vol. 64, no. 3, pp. 731–739, March 2017.

[5.23] Y.-J. Ren and K. Chang, "5.8 GHz circularly polarized dual-diode rectenna and rectenna array for microwave power transmission," IEEE Trans. MTT., vol. 54, no. 4, pp. 1495–1502, June 2006.

[5.24] M. Roberg, T. Reveyrand, I. Ramos, E.A. Falkenstein and Z. Popovic, “High-efficiency harmonically terminated diode and transistor rectifiers,” IEEE Trans. MTT., vol. 60, no. 12, pp. 4043–4052, Dec. 2012.

[5.25] B. Li, X. Shao, N. Shahshahan, N. Goldsman, T. Salter and G.M. Metze, “An antenna co-design dual band RF energy harvester,” IEEE Trans. Circuits and Systems, vol. 60, no. 12, pp. 3256–3266, Dec. 2013.

[5.26] J. Guo, H. Zhang and X. Zhu, “Theoretical analysis of RF-DC conversion efficiency for class-F rectifiers,” IEEE Trans. MTT., vol. 62, no. 4, pp. 977–985, Apr. 2014.

[5.27] K. Niotaki, A. Georgiadis, A. collado, and J.S. Vardakas, “Dual-band resistance compression networks for improved rectifier performance,” IEEE Trans. MTT., vol. 62, no. 12, pp. 3512–3521, Dec. 2014.

[5.28] C. R. Valenta, M. M. Morys, and G. D. Durgin, “Theoretical energy-conversion efficiency for energy-harvesting circuits under power-optimized waveform excitation,” IEEE Trans. MTT., vol. 63, no. 5, pp. 1758–1767, May 2015.

[5.29] T. S. Rappaport, S. Sun, R. Mayzus, H. Zhao, Y. Azar, K. Wang, G. N. Wong, J. K. Schulz, M. Samimi, and F. Gutierrez, “Millimeter Wave Mobile Communications for 5G Cellular: It Will Work,” IEEE Access, vol. 1, pp. 335- 349, May 2013.

[5.30] P. Guan, D. Wu, T. Tian, J. Zhou, X. Zhang, L. Gu, A. Benjebbour, M. Iwabuchi, and Y. Kishiyama, “5G Field Trials - OFDM-based Waveforms and Mixed Numerologies,” IEEE Journal on Selected Areas in Communications, vol. PP, no. 99, pp. 1–1, 2017.

[5.31] F.-L. Luo and C. Zhang, “Major 5G Waveform Candidates: Overview and Comparison,” Signal Processing for 5G: Algorithms and Implementations, Wiley-IEEE Press, 2016.

[5.32] B. D. Tensubam and S. Singh, “A Review on FBMC: An Efficient Multicarrier Modulation System”, International Journal of Computer Applications (0975 – 8887) Volume 98– No.17, July 2014F.-L. Luo and C. Zhang, “From OFDM to FBMC: Principles and Comparisons,” Signal Processing for 5G: Algorithms and Implementations, Wiley-IEEE Press, 2016.

[5.33] A. Basaligheh, P. Saffari, M. Taherzadeh-Sani, and F. Nabki, "A highly efficient and linear Broadband common-drain CMOS power amplifier with transformer-based input-matching network," *IEEE Microwave and Wireless Components Letters*, vol. 25, no. 12, pp. 814–816, Dec. 2015.

[5.34] S. Stefanatos and F. Foukalas, "A filter-bank Transceiver architecture for massive non-contiguous carrier aggregation," *IEEE Journal on Selected Areas in Communications*, pp. 1–1, 2016.

[5.35] H. Jeon et al., "A triple-mode balanced linear CMOS power amplifier using a Switched-Quadrature coupler," *IEEE Journal of Solid-State Circuits*, vol. 47, no. 9, pp. 2019–2032, Sep. 2012.

[5.36] R. Kalyan, K. Rawat, and S. K. Koul, "Reconfigurable and concurrent dual-band Doherty power amplifier for Multiband and Multistandard applications," *IEEE Transactions on Microwave Theory and Techniques*, vol. 65, no. 1, pp. 198–208, Jan. 2017.

[5.37] H. Jeon, Y. Yoon, H. Kim, Y. Huang, and C. Lee, "Highly efficient balanced CMOS linear power amplifier with load immunity," *IET Electronics Letters*, vol. 47, no. 19, p. 1095, 2011.

[5.38] R. Ma, K. H. Teo, S. Shinjo, K. Yamanaka and P. M. Asbeck, "A GaN PA for 4G LTE-Advanced and 5G: Meeting the Telecommunication Needs of Various Vertical Sectors Including Automobiles, Robotics, Health Care, Factory Automation, Agriculture, Education, and More," in IEEE Microwave Magazine, vol. 18, no. 7, pp. 77-85, Dec. 2017.

[5.39] S. Stefanatos and F. Foukalas, "A filter-bank Transceiver architecture for massive non-contiguous carrier aggregation," IEEE Journal on Selected Areas in Communications, pp. 1–1, 2016.

[5.40] S. C. Cripps, RF Power Amplifiers for Wireless Communications, Norwood, MA, USA: Artech House, 2006.

[5.41] B. Moret, V. Knopik and E. Kerherve, "A 28GHz self-contained power amplifier for 5G applications in 28nm FD-SOI CMOS," 2017 IEEE 8th Latin American Symposium on Circuits & Systems (LASCAS), Bariloche, 2017, pp. 1-4.

[5.42] J. K V. Radisic, D. W. Scott, A. Cavus and C. Monier, "220-GHz High-Efficiency InP HBT Power Amplifiers," in IEEE Transactions on Microwave Theory and Techniques, vol. 62, no. 12, pp. 3001-3005, Dec. 2014.

[5.43] J H. Jeon et al., "A triple-mode balanced linear CMOS power amplifier using a Switched-Quadrature coupler," IEEE Journal of Solid-State Circuits, vol. 47, no. 9, pp. 2019–2032, Sep. 2012.

[5.44] C.-F. Chen, S.-F. Chang, and B.-H. Tseng, "Compact Microstrip dual-band Quadrature coupler based on Coupled-Resonator technique," IEEE Microwave and Wireless Components Letters, vol. 26, no. 7, pp. 487–489, Jul. 2016.

[5.45] B. Bukvić and M. M. Ilić, "Simple Design of a Class-J Amplifier with Predetermined Efficiency," in IEEE Microwave and Wireless Components Letters, vol. 26, no. 9, pp. 699-701, Sept. 2016.

Chapter 6 Conclusions and Future Work

This Chapter summarises the contributions to knowledge achieved in this thesis and gives the potential for future work based on the areas covered in this topic. The main aim of this thesis is to investigate current techniques that improve the linearity and efficiency of mobile wireless networks and develop these techniques for next generation networks. Novel designs that will improve the overall linearity and efficiency of the wireless transceivers with significant size reduction and ease of implementation is the main focus of this research. This thesis investigated the RF second harmonic injection technique that was initially successful in compensating for nonlinear distortions in the wireless transmitters but as the mobile wireless networks advanced, it started becoming limited in its abilities to meet the demands of modern-day wireless systems. The challenges of the injection technique were fully addressed in this thesis. This was done by evaluating the distortions in the wireless transmitters and demonstrating the effects of the nonlinear distortions on mobile network signals. Once, the nonlinear distortion properties were established, the second harmonic injection technique was used to compensate for the uncharacteristic nonlinear performance that limits the performance of the wireless transmitters and limits the data rate achievable. The second harmonic injection technique was modified with the aid of a well-designed compact inkjet-printed band-stop (notch) filter. The notch filter was also integrated in the injection architecture for better reduction in intermodulation distortion for modern day carrier aggregation (CA) wireless transmitters.

To meet the needs of the next generation 4G and 5G wireless transceivers, a compact branch line coupler (BLC) or quadratic hybrid coupler (QHC) was designed. This coupler was designed with unique properties for efficiency and linearity improvements for different applications. The coupler was combined with rectifiers and achieved improved performance for energy harvesting. The coupler was also used to design a balanced power amplifier that achieved improved efficiency and linearity for large bandwidths necessary for next generation 5G wireless transceivers.

Chapter 1 has given a detailed outline of the thesis, the aims and objectives. Past research work have been thoroughly investigated with regards to techniques for compensation of nonlinear distortions in wireless transmitters and the current state of the art.

Chapter 2 investigated the theoretical background directly relating to this research. A brief evolution of the generation of mobile networks was provided to know the rationale behind moving from one generation to another. More emphasis was given to modern day 4G and next generation 5G networks that will form the basis of this research. 4G LTE's OFDM and carrier aggregation was explained and the waveform candidates for 5G networks were compared. This chapter examined the basic wireless transmitter concepts for the power amplifier and finalised with the microstrip technology that will form the basis of any component design to be used in these wireless systems.

The microstrip technology formed the basis of the band-stop filter design in chapter 3. Conventional filters were designed using the technology initially to investigate merits and demerits. This technology was investigated and utilised to design a novel compact band-stop filter for wireless networks. The filter was designed and was able to achieve very good

performance properties for interference rejection and suppression. This design was then modified using the emerging inkjet-printing technology to achieve miniaturisation and multiband properties.

In chapter 4, the distortions in the power amplifier of the wireless transmitters were evaluated. The second harmonic injection was used to compensate for the nonlinear distortion. The designed filter in chapter 3 was then used to modify the technique due to its draw backs and its limitations for higher bandwidths. The integration of the band-stop filter in the injection technique was also successful for intra-band and inter-band carrier aggregation transmitters.

Chapter 5 was mainly to do with the design of a novel, compact microstrip couplers and its application for next generation networks. The 3 dB quadratic hybrid coupler was designed and achieved miniaturisation against other couplers. It was fabricated. A multi-band inkjet coupler was also designed and used for improved energy harvesting performance. The QHC was then used to design a balanced PA for 4G and 5G applications. The proposed technique improved on the drawbacks of other linearization techniques that struggled for higher bandwidths. The proposed balanced PA with QHC was able to improve linearity and efficiency for even higher bandwidths in a 5G wireless transmitter system.

6.1 Contributions of the Thesis

The injection technique proposed has been modified with the aid of a novel inkjet-printed based notch filter. This technique has not yet been explored on carrier aggregation as it has been done in this thesis. The injection technique and other techniques have struggled for nonlinear distortion improvements for higher bandwidths. The integration of the filter was able to achieve better results for higher bandwidth cases and carrier aggregation. This entire study is based on attempts of original approaches to introduce new ideas to contribute to knowledge and further development of the state of the art in the scientific community. The inkjet-printed filter design itself is new and has never been designed before.

This research shows a lot of contributions not only in linearity but also takes compactness and cost effectiveness into consideration. By employing the use of inkjet printing, the notch filter design is very small in size so as not to considerably add to the size of the overall architecture as miniaturisation is a very important commercial interest of the mobile industry.

This research also presents novel couplers (QHC). These couplers were new, had great performance requirements and achieved very high miniaturisation when compared to other couplers. The designed couplers were fabricated. The coupler was used with a rectifier to achieve improved performance for energy harvesting. The QHC was also used to design balanced power amplifiers and was able to achieve high linearity and efficiency in simulations and in practice. Most notably, the proposed balanced PA with QHC was able to improve both efficiency and linearity for the first time for higher bandwidths in a 5G system. This is a major contribution as previous techniques have been limited in their applications for increasing bandwidths but the proposed balanced PA with coupler was able to increase efficiency whilst achieving good linearity as well even though they are meant to be trade-off requirements and

for large bandwidths. The proposed design will contribute to the advent of 5G that require high linearity and efficiency performance for very large bandwidths above 100 MHz.

This work has been inspired by the fact that theoretical data speeds and expectations have not been met in reality/practice. The industries quest for higher data rates means that linearity, efficiency and miniaturisation will continue to be key elements for researchers in this field. This research continues to play a vital role for next generation mobile wireless communication systems. 5G is the next future of mobile wireless communications and these key areas continue to be vital and there is room for more findings and developments that could help shape the future of mobile wireless communications.

6.2 Suggestions for Future Work

This work is currently aiming to achieve highest possible reduction in nonlinear distortion for different fabricated power amplifier under test (ZFL-500 and ZHL-4240W) for both analog and digital modulated signals used currently as stated above and to effectively obtain further reduction with different approaches.

The ink-jet printed filters and couplers have not yet been fabricated due to fabrication equipment issues.

The proposed coupler has been fabricated using PCB, but it should also be fabricated using inkjet printing technologies and other new technologies that could achieve further miniaturisation with better multiband properties. This technique could be combined with other linearization techniques like DPD to further improve distortion performance.

The proposed balanced PA should also be further tested in simulations and experimental verification for 5G signals for frequency bandwidths above 100 MHz.

6.3 Conclusions

This thesis has been able to consider some of the main challenges affecting the next generation mobile wireless transceivers and has proposed some solutions to the ongoing problems. Some of the challenges facing the mobile industry is how to improve speeds, reduce size, improve efficiency and maintain linearity. The ability of the mobile wireless transmitters to attain the predicted theoretical speeds have not been realised in practice. Predicted speeds of about 1 Gbps for 4G LTE-Advanced for stationary and 100 Mbps for mobility cases have not been close in reality. This issue will also play a vital role in the ability of the upcoming 5G networks to attain the theoretical data-rates. The wireless transmitters are limited by the fact that efficiency cannot be maximised due to the trade-off with linearity.

This thesis has considered some of the current linearization techniques and proposed some novel ways to deal with the diverse issues facing the industry. However, the nonlinear distortion reduction has reduced for the current linearization techniques for increasing bandwidth. Hence, this thesis has considered ways in which the compensation of nonlinear

distortions could be maintained for even higher bandwidth cases. This work has successfully reduced the complex nature of modern-day linearization techniques with the aim for size reduction while ensuring that the suppression of the nonlinear distortions and interference are maintained even for higher frequency bandwidth cases such as 4G LTE and 5G systems that will require bandwidths up to and above 100 MHz. This thesis has also achieved the miniaturisation of critical elements in the RF/Microwave wireless transmitter system.

This thesis has considered the fact that a flexible bandstop filter could be adapted into any of the wireless transceiver applications to contribute to its linear properties by adopting it prior to amplification rather than just rejecting at the output. This idea is great, but it also has the limitation of increase in size as the conventional bandstop and bandpass filters are very large in size. This is an issue for next generation networks which have imposed strict conditions on size. In this thesis, a very compact bandstop filter was designed in inkjet-printed technology using a novel transmission line concept for ease of integration and miniaturization purposes. This narrowband bandstop (notch) filter can be designed at any desired centre frequency and was smaller in area than other published filters. The filters designed are very compact and will not considerably increase the overall size of the wireless transceiver architecture. The notch filters were successful in rejecting interfering signals prior to amplification to give a more linear output.

The second harmonic injection technique has been a successful technique for low bandwidth applications such as 2G. However, as the bandwidth increased, the technique has struggled to maintain its reduction capabilities. This has also limited the technique's use for linearization in 4G LTE networks. The injection technique was modified to successfully reduce nonlinear distortions for 4G LTE and LTE-Advanced cases with two and three carrier components. The notch filters designed were also used successfully with the injection technique to reject interference and reduce non-linear distortions.

The notch filters when implemented in multi-standard wireless transmitter systems, maintained the IM3 reduction abilities as bandwidth increased from 1.4 MHz to 5 MHz which improved on the increasing bandwidth drawback problem that the conventional second harmonic injection technique and other linearization techniques had struggled with. The modified injection technique with notch filter will be important for modern day LTE-A CA and 5G wireless systems as channel bandwidths up to and above 100 MHz will be utilized.

A novel microstrip coupler was also designed and fabricated in this thesis. The BLC is compact and can be easily integrated in 4G and 5G wireless transceiver systems for improved efficiency and linearity. The coupler was implemented and tested thereby improving efficiency at the back-off region whilst also maintaining the linearity of the system for increasing channel bandwidth for 4G and 5G systems. The coupler also improved the RF-dc conversion efficiency and maintain linearity for RF energy harvesting applications.

This thesis has successfully designed and fabricated compact microstrip filters and couplers that have contributed in improving efficiency, reducing nonlinear distortions and maintaining the linearization effect on the system for increasing channel bandwidths.

List of Publications

1. O. Olukoya, A. Tarczynski and D. Budimir, "Miniaturised inkjet-printed quadrature hybrid couplers for multiband wireless systems," *2017 USNC-URSI Radio Science Meeting (Joint with AP-S Symposium)*, San Diego, CA, 2017, pp. 83-84.
2. O. Olukoya and D. Budimir, "Inkjet-printed bandstop filters for interference suppression in multi-standard wireless systems," *2016 Asia-Pacific Microwave Conference (APMC)*, New Delhi, 2016, pp. 1-4.
3. O. Olukoya and D. Budimir, "Compact inkjet-printed bandstop filters using defected microstrip structure on flexible substrate," *Active and Passive RF Devices Seminar*, London, 2016, pp. 1-3.
4. O. Olukoya and D. Budimir, "Highly Linear Balanced Power Amplifiers with Miniaturised Quadrature Hybrid Couplers for Carrier Aggregation," *Microwave Optical Tech. Letters*, 2017, vol. 60, no. 3, pp. 529-534, March 2018.
5. G. Unichi, O. Olukoya and D. Budimir, "Rectifiers Based on Quadrature Hybrid Coupler with Improved Performance for Energy Harvesting," *IEEE Wireless Power Transfer Conference (WPTC)*, Montreal, Quebec, Canada, July 2018.
6. O. Olukoya and D. Budimir, "Rectifier Nonlinearity Effects on 4G and 5G Wireless Systems," *Intl. Microwave and RF Conference*, India, November 2018.
7. O. Olukoya, A. Ilic, A. Basu and D. Budimir, "Miniaturized Quadrature Hybrid Couplers based on Novel U-shaped Transmission Lines," *Microwave Optical Tech. Letters*, December 2018.
8. Olukoya, O., Kodogiannis, V. and Budimir, D. (2018) *Highly Efficient Balanced Power Amplifiers for 4G Applications. In: 41st International Conference on Telecommunications and Signal Processing*, Athens, July 2018.